January 1, 2010

High Geologic Slip Rates since Early Pleistocene Initiation of the San Jacinto and San Felipe Fault Zones in the San Andreas Fault System

Contents

THE GEOLOGICAL SOCIETY OF AMERICA®

3300 Penrose Place ▪ P.O. Box 9140
Boulder, CO 80301-9140, USA

ISBN 978-0-8137-2475-1
9 780813 724751

by S.U. Janecke, R.J. Dorsey, D. Forand, A.N. Steely, S.M. Kirby, A.T. Lutz, B.A. Housen, B. Belgarde, V.E. Langenheim, and T.M. Rittenour

High Geologic Slip Rates since Early Pleistocene Initiation of the San Jacinto and San Felipe Fault Zones in the San Andreas Fault System, Southern California, USA

Special Paper 475

High Geologic Slip Rates since Early Pleistocene Initiation of the San Jacinto and San Felipe Fault Zones in the San Andreas Fault System, Southern California, USA

by Susanne U. Janecke, Rebecca J. Dorsey, David Forand, Alexander N. Steely, Stefan M. Kirby, Andrew T. Lutz, Bernard A. Housen, Benjamin Belgarde, Victoria E. Langenheim, and Tammy M. Rittenour

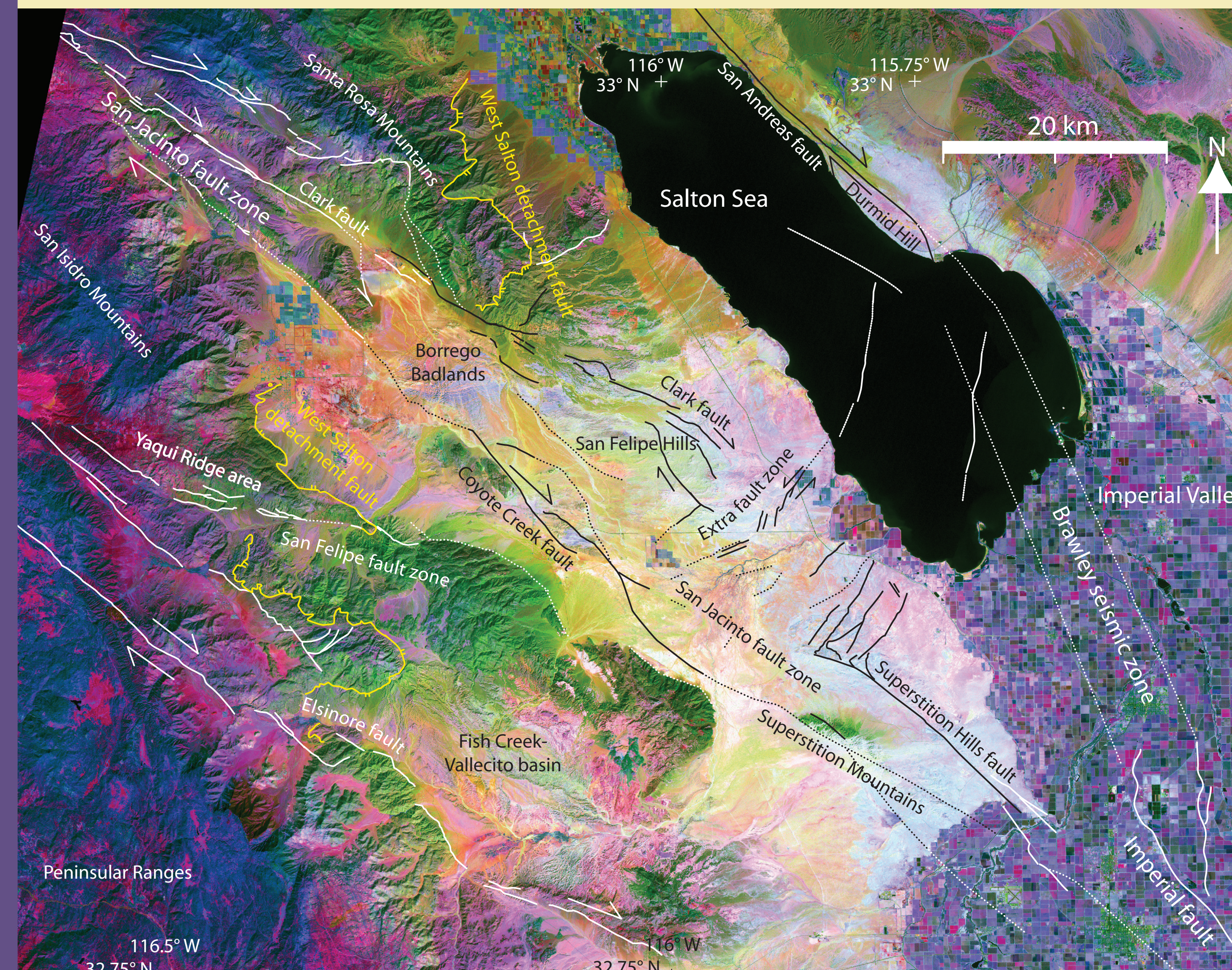

THE GEOLOGICAL SOCIETY OF AMERICA®

Special Paper 475

The Geological Society of America
Special Paper 475
2010

High Geologic Slip Rates since Early Pleistocene Initiation of the San Jacinto and San Felipe Fault Zones in the San Andreas Fault System: Southern California, USA

Susanne U. Janecke*
Department of Geology, 4505 Old Main Hill, Utah State University, Logan, Utah 84322-4505, USA

Rebecca J. Dorsey
Department of Geological Sciences, 1272 University of Oregon, Eugene, Oregon 97403-1272, USA

David Forand
Department of Geology, 4505 Old Main Hill, Utah State University, Logan, Utah 84322-4505, USA, and Chevron U.S.A. Inc., 15 Smith Road, Midland, Texas 79705-5423, USA

Alexander N. Steely
Department of Geology, 4505 Old Main Hill, Utah State University, Logan, Utah 84322-4505, USA

Stefan M. Kirby
Department of Geology, 4505 Old Main Hill, Utah State University, Logan, Utah 84322-4505, USA, and
Utah Geological Survey, 1594 W. North Temple, P.O. 146100, Salt Lake City, Utah 84114-6100, USA

Andrew T. Lutz
Fugro William Lettis & Associates, Inc., 1777 Botelho Drive, Suite 262, Walnut Creek, California 94596, USA

Bernard A. Housen
Geology Department, 516 High Street, Western Washington University, Bellingham, Washington 98225-9080, USA

Benjamin Belgarde
Department of Geology, 4505 Old Main Hill, Utah State University, Logan, Utah 84322-4505, USA, and
ExxonMobil, 222 Benmar Drive, Houston, Texas 77060, USA

Victoria E. Langenheim
U.S. Geological Survey, 345 Middlefield Road, Menlo Park, California 94025, USA

Tammy M. Rittenour
Department of Geology, 4505 Old Main Hill, Utah State University, Logan, Utah 84322-4505, USA

*susanne.janecke@usu.edu

Janecke, S.U., Dorsey, R.J., Forand, D., Steely, A.N., Kirby, S.M., Lutz, A.T., Housen, B.A., Belgarde, B., Langenheim, V.E., and Rittenour, T.M, 2010, High Geologic Slip Rates since Early Pleistocene Initiation of the San Jacinto and San Felipe Fault Zones in the San Andreas Fault System: Southern California, USA: Geological Society of America Special Paper 475, 48 p., doi: 10.1130/2010.2475. For permission to copy, contact editing@geosociety.org.

ABSTRACT

The San Jacinto right-lateral strike-slip fault zone is crucial for understanding plate-boundary dynamics, regional slip partitioning, and seismic hazards within the San Andreas fault system of southern California, yet its age of initiation and long-term average slip rate are controversial. This synthesis of prior and new detailed studies in the western Salton Trough documents initiation of structural segments of the San Jacinto fault zone at or slightly before the 1.07-Ma base of the Jaramillo subchron. The dextral faults changed again after ca. 0.5–0.6 Ma with creation of new fault segments and folds. There were major and widespread basinal changes in the early Pleistocene when these new faults cut across the older West Salton detachment fault. We mapped and analyzed the complex fault mesh, identified structural segment boundaries along the Clark, Coyote Creek, and San Felipe fault zones, documented linkages between the major dextral faults, identified previously unknown active strands of the Coyote Creek fault 5 and 8 km NE and SW of its central strands, and showed that prior analyses of these fault zones oversimplify their complexity. The Clark fault is a zone of widely distributed faulting and folding SE of the Santa Rosa Mountains and unequivocally continues 20–25 km SE of its previously inferred termination point to the San Felipe Hills. There the Clark fault zone has been deforming basinal deposits at an average dextral slip rate of ≥10.2 +6.9/–3.3 mm/yr for ~0.5–0.6 m.y.

Five new estimates of displacement are developed here using offset successions of crystalline rocks, distinctive marker beds in the late Cenozoic basin fill, analysis of strike-slip–related fault-bend folds, quantification of strain in folds at the tips of dextral faults, and gravity, magnetic, and geomorphic data sets. Together these show far greater right slip across the Clark fault than across either the San Felipe or Coyote Creek faults, despite the Clark fault becoming "hidden" in basinal deposits at its SE end as strain disperses onto a myriad of smaller faults, strike-slip ramps and flats, transrotational systems of cross faults with strongly domain patterns, and a variety of fault-fold sets. Together the Clark and Buck Ridge–Santa Rosa faults accumulated ~16.8 +3.7/–6.0 km of right separation in their lifetime near Clark Lake. The Coyote Ridge segment of the Coyote Creek fault accumulated ~3.5 ± 1.3 km since roughly 0.8–0.9 Ma. The San Felipe fault accumulated between 4 and 12.4 km (~6.5 km preferred) of right slip on its central strands in the past 1.1–1.3 Ma at Yaqui and Pinyon ridges.

Combining the estimates of displacement with ages of fault initiation indicates a lifetime geologic slip rate of 20.1 +6.4/–9.8 mm/yr across the San Jacinto fault zone (sum of Clark, Buck Ridge, and Coyote Creek faults) and about ~5.4 +5.9/–1.4 mm/yr across the San Felipe fault zone at Yaqui and Pinyon ridges. The NW Coyote Creek fault has a lifetime slip rate of ~4.1 +1.9/–2.1 mm/yr, which is a quarter of that across the Clark fault (16.0 +4.5/–9.8 mm/yr) nearby. The San Felipe fault zone is not generally regarded as an active fault in the region, yet its lifetime slip rate exceeds those of the central and southern Elsinore and the Coyote Creek fault zones. The apparent lower slip rates across the San Felipe fault in the Holocene may reflect the transfer of strain to adjacent faults in order to bypass a contractional bend and step at Yaqui Ridge.

The San Felipe, Coyote Creek, and Clark faults all show evidence of major structural adjustments after ca. 0.6–0.5 Ma, and redistribution of strain onto new right- and left-lateral faults and folds far removed from the older central fault strands. Active faults shifted their locus and main central strands by as much as 13 km in the middle Pleistocene. These changes modify the entire upper crust and were not localized in the thin sedimentary basin fill, which is only a few kilometers thick in most of the western Salton Trough. Steep microseismic alignments are well developed beneath most of the larger active faults and penetrate basement to the base of the seismogenic crust at 10–14 km.

We hypothesize that the major structural and kinematic adjustments at ca. 0.5–0.6 Ma resulted in major changes in slip rate within the San Jacinto and San Felipe

fault zones that are likely to explain the inconsistent slip rates determined from geologic (1–0.5 m.y.; this study), paleoseismic, and geodetic studies over different time intervals. The natural evolution of complex fault zones, cross faults, block rotation, and interactions within their broad damage zones might explain all the documented and implied temporal and spatial variation in slip rates. Co-variation of slip rates among the San Jacinto, San Felipe, and San Andreas faults, while possible, is not required by the available data.

Together the San Jacinto and San Felipe fault zones have accommodated ~25.5 mm/yr since their inception in early Pleistocene time, and were therefore slightly faster than the southern San Andreas fault during the same time interval. If the westward transfer of plate motion continues in southern California, the southern San Andreas fault in the Salton Trough may change from being the main plate boundary fault to defining the eastern margin of the growing Sierra Nevada microplate, as implied by other workers.

INTRODUCTION

The Pacific–North America plate boundary south of the Big Bend in the San Andreas fault is broad (~70–80 km wide), with slip currently distributed between the southern San Andreas, San Jacinto, San Felipe, and Elsinore faults and other smaller structures in the Peninsular Ranges, Salton Trough (the name applied to Coachella, Imperial, and Cerro Prieto valleys) and Borderlands area (Fig. 1). The Agua Blanca and San Miguel faults in northern Baja California may be broadly related to the fault array because they also allow plate motion to bypass the Big Bend in the San Andreas fault (Fig. 1, Allen et al., 1960). The geologic evolution and present-day distribution of slip rates across faults south of the Transverse Ranges are uncertain and controversial. Some studies dating back to the 1960s suggest that the San Jacinto fault zone carries a substantial portion of plate-boundary slip (~17–22 mm/yr), similar to that of the adjacent San Andreas fault (Table 1) (Coolidge in Sharp, 1967; Thatcher et al., 1975; Savage and Prescott, 1976; Savage et al., 1979; King and Savage, 1983; Sanders, 1989; Sanders et al., 1986; Morton and Matti, 1993; Kendrick et al., 2002; Anderson et al., 2003; Fialko, 2006; Rockwell et al., 2006; Lundgren et al., 2009). Other studies suggest much slower slip rates across the San Jacinto fault (8–12 mm/yr) (Sharp, 1981; Rockwell et al., 1990; Bennett et al., 1996; McCaffrey, 2005; Meade and Hager, 2005; Fay and Humphreys, 2005; Becker et al., 2005). Studies of slip rate can be limited by the difficulty of correlating and dating offset geologic features, particularly planar ones, by deformation that is distributed across broad damage zones, and by simplifying assumptions about crustal rheology, localized slip, locking depth, effects of post-seismic relaxation that are required to convert geodetic data into slip rates, and by comparisons of slip rates over differing time spans. Here we minimize or avoid some of these problems by determining long-term geologic slip rates since inception of the Clark, Coyote Creek, and San Felipe fault zones. In addition to these lifetime slip rates, we present incremental slip rates since the middle Pleistocene across segments of two faults.

The bulk of the Big Bend in the San Andreas fault formed sometime between 12 and 6 Ma when the transform fault south of the Transverse Ranges stepped from an offshore position into the Gulf of California during capture of the Baja microplate by the Pacific plate (Stock and Hodges, 1989; Nicholson et al., 1994; Ingersoll and Rumelhart, 1999; Fletcher et al., 2007). After this major reorganization, plate motion in the northern Salton Trough was accommodated by slip on the southern San Andreas fault and eastern California shear zone, with some strain being taken up by the east-northeast–dipping West Salton detachment fault (Powell, 1993; Axen and Fletcher, 1998). Later, in late Pliocene to Pleistocene time, dextral faults including the San Jacinto, San Felipe, and Elsinore faults were initiated in the Peninsular Ranges and Salton Trough. These dextral faults cut across, replaced, and deactivated the West Salton detachment fault, and substantially modified the slip budget of the southern San Andreas fault system (Morton and Matti, 1993; Matti and Morton, 1993; Dorsey and Axen, 2009; Steely et al., 2009).

The age of the San Jacinto fault zone is controversial. The popular interpretation that it initiated at ca. 2–2.5 Ma is based on widely cited late Quaternary slip rates of ~9–12 mm/yr at Anza (Sharp, 1981; Rockwell et al., 1990), a rate that would require ~2–2.5 m.y. to produce the 24–29 km of right slip on the fault (Sharp, 1967; Hill, 1984), if the slip rate at Anza is representative and was steady for its lifetime. Indirect evidence for this late Pliocene initiation age is derived from an anticline in the western San Bernardino Mountains that was thought to have initiated ca. 2–2.5 Ma near the subsurface lateral ramp and branch point between the San Andreas and San Jacinto faults (Meisling and Weldon, 1989; Weldon et al., 1993; Morton and Matti, 1993). In contrast, stratigraphic and structural studies near San Bernardino concluded that contraction and structural complexities in San Gorgonio Pass led to initiation of the San Jacinto fault zone between 1.4 and 1.2 Ma in order to partially bypass the eastern 55 km of the Big Bend in the San Andreas fault (Matti and Morton, 1993; Morton and Matti, 1993; Albright, 1999). Early Pleistocene initiation was also documented in the western Salton

Trough (Johnson et al., 1983; Dorsey, 2002; Lutz et al., 2006; Kirby et al., 2007; Dorsey and Axen, 2009). This latter view is supported by reanalysis of stratigraphic and structural data and documentation of a ca. 1.5 Ma, not 2–2.5 Ma initiation of the San Bernardino anticline (Kenney, 1999; Kenney and Weldon, 1999).

Very different conclusions might be reached about the age of the San Jacinto fault zone, if some of the higher slip rates inferred from analysis of global positioning system (GPS) data sets and interferometric synthetic aperture radar (InSAR) and geologic studies were extrapolated at a steady rate back in time (Table 1; Morton and Matti, 1993; Fialko, 2006; Lundgren et al., 2009). One hypothesis that reconciles the seemingly conflicting slip rates proposes that the San Jacinto fault quickly accelerated and slipped faster than the southern San Andreas fault between ca. 1 Ma and 100 ka, and then slowed to its current rate (Bennett et al., 2004). This model reconciles some of the slow late Pleistocene to Holocene slip on the San Jacinto fault based on paleoseismic and neotectonic studies (8–12 mm/yr) with a faster long-term rate implied by the young initiation ages of Morton and Matti (1993) and supported by Kenney (1999). It does not reconcile the discrepancy between the faster slip rates inferred by most recent analyses of GPS data sets and the slower rates of paleoseismic and neotectonic interpretations (Table 1).

The large disparity between slip rates derived from different data sets and over different time scales motivated our study to determine the time of initiation and long-term average slip rates of the San Jacinto and San Felipe fault zones in the western Salton Trough. The age of fault initiation places critical constraints on the

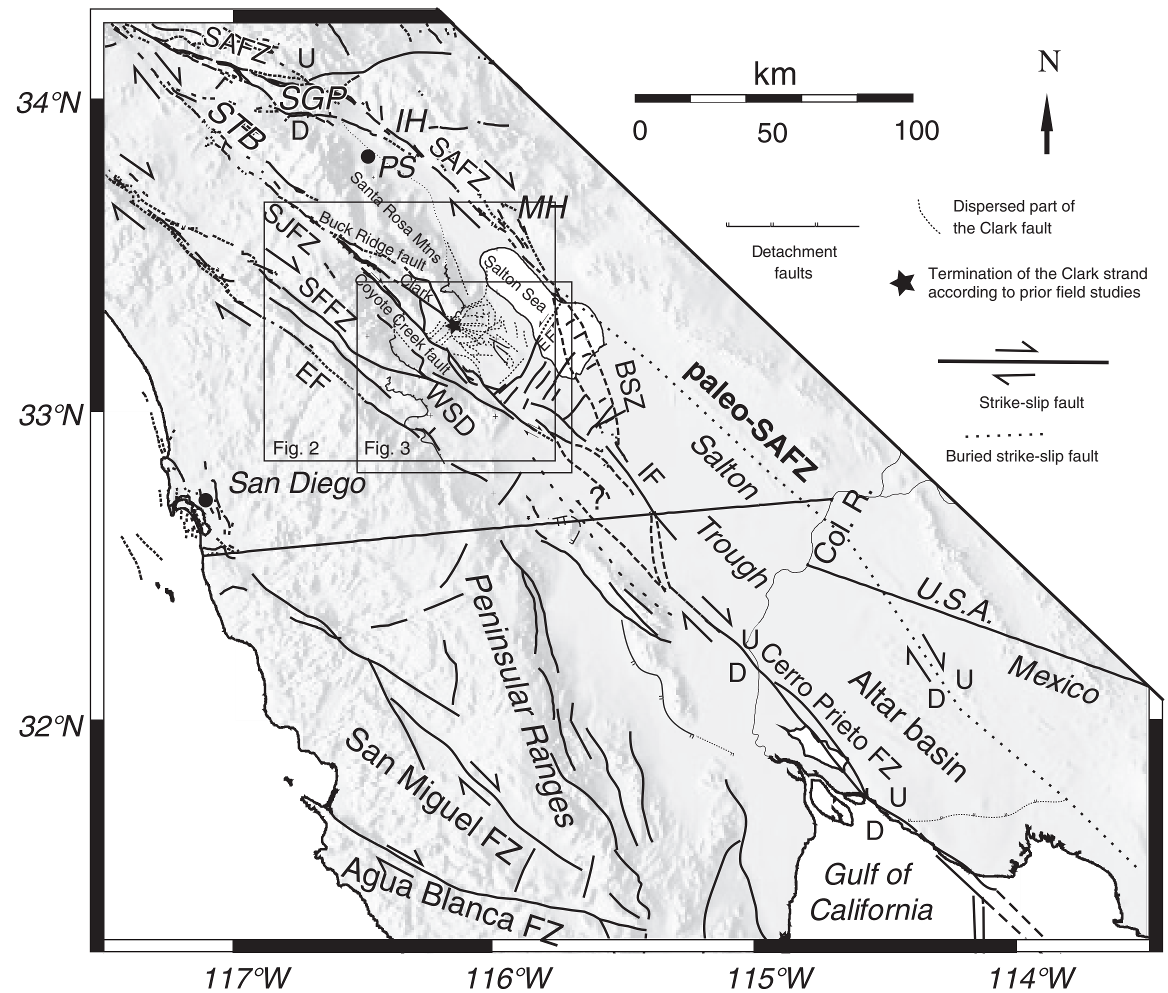

Figure 1. Regional fault map showing the linkage of the San Jacinto fault and San Felipe fault with each other, San Andreas fault, Brawley seismic zone, and Imperial faults farther to the southeast. Modified from many sources, including Jennings (1977, 1994), Janecke et al. (2004), Kirby (2005), Hudnut et al. (1989), Axen and Fletcher (1998), Steely (2006), Lutz (2005), Kirby (2005), Pacheco et al. (2006), Janecke, unpublished mapping. San Felipe fault zone (SFFZ) is counterclockwise to most other strike-slip faults; SAFZ—San Andreas fault zone; SJFZ—San Jacinto fault zone; EF—Elsinore fault; BSZ—Brawley seismic zone; IF—Imperial fault; IH—Indio Hills; MH—Mecca Hills; SFFZ—San Felipe fault zone; SGP—San Gorgonio Pass; STB—San Timoteo Badlands; PS—Palm Springs. Oblique-slip detachment faults include the West Salton detachment fault (WSD).

TABLE 1. SUMMARY OF SLIP RATES ACROSS THE SAN JACINTO FAULT ZONE (SJFZ)

Author (in chronological order)	Method	Rate for SJFZ	Rate for SAF	Time scale	Comments
Coolidge and Whitten (1956), as cited in Sharp (1967)	Geodetic network Very long baseline	24 mm/yr[¥]	ND	Short	
Sharp (1967)	Geologic	25 mm/yr	ND	ca. 1 Ma	
Savage and Prescott (1976)	Geodetic network	25 mm/yr[¥]	ND	6 yr	
Savage et al. (1979)	Long baseline	17 ± 9 mm/yr[¥]	25 ± 8 mm/yr	4 yr	
Sharp (1981)	Paleoseismology	10 ± 2 mm/yr 8–12 mm/yr	ND	Since 0.73 Ma	Lowest rate from paleoseismic or neotectonic study
King and Savage (1983)	Long baseline	(SJFZ = 88% of SAF) 21.9 mm/yr[#]	(SJFZ = 88% of SAF) 25 mm/yr[#]	8 yr	
Rockwell et al. (1990)	Paleoseismology and neotectonic	10 ± 2 mm/yr 8–12 mm/yr is preferred; 6–23 mm/yr is the total range	ND	50 k.y.	
Morton and Matti (1993)	Geologic	25–30 km/1.5 m.y. 17.4–20 mm/yr		1.4 Ma	
Matti and Morton (1993)	Geologic	25–30 km/1.2 m.y. 20.1 to 25 mm/yr		1.2 Ma	
Bennett et al. (1996)	GPS	9 ± 2 mm/yr	23 ± 2 mm/yr	15 yr	Lowest rate from GPS analysis
Kendrick et al. (2002)	Neotectonic	>20 mm/yr			
Anderson et al. (2003)	GPS	SJFZ ≥ SAF ≥19.5 mm/yr[#]	SJFZ ≥ SAF ≤19.5 mm/yr[#]	15 yr	
McCaffrey (2005)	GPS	13.5 mm/yr	25.3 mm/yr	15 yr	
Meade and Hager (2005)	GPS block model	11.9 ± 1.2 mm/yr	23.3 ± 0.5	15 yr	
Fay and Humphreys (2005)	GPS	14.5 ± 0.8 mm/yr	22.3 ± 0.7 mm/yr	15 yr	
Becker et al. (2005)	GPS plus stress inversion	15.3 ± 11 14.5 ± 9	23 ± 8 mm/yr 22.9 ± 8 mm/yr	15 yr	
Rockwell et al. (2006)	Paleoseismology	>16 mm/yr	ND	4 k.y.	Highest rate from paleoseismic or neotectonic study
Fialko (2006)	InSAR plus GPS	20 ± 1 mm/yr	25 ± 3 mm/yr	8 yr—InSAR, 20 yr GPS	
Lundgren et al. (2009)	InSAR plus GPS	24–26 mm/yr	16–18 mm/yr	7 yr—InSAR, 20 yr—GPS	Highest rate from GPS and InSAR analysis
					Slip rate across the Coyote Creek fault is among the highest of any study.
This study	Lifetime geologic slip rate	20.1 +6.4/–9.8 mm/yr	ND	0.8–1.3 Ma	
This study	Slip rate since ca. 0.5 Ma	≥14.0 + 7.1/–4.5 mm/yr		0.5–0.6 Ma	

Note: GPS—global positioning system; InSAR—interferometric synthetic aperture radar; ND—no data.

[¥] Linear slip rate was calculated from the rotational strain rate reported in this article.

[#] We calculated a rate of slip by assuming a combined slip rate of 38.9 mm/yr across both the San Jacinto and southern San Andreas fault (SAF). This value is the average of all the rates in this table.

fault-displacement field and slip partitioning through time and is important for assessing seismic hazards in southern California.

This paper presents, summarizes, and interprets three complementary data sets: (1) prior stratigraphic and magnetostratigraphic studies by our group (Kirby, 2005; Kirby et al., 2007; Lutz, 2005; Lutz et al., 2006; Steely, 2006; Steely et al., 2009; Belgarde, 2007; Janecke and Belgarde, 2008) that define the initiation ages of three separate faults and describe many detailed data sets that cannot be reproduced here; (2) abundant new and revised data for total offsets across three dextral faults, optically stimulated luminescence dating of sediment on pediment within the fault zones, and in-depth structural analysis of the fault zones; and (3) data from two unpublished theses (Belgarde, 2007; Forand, 2010) and the unpublished prepublication manuscripts in partly published theses of Kirby (2005) and Steely (2006). We present the estimates of displacement from NE to SW across segments of the Clark and Coyote Creek faults of the San Jacinto fault zone and the San Felipe fault zone in the southwest. We calculate slip rates from these data, and explore the implications of the slip rates and structural geometries of the fault zones for understanding plate-boundary kinematics, seismic hazards, and the distribution of slip rates at time scales from the present-day to 10^6 yr. A separate study (Janecke and DeMets, 2010) addresses how the inception of the new dextral faults reflects a widespread reorganization of the North American plate boundary.

STRUCTURAL GEOLOGY OF DEXTRAL FAULT ZONES IN THE WESTERN SALTON TROUGH

The San Jacinto, San Felipe, and Elsinore fault zones lie southwest of the San Andreas fault and cut obliquely across the northern Peninsular Ranges and western Salton Trough (Figs. 1–3). Each fault zone consists of separate faults connected by steps, branch points, and transrotational linkages (Figs. 1–3; Sharp, 1967; Sanders, 1989; Kirby, 2005; Kirby et al., 2007; Lutz, 2005; Lutz et al., 2006; Steely, 2006, Belgarde, 2007).

San Jacinto Fault Zone

Estimates of total right-lateral slip across the San Jacinto fault zone in the Peninsular Ranges and Salton Trough vary from 19 to 29 km (Sharp, 1967; Bartholomew, 1970; Hill, 1984; Matti and Morton, 1993; Janecke et al., 2005b; Forand, 2010). Near the western margin of the Salton Trough the major strands of the San Jacinto fault zone are the Buck Ridge, Clark, and Coyote Creek faults (Figs. 2 and 3; Dibblee, 1954, 1984; Sharp, 1967, 1975). The dextral Buck Ridge fault diverges from the Clark fault near Anza and reconnects at the southern tip of the Santa Rosa Mountains by bending to a more southerly strike and becoming the normal-oblique Santa Rosa fault NW of branch point (Figs. 2 and 3; Dibblee, 1954, 1984; Belgarde, 2007; this study). Our mapping east of Clark Lake shows that Dibblee was correct in connecting the Buck Ridge and Santa Rosa faults in the SE Santa Rosa Mountains even though Sharp (1967) and most subsequent workers (e.g., Jennings, 1994) rejected this interpretation (Figs. 2 and 3; Janecke and Belgarde, 2008; plate 1 in Belgarde, 2007; Forand, 2010). The Santa Rosa fault consists of several mappable SW-dipping strands near its SE branch point with the Clark fault that are embedded within a kilometer-scale breccia zone of tonalite and mylonite in the southern Santa Rosa Mountains (Fig. 3; Sharp, 1967; Janecke and Belgarde, 2008; Belgarde, 2007). Short fault scarps are preserved on strands of the Buck Ridge and Santa Rosa fault zones, and block rotation, distributed faulting, and kilometer-scale breccia zones characterize the rocks between the Buck Ridge and Clark fault NW of Clark Lake Valley (Janecke, unpublished mapping, 2008).

The Clark strand of the San Jacinto fault has 16.8 +3.7/–6.0 km of right separation based on offset crystalline rocks (Sharp, 1967; Bartholomew, 1970; Forand, 2010). This slip estimate includes all the slip across the SE part of the Clark fault plus much of the slip on the Buck Ridge fault in the Santa Rosa Mountains (Figs. 2A and 2B; Janecke et al., 2005a; Belgarde, 2007).

Despite having roughly 17 km of right separation near Clark Lake, the Clark strand is difficult to locate in the Salton Trough southeast of the Santa Rosa Mountains and is typically depicted as terminating near there in Smoke Tree Canyon and Palo Verde Wash (Figs. 1–3) (Dibblee, 1954, 1984; Sharp, 1967, 1972b, 1975, 1981; Bartholomew, 1970; Sanders, 1989; Pettinga, 1991; Sanders and Magistrale, 1997). New field studies, structural analysis, gravity and magnetic gradients, and mapping for this study show that, instead, the Clark fault is a zone of widely distributed faulting and folding SE of the Santa Rosa Mountains and unequivocally continues 20–25 km SE of its previously inferred termination point to within ~3 km of the crossing NE-striking Extra fault zone at the surface (Figs. 1–3; Dibblee, 1984; Hudnut et al., 1989; Kirby, 2005; Kirby et al., 2007; and Belgarde and Janecke, unpublished mapping, 2006; Belgarde, 2007). This new interpretation is based on recognition that the Clark fault is a zone of widely distributed faults and folds SE of the Santa Rosa Mountains and required a detailed mapping to identify its highly complex dispersed elements (Kirby et al., 2007; Belgarde, 2007; Janecke and Belgarde, 2008). Folded Pleistocene and Holocene sedimentary rocks occupy the zone between the SE tip of the Clark fault zone and the Extra fault zone in the SE San Felipe Hills (Figs. 3 and 4; Kirby, 2005; Kirby et al., 2007; S.U. Janecke, unpublished mapping). The traditional interpretation—that there is very little slip across the Clark fault SE of Smoke Tree Canyon—is incompatible with the strongly folded and faulted Upper Pliocene and Pleistocene sedimentary rocks in the SE San Felipe Hills (Kirby, 2005). The fault zone is very broad and splays out to a width of at least 18 km perpendicular to the strike of the main strands (Belgarde, 2007; Kirby et al., 2007).

Boundaries between structural segments of the dextral Clark fault coincide with bends and steps in the fault zone, branch points, crossing blocks of sinistral faults, and changes in structural style, and include a newly defined Tarantula Wash segment in the San Felipe Hills (Fig. 2B). To avoid confusion we adopt this name in place of the original name "San Felipe Hills segment" of Belgarde (2007). We modified the positions of boundaries between structural segments (Fig. 2B) based on our mapping of each fault zone but retained many of the names of segments from Sanders (1989) and Sanders and Magistrale (1997). Figure 2 shows the structural segments of the Clark fault (by color), as well as those of the Coyote Creek and central San Felipe fault zones (triangles).

The Coyote Creek fault is the most continuous strand of the San Jacinto fault zone within the Salton Trough (Sharp, 1967; Sanders, 1989; Sanders and Magistrale, 1997; Dorsey, 2002; Janecke et al., 2005a, 2005b; Steely, 2006). The Coyote Creek fault (Fig. 2A) was previously thought to have ~4–6 km of right slip (Sharp, 1967; Bartholomew, 1970; Dorsey, 2002). It terminates to the northwest in tonalite of the Peninsular Ranges batholith ~20 km northwest of the Salton Trough without a direct surface connection to the Clark fault (Sharp, 1967). Rotated normal, thrust and sinistral-oblique faults provide the surface connection between the Clark and Coyote Creek faults at the NW part of Coyote Ridge (Sharp, 1979), whereas some oblique dextral faults perform this function in the SE part of the ridge (Figs. 2A, 2B, and 3; Janecke and Forand, plate in Forand, 2010). Small steps and lateral bends have uplifted sedimentary and crystalline rocks along the Coyote Creek fault between Coyote Ridge and the Superstition Mountains (Fig. 2). Southeast of the Superstition Hills and Superstition Mountain, the Coyote Creek fault zone lacks surface expression and its location was poorly constrained until three NW-trending microseismic alignments were identified along the fault zone, verifying that the San Jacinto fault zone branches from the NW end of the Imperial fault (Fig. 1; Magistrale, 2002; Shearer et al., 2005; Lin et al., 2007). At least one fault strand projects southeastward toward the Cerro Prieto fault (Fig. 1; Magistrale, 2002; Lin et al., 2007).

Our 1:12,000–1:40,000 scale mapping, photogeologic and satellite-based mapping, as well as the distribution of precisely relocated earthquakes (Shearer et al., 2005; Lin et al., 2007) all show that the dextral fault array in the Peninsular Ranges and southwest Salton Trough is a >50-km-wide fault web and map-scale fault mesh (Figs. 1–3). This fault mesh is far more complex and interconnected than existing maps depict (e.g., Jennings, 1994, Fig. 3). The highly faulted region contains a small number of continuous right-lateral fault zones (master faults such as the Buck Ridge, Clark, Coyote Creek, San Felipe, Earthquake Valley, and Elsinore faults) that are surrounded and connected by a complex mesh of shorter, smaller offset, left-lateral, normal, and thrust faults, and many large and small folds (Fig. 3). We refer to these shorter faults between the master faults as connector, cross, or rung faults depending on their geometry. Folds deform some of the crystalline rocks (e.g., Kirby et al., 2007; Steely et al., 2009) but are far more common and well developed in the sedimentary basin fill.

The presence of this very complex fault and fold mesh complicates analysis of the kinematic and geometric relationships between dextral faults and makes it difficult to confidently assign every structure to a specific fault zone (Figs. 2 and 3). Deformation occurs in domains that are separated by abrupt lateral changes in fault patterns. This suggests that slip amounts and slip rates are likely to vary considerably along strike of the principal faults as strain is transferred to and from adjacent structures. We address this issue by being as site-specific as possible in our analysis and by emphasizing that displacement values and age controls apply to particular structural and rupture segments of the dextral faults and may not apply to adjacent parts of the fault (e.g., Table 2).

Clark Fault Zone

Right Slip across the Clark Fault Zone in Crystalline Rocks

Sharp (1967) determined that the Clark strand of the San Jacinto fault zone in the Clark Valley area has ~14–15 km of right separation based on offset crystalline rocks (but see below for a revised value). This slip magnitude is widely accepted but is low relative to separations along the remainder of the Clark fault (Sharp, 1967). Farther to the northwest, five offset markers are correlable across the Clark fault (Sharp, 1967). The right separations of these marker units are very similar to each other: 24, 23.2, 21.9, 22.9, and 23.5 km from southeast to northwest (Sharp, 1967). These separations average 23.1 km. We remapped and remeasured the southeasternmost of these offset plutons (with 24 km of right separation [Sharp, 1967]) using Landsat, Google Earth, and Sharp's original map. Our analysis confirms the original report of Sharp (1967) (Fig. 2) and refines the displacement of the northern edge of the Coahilla pluton to 23.4 km (Fig. 2, red lines). The equivalent pluton on the northeast side of the Clark fault is called the Clark Valley pluton and its northwest edge is well exposed along Rock House Canyon (Sharp, 1967). After addition of separation across the adjacent part of the Coyote Creek fault at Monkey Hill (2.3 km; Sharp, 1967), this sums to a total right separation of 25.6 km on the San Jacinto fault zone where it enters the Clark and Borrego Valleys in the northwest part of our study area (Fig. 2; NW part of Fig. 3). This value contrasts with that of Blisniuk et al. (2010), who inferred a significant decrease in total bedrock offset along the Clark fault from Anza to Rockhouse Canyon. We address the sources and implications of this discrepancy in the Discussion section of this paper.

Previous estimates of right separation across the Clark fault along the Santa Rosa segment (SRS, Fig. 2B) range from ~14.4 to 22.4 km based on a displaced east-dipping mylonite zone (Sharp, 1967; Bartholomew, 1970; Erskine, 1985). Possible right drag and folding within the damage zone of the Clark fault was suspected to increase the right separation measured by Sharp (1967) to 18 km (Janecke et al., 2005a), but field and structural analyses show that the largest folds in the damage zone of the San Jacinto fault zone have ductile overturned limbs, and are therefore Cretaceous folds that are unrelated to the brittle Quaternary San Jacinto fault zone (Fig. 5; Forand, 2010).

Careful mapping of the marker succession (tonalite, marble, and migmatite) on either side of the Clark fault yields a new estimate of 16.8 +3.7/–6.0 km for the right separation on this fault

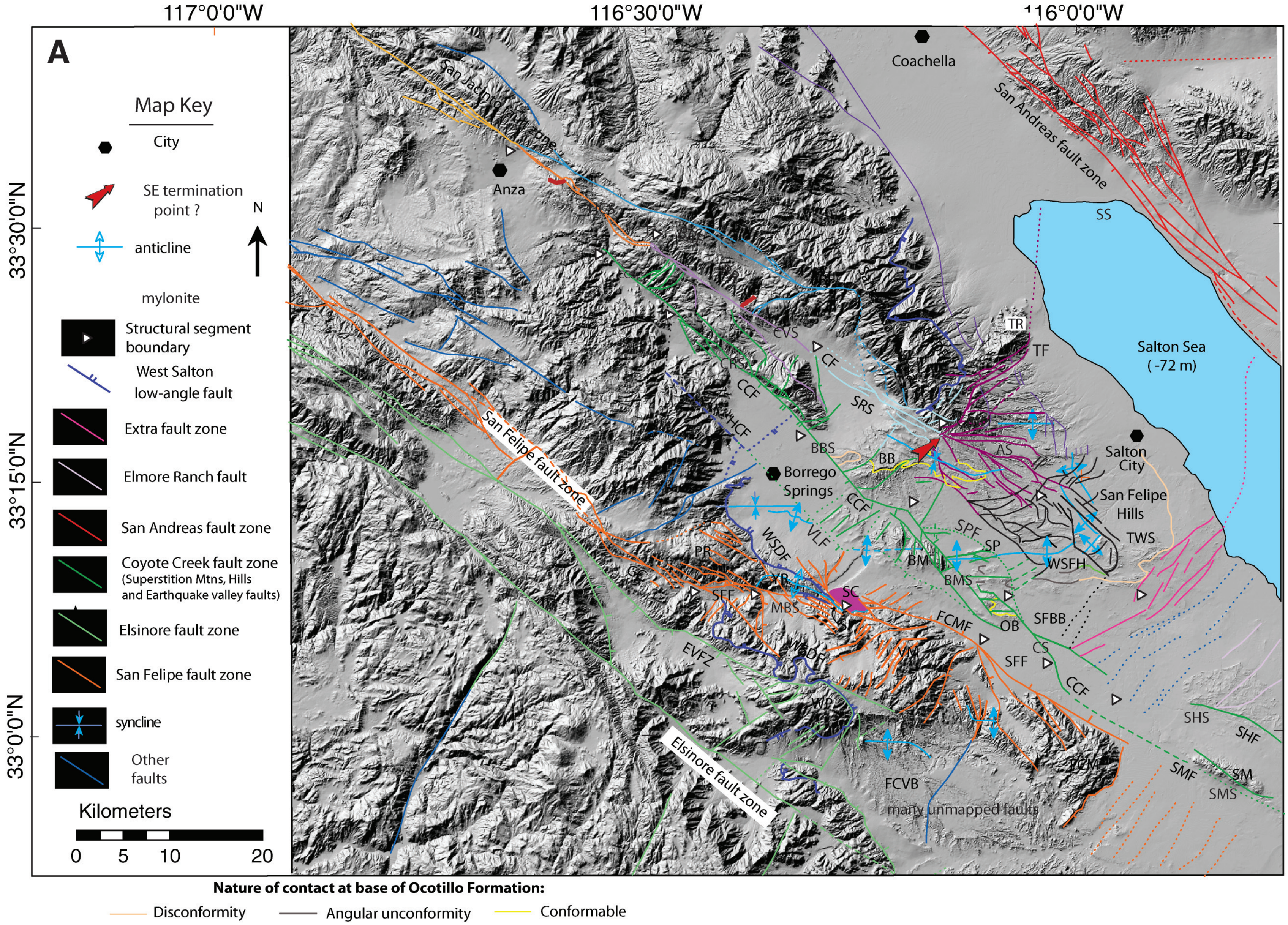

Figure 2 (*continued on following page*). (A) Important structural features of southern California and the nature of the basal contact of the Ocotillo Formation in the SW Salton Trough. Location shown in Figure 1. The offset northern and northwestern margins of a distinctive pluton are show with a thick red line on either side of the Clark fault. This pluton margin is displaced 23.4 km. Note that the West Salton low-angle fault is folded and cut by dextral strike-slip fault zones. A Cretaceous mylonite zone (light blue) is offset ~16.8 +3.7/–6.0 km across the Clark fault; yet the fault was thought to terminate at the red arrow by most prior workers.

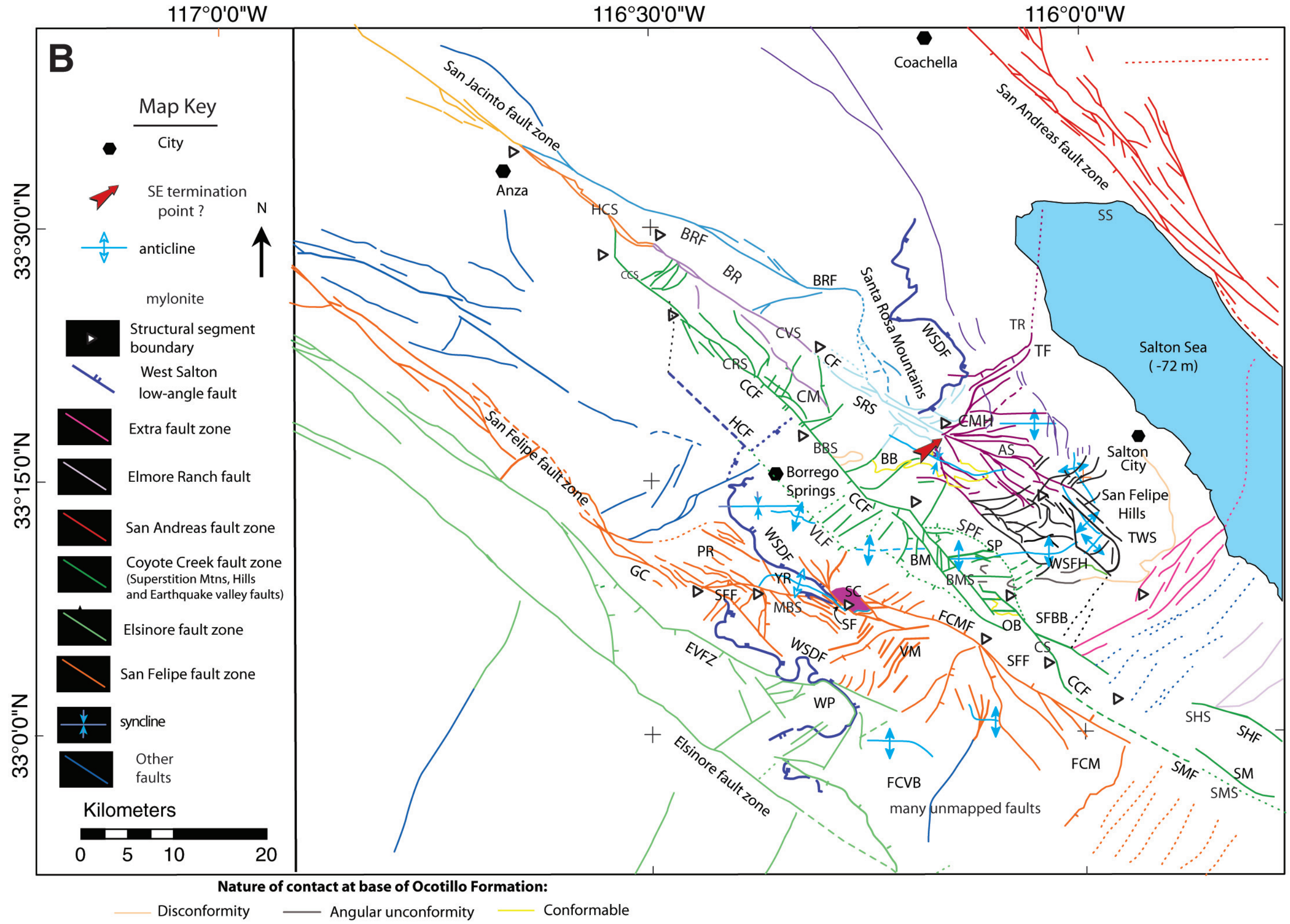

Figure 2 (*continued*). (B) Same as (A) with faults highlighted. Names of structural segments and positions of boundaries between them (triangles) are modified from Sanders (1989), Kirby (2005), Steely (2006), and this study and are placed at major bends, steps, and changes in structural style. BRF—Buck Ridge fault; BR—Buck Ridge. Segments of Clark fault: AS—Arroyo Salada segment; CVS—Clark Valley segment; HCS—Horse Canyon segment; TWS—Tarantula Wash segment; SRS—Santa Rosa segment. Segments of Coyote Creek fault: BBS—Borrego Badlands segment; BMS—Borrego Mountain segment; CRS—Coyote Ridge segment; CS—central segment; SS—Superstitions segment; SHS—Superstition Hills segment; SMS—Superstition Mountains segment. Segments of San Felipe fault zone: GC—Grapevine Canyon segment, which is in Grapevine Canyon; MBS—Mescal Bajada segment; PR—Pinyon Ridge segment, which is directly south of Pinyon Ridge; FCMF—Fish Creek Mountain fault. Other names: BB—Borrego Badlands; BM—Borrego Mountain; BRF—Buck Ridge fault; CCF—Coyote Creek fault; CCS—Coyote Creek segment; CF—Clark fault; CM—Coyote Mountain; CMH—Calcite Mine hill; EVFZ—Earthquake Valley fault zone; FCM—Fish Creek Mountains; FCMF—Fish Creek Mountains fault; FCVB—Fish Creek–Vallecito basin; HCF—Hellhole Canyon fault; OB—Ocotillo Badlands; SC—Sunset conglomerate of the Ocotillo Formation (hot pink); SF—Sunset fault; SFBB—San Felipe–Borrego basin; SFF—San Felipe fault; SHF—Superstition Hills fault; SM—Superstition Mountain; SMF—Superstition Mountains fault; SP—Squaw Peak; SPF—Squaw Peak fault; TF—Travertine fault; TR—Travertine Ridge; VLF—Veggie Line fault; VM—Vallecito Mountains; FCVB—Fish Creek–Vallecito basin; WP—Whale Peak; WSDF—West Salton detachment fault; WSFH—west San Felipe Hills; YR—Yaqui Ridge. Faults are compiled and modified from Rogers (1965), Jennings (1977), Morton (1999), Kirby (2005), Lutz (2005), Kennedy (2000, 2003), Kennedy and Morton (2003), Morton and Kennedy (2003), and this study. Mylonite was modified from Sharp (1979), Kairouz (2005), and Steely (2006).

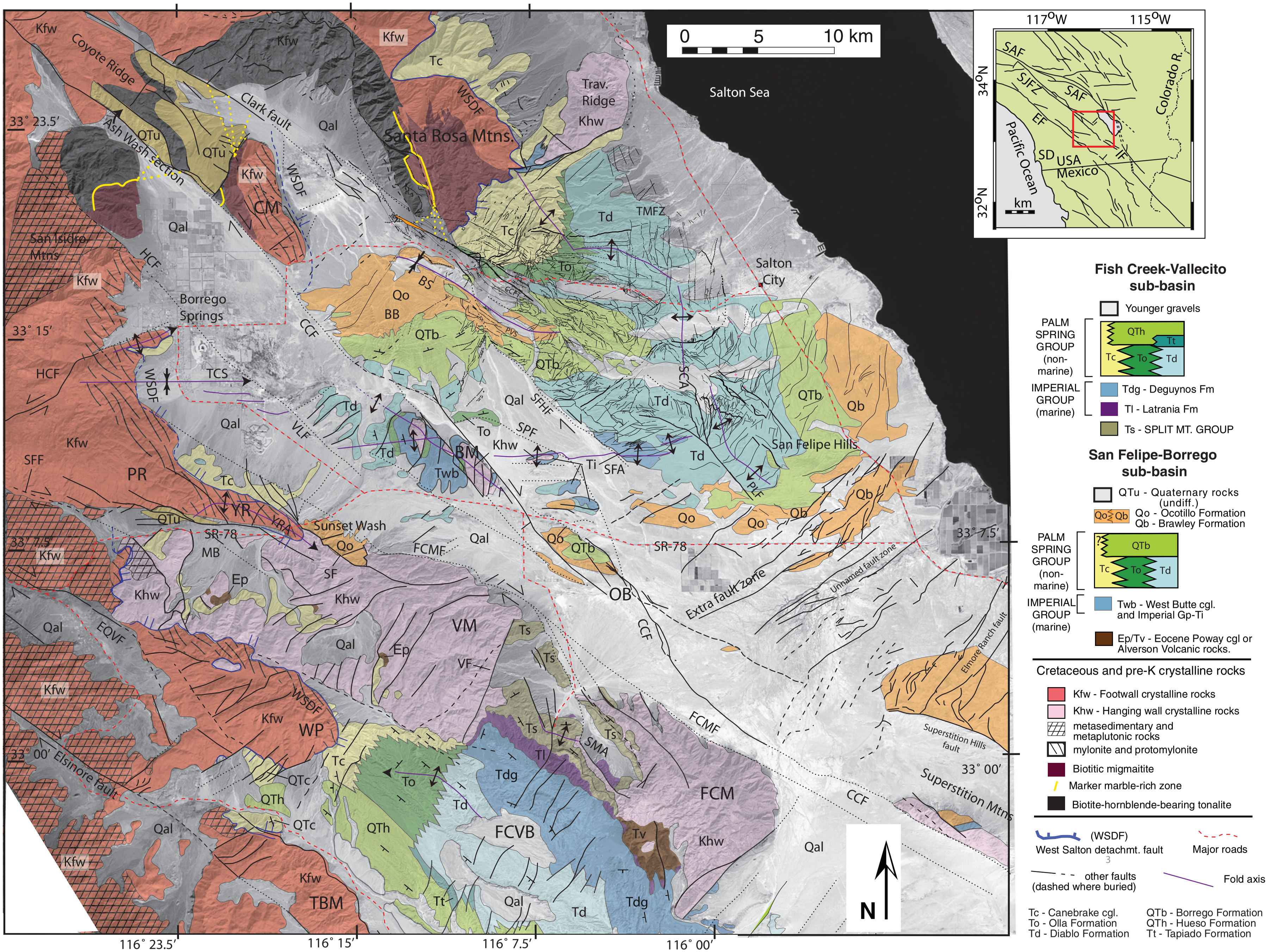

0 5 10 km
Salton Sea
Santa Rosa Mtns.
Coyote Ridge
Clark fault
Ash Wash section
San Isidro Mtns
Borrego Springs
Salton City
San Felipe Hills
Trav. Ridge
Sunset Wash
Extra fault zone
Unnamed fault zone
Elmore Ranch fault
Superstition Hills fault
Superstition Mtns
Elsinore fault
33° 23.5′
33° 15′
33° 7.5′
33° 00′
116° 23.5′
116° 15′
116° 7.5′
116° 00′
117°W
115°W
34°N
32°N
Pacific Ocean
Colorado R.
USA
Mexico
Fish Creek-Vallecito sub-basin
Younger gravels
PALM SPRING GROUP (non-marine)
IMPERIAL GROUP (marine)
Tdg - Deguynos Fm
Tl - Latrania Fm
Ts - SPLIT MT. GROUP
San Felipe-Borrego sub-basin
QTu - Quaternary rocks (undiff.)
Qo - Ocotillo Formation
Qb - Brawley Formation
Twb - West Butte cgl. and Imperial Gp-Ti
Ep/Tv - Eocene Poway cgl or Alverson Volcanic rocks.
Cretaceous and pre-K crystalline rocks
Kfw - Footwall crystalline rocks
Khw - Hanging wall crystalline rocks
metasedimentary and metaplutonic rocks
mylonite and protomylonite
Biotitic migmaitite
Marker marble-rich zone
Biotite-hornblende-bearing tonalite
(WSDF) West Salton detachmt. fault
Major roads
other faults (dashed where buried)
Fold axis
Tc - Canebrake cgl.
To - Olla Formation
Td - Diablo Formation
QTb - Borrego Formation
QTh - Hueso Formation
Tt - Tapiado Formation
N

Figure 3. Geologic map of the western Salton Trough overlain on Landsat image. Inset map shows relationship of the region to major dextral faults in southern California. Compiled from Dibblee (1954, 1984, 1996), Rogers (1965), Winker (1987), Winker and Kidwell (1996), Treiman and Lundberg (1999), Heitman, (2002), Lilly (2003), Kirby (2005), Belgarde (2007), Steely (2006), Lutz (2005), Kairouz (2005), Sharp (1967), Shirvell (2006), and S.U. Janecke unpublished mapping (2001–present); Axen, unpublished mapping (2006); Dorsey unpublished mapping (2002–2006); Forand, unpublished mapping (2008). BB—Borrego Badlands; BM—Borrego Mountain; BS—Borrego Syncline; CCF—Coyote Creek fault; CM—Coyote Mountain; EQVF—Earthquake Valley fault zone; FCM—Fish Creek Mountains; FCMF—Fish Creek Mountains fault; FCVB—Fish Creek–Vallecito basin; HCF—Hellhole Canyon fault; MB—Mescal Bajada; OB—Ocotillo Badlands; PLF—Powerline fault; PR—Pinyon Ridge; SCA—Salton City anticline; SF—Sunset fault; SFF—San Felipe fault; SFA—San Felipe anticline; SFHF—San Felipe Hills fault; SMA—Split Mountain anticline; SPF—Squaw Peak fault; SR—Santa Rosa fault; TCS—Tubb Canyon syncline; TBM—Tierra Blanca Mountains; TMFZ—Torrez Martinez fault zone; VF—Vallecito fault; VLF—Veggie Line fault; VM—Vallecito Mountains; WP—Whale Peak; WSDF—West Salton detachment fault; YRA—Yaqui Ridge anticline. For clarity, we show most of the complex fault mesh in the Clark fault zone SE of the Santa Rosa Mountains (Belgarde, 2007) with thinner fault lines. cgl—conglomerate; Trav.—travertine.

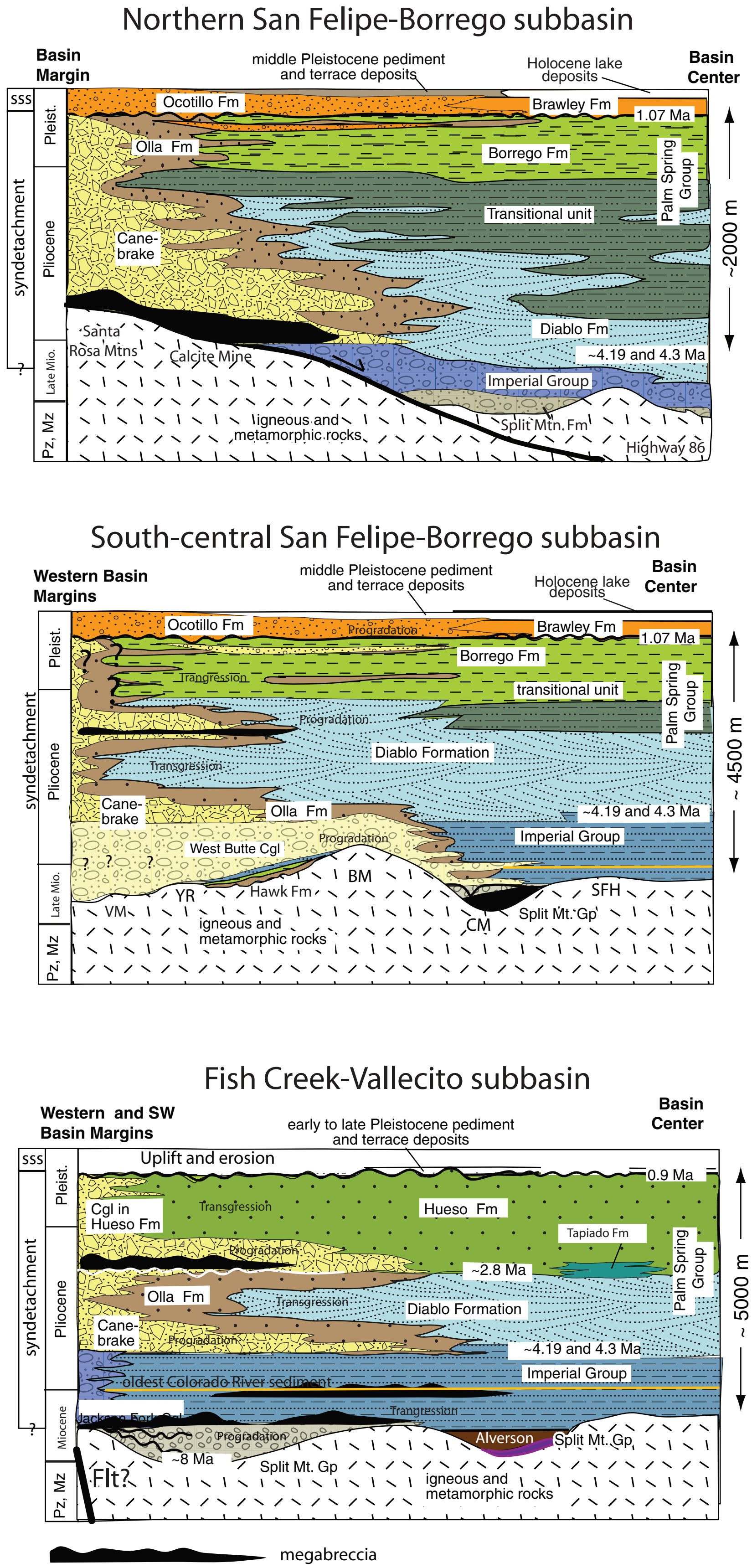

Figure 4. Stratigraphy of the Fish Creek–Vallecito and San Felipe–Borrego subbasins. Data were synthesized from many sources, including Dibblee (1954, 1984, 1996); Woodward (1963, 1974); Winker and Kidwell (1996); Dorsey (2002, 2006); Dorsey et al. (2007); Kairouz (2005); Kirby (2005); Lutz (2005); Steely (2006); Shirvell (2006); Belgarde (2007); this study. Pz—Paleozoic; Mz—Mesozoic; SSS—syn-strike-slip.

TABLE 2A. LIFETIME SLIP RATES ACROSS THE SAN JACINTO FAULT ZONE

Fault zone	Fault within fault zone	Structural segment(s) along the fault (see Fig. 3B)	Slip estimate (since ca. 0.5 Ma)	Offset feature	Estimated age of initiation of the fault segment	Lifetime slip rate	Source of data used to calculate the slip rate
San Jacinto	Clark	Santa Rosa and Arroyo Salada	16.8 +3.7/–6.0 km*	Succession of tonalite, marble, migmatite, mylonite	1.0 to 1.3 Ma; 1.05 Ma is the preferred age	16.0 +4.5/–7.7 mm/yr	Sharp (1967); Lutz et al. (2006); Kirby et al. (2007); this study
San Jacinto	Coyote Creek	Coyote Ridge	3.5 ± 1.3 km*	Tonalite, marble, migmatite, mylonite	1.1 to 0.8 Ma	4.1 +1.9/–2.1 mm/yr	This study, updated from data in Sharp (1967); Dorsey (2002)
Total slip rate across the San Jacinto fault zone in its lifetime					SUM	20.1 +6.4/–9.8 mm/yr	This study

TABLE 2B. SLIP RATES ACROSS THE SAN JACINTO FAULT ZONE SINCE CA.0.5 TO 0.6 MA

Fault zone	Fault within fault zone	Structural segment(s) along the fault (see Fig. 3B)	Slip estimate (since ca. 0.5 Ma)	Offset feature	Estimated age of initiation of the fault segment	Interval slip rate	Source of data used to calculate the slip rate
San Jacinto	Clark	San Felipe Hills	(5.6 ± 0.4 km)†	Calculated from amount of N-S shortening in Pliocene–Pleistocene sedimentary rocks	<~0.55 ± 0.2 Ma	≥10.2 +6.9/–3.3 mm/yr	Kirby (2005); Janecke et al. (2005b); this study
San Jacinto	Coyote Creek	Borrego Mountain and Borrego Badlands	2.3 ± 0.7 km†	North-dipping marker bed near contact between Olla and Diablo formations, gravity contours	<0.6 Ma	>3.8 ± 1.2 mm/yr	Steely (2006); this study
Minimum slip rate across the San Jacinto fault zone since ca. 0.5 to 0.6 Ma					SUM	≥14.0 +7.1/–4.5 mm/yr	This study

TABLE 2C. LIFETIME SLIP RATE ACROSS PARTS OF THE SAN FELIPE FAULT ZONE

Fault zone	Fault within fault zone	Structural segment(s) along the fault (see Fig. 3B)	Slip estimate (since ca. 0.5 Ma)	Offset feature	Estimated age of initiation of the fault segment	Lifetime slip rate	Source of data used to calculate the slip rate
San Felipe	Sunset	Sunset	<2.5 km	Provenance link between displaced Ocotillo formation and its possible source area in the La Posta pluton	1.3 to 1.1 Ma	<2.1 ± 0.2 mm/yr	Steely (2006)
San Felipe	San Felipe	Pinyon Mountain and Mescal Bajada	4 to 12.4 km* 6.5 km preferred‡	West Salton detachment fault and base of the Eastern Peninsular Ranges mylonite zone	1.3 to 1.1 Ma	~5.4 +5.9/–1.4 mm/yr	Steely (2006); this study

*Displacement of crystalline markers or preexisting structural feature.
†Displacement is based on deformed or offset Pliocene–Pleistocene sedimentary rocks.
‡Three separate methods were used to estimate the right slip, and ~6.5 km is the overlap between methods.

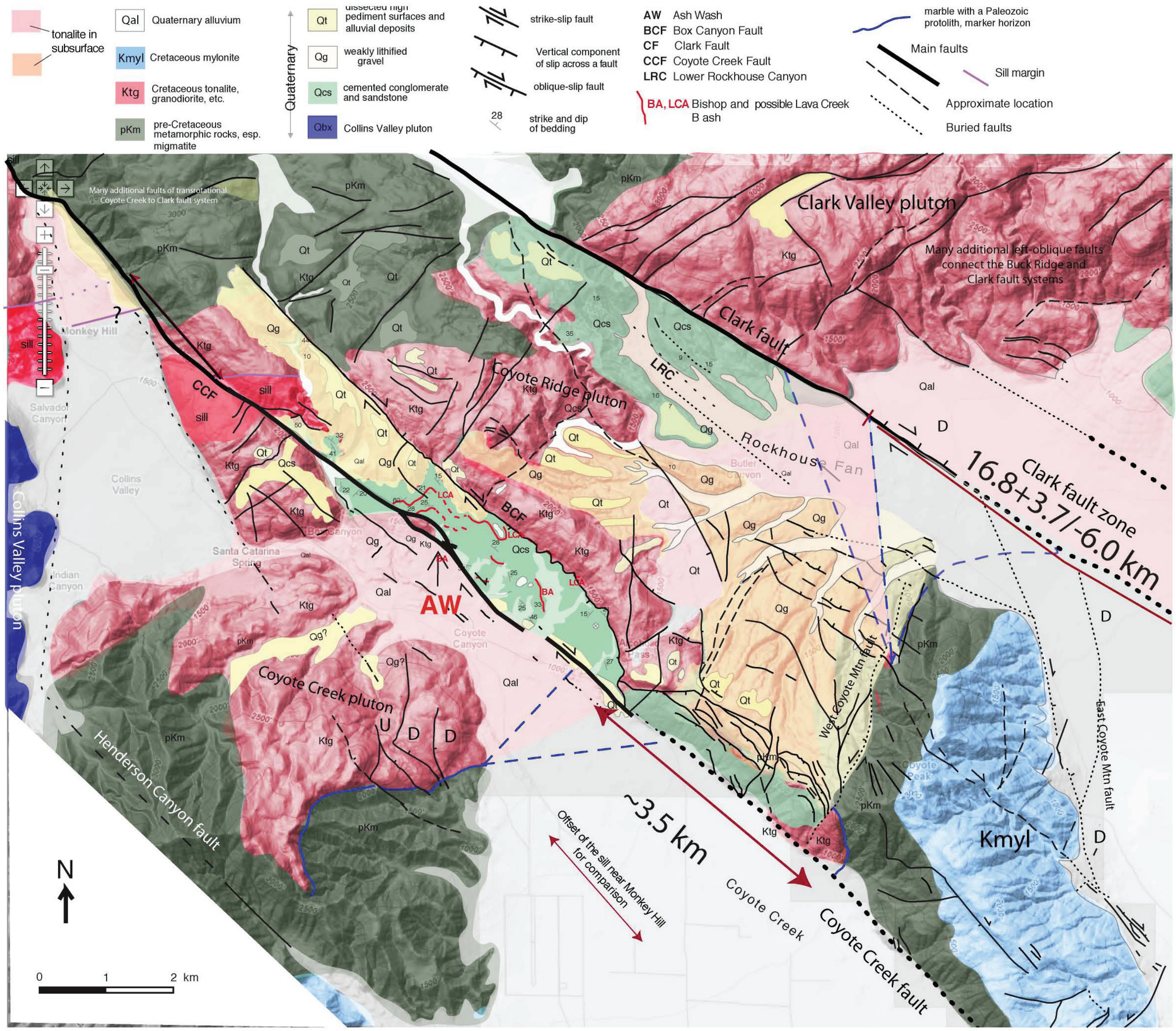

Figure 5. Geologic map of the Coyote Mountain area showing 3.5 ± 1.3 right slip across the Coyote Creek fault and marker succession and projections that define 16.8 km slip across the Clark fault. Mapping compiled from Sharp (1967), Dorsey (2002), and Forand (2010). Pink shading depicts inferred distribution of biotite-hornblende–bearing tonalite in the subsurface.

(Table 2; Figs. 4 and 5; Forand, 2010), 2.4 km more than the 14.4 km of Sharp (1967). This slip estimate has a large uncertainty due to the Quaternary cover between the bedrock marker succession and the Clark fault and the possible changes in the strike of the marker succession beneath the Quaternary deposits (Forand, 2010). We used Sharp's low slip value in our prior calculations of slip rate (Janecke et al., 2005a, 2005b, 2010), so those estimates should be updated to the new values reported here.

A southwest-down component of slip across the Santa Rosa segment of the Clark fault would decrease the right slip calculated from this separation by at most a few kilometers. We argue that this is a secondary and minor component of the total right separation across the Clark fault for several reasons. First, the Clark fault has both NE-up and SW-up scarps along the 25-km-long trace for which this measurement was made, and therefore does not show consistent SW-down motion since late Pleistocene (Sharp, 1972b; Belgarde and Janecke, 2007; Belgarde, 2007; this study). Second, the structural relief across the fault zone in the SE Santa Rosa Mountains is small relative to its dextral offset, because the same stratigraphic units are exposed NE and SW of the central main traces of the fault within the Cenozoic basin (Fig. 3; Dibblee, 1984; Bartholomew, 1970; Belgarde, 2007; Kirby et al., 2007). Third, the one focal mechanism of a moderate earthquake that nucleated on this part of the Clark fault zone shows dominant right slip and only ~5% dip slip (Sanders et al., 1986; Doser, 1990). The M 6.2 1954 Arroyo Salado earthquake (also known as the Salada Wash earthquake) had a slip vector raking either 5° ± 6° or 0° from horizontal (Sanders et al., 1986; Sanders, 1989; Doser, 1990). There were similar small to negligible dip-slip components of deformation evident in focal mechanisms from a handful of other moderate earthquakes that nucleated on the Clark fault nearby (Sanders and Kanamori, 1984). Fourth, a gravity gradient with consistent southwest-side down displacement suggests that at most ~20% dip-slip cumulative displacement (3 km versus 16.8 km) along the fault in Clark Lake Valley.

Right Slip across the Clark Fault Zone in Sedimentary Rocks

It is presently difficult to quantify the total surface slip across the Clark fault zone in the Salton basin since its inception because much of the offset is localized along bedding planes and is distributed across a myriad of small-displacement faults that span at least 18 km perpendicular to the fault zone (Figs. 2 and 3; Janecke et al., 2005a, 2005b; Belgarde and Janecke, 2006; Belgarde, 2007). In the SE San Felipe Hills, however, we have estimated a *minimum* slip amount since ca. 0.5 Ma based on analysis of folded Pleistocene sedimentary rocks (Kirby, 2005). Faults at the southeast tip of the Clark fault in the southeast San Felipe Hills do not cut the Pleistocene Ocotillo and Brawley formations at the surface, but instead slip is transferred to several domains of tight folds with up to 35% N-S shortening (domains A–D in Fig. 6; Heitman, 2002; Lilly, 2003; Kirby, 2005; Kirby et al., 2007; Belgarde, 2007). Some displacement may also transfer southwest to the Coyote Creek fault along several newly mapped sinistral faults SW of the Powerline fault (Fig. 3). These left-lateral faults cut Pleistocene pediment deposits, have degraded scarps along contractional and extensional parts of their traces, and produce barriers to groundwater that are reflected in vegetation lineaments and contrasting soil moisture (Janecke, unpublished mapping, 2007).

Folding strains in the SE part of the Clark fault zone, in the Tarantula Wash structural segment, are localized east of each fault tip and north of the inferred subsurface intersection between the Clark and Extra fault zones (Figs. 3 and 6). The folds likely formed from the transformation of dextral slip into N-S shortening as the Clark fault strands die out to the SE at the surface (Fig. 6) (Feragen, 1986; Wells and Feragen, 1987; Heitman, 2002; Lilly, 2003; Kirby, 2005; Kirby et al., 2007). Some additional shortening and reorientation of fold axes occurred where SE-moving fault blocks NE of the Clark fault strands impinge against the crossing Extra fault zone. Folding strains are much higher adjacent to the tips of dextral fault strands than elsewhere in the San Felipe Hills and domains B and C have the highest percent strains (20% and 35%, Fig. 6; Kirby, 2005; Belgarde, 2007).

Folding near the intersection of the Clark and the Extra fault zones produced a total of at least 3 km of north-south shortening in SE of the tip of three central principal strands of the Clark fault zone in the Tarantula Wash segment (Fig. 6) (Kirby, 2005; Belgarde, 2007). Making simple geometric assumptions about the relationship between folding and the SE tip of the right-lateral strike-slip fault zones in the Tarantula Wash segment of the Clark fault (e.g., Wells, 1987) (Fig. 6), we calculate that this folding strain was produced by 5.6 ± 0.4 km of right slip across this part of the Clark fault zone (Table 2; Kirby, 2005). This estimate is a minimum because right slip on the other two principal fault strands was not included, some strain may be transferred to the SW onto the Coyote Creek fault instead of being transferred into the folds, and some dextral strain could be blind beneath fault zone. In particular, fairly substantial folding strains in domain A, east of the SE tip of the San Felipe Hills fault (Fig. 6), are not included in our analysis because that domain shortened over a protracted period of time, and we cannot separate the strain of the paleo–San Felipe anticline (early to middle Pleistocene) from strains produced east of the SE tip of the younger cross-cutting San Felipe Hills strand of the Clark fault (middle Pleistocene to Holocene). Gravity data suggest as much as 2 km of right separation of the basement-cover contact on the north flank of the San Felipe anticline across the San Felipe Hills fault (Fig. 7).

The absence of growth strata across the crest and troughs of the closely spaced folds in the Tarantula Wash segment of the Clark fault zone shows that the closely spaced folds must postdate all the deformed strata there except for the much younger pediment deposits, strath terraces, and Lake Cahuilla sediment (Reitz, 1977; Kirby, 2005; Belgarde, 2007). The youngest deformed unit, the Brawley Formation, forms an arcuate outcrop belt along the edges of the Tarantula Wash segment of the Clark fault. This makes the folds younger than the youngest Brawley Formation (ca. 0.5–0.6 Ma, see below) (Kirby, 2005). The closely spaced

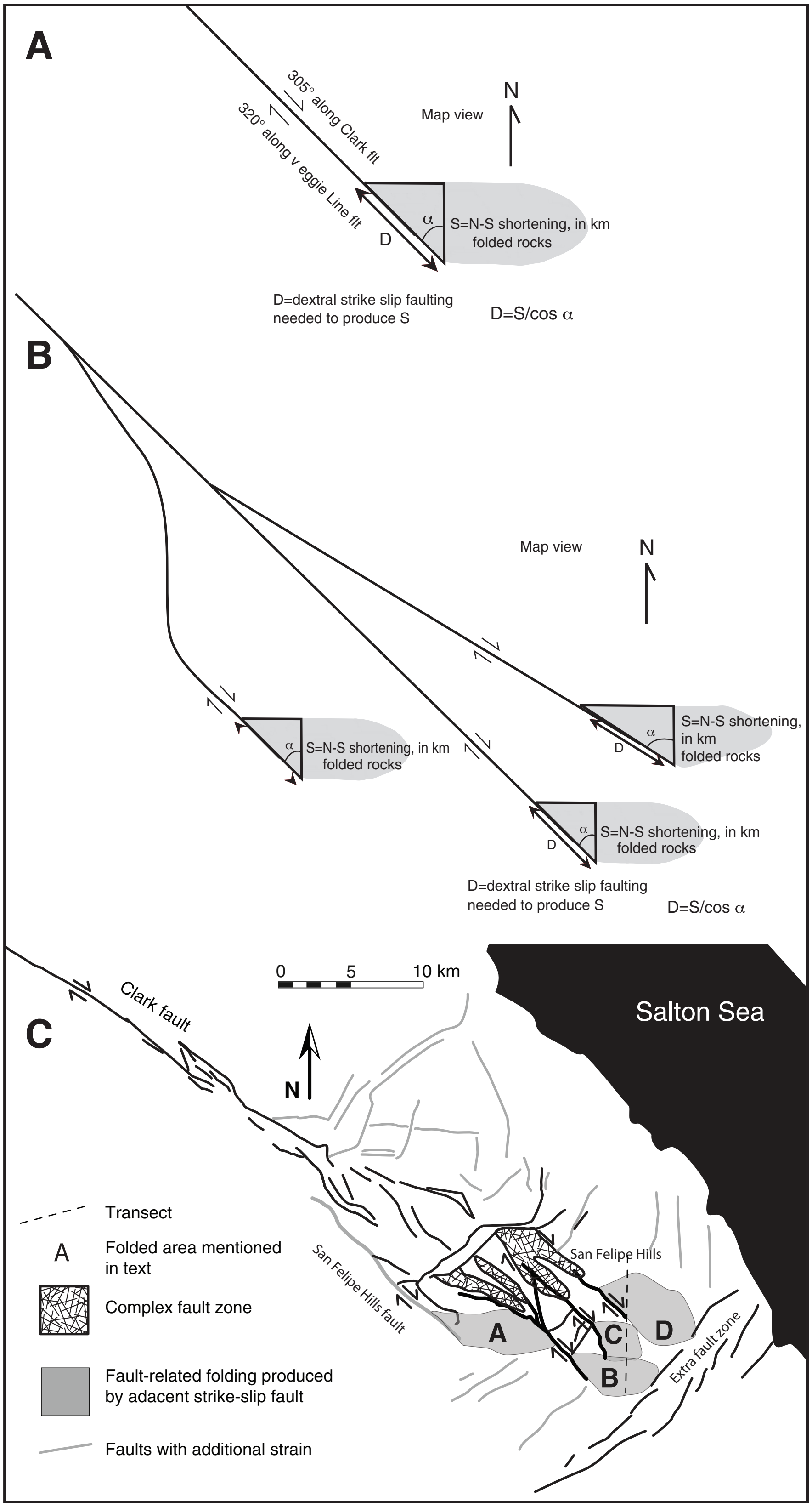

Figure 6. (A) Method for calculating the slip across a strike-slip fault from the shortening (S) in the folds at its tip. (B) Modification of the method for diverging fault strands. (C) Simplified relationships along the Clark fault zone emphasizing folding in the SE San Felipe Hills. Four fault strands terminate in folded domains near their SE tips. Our transect quantifies strain in domains (B), (C), and (D). See the text for discussion of domain (A) and the San Felipe Hills fault. Table 2 does not quantify the strain associated with gray faults.

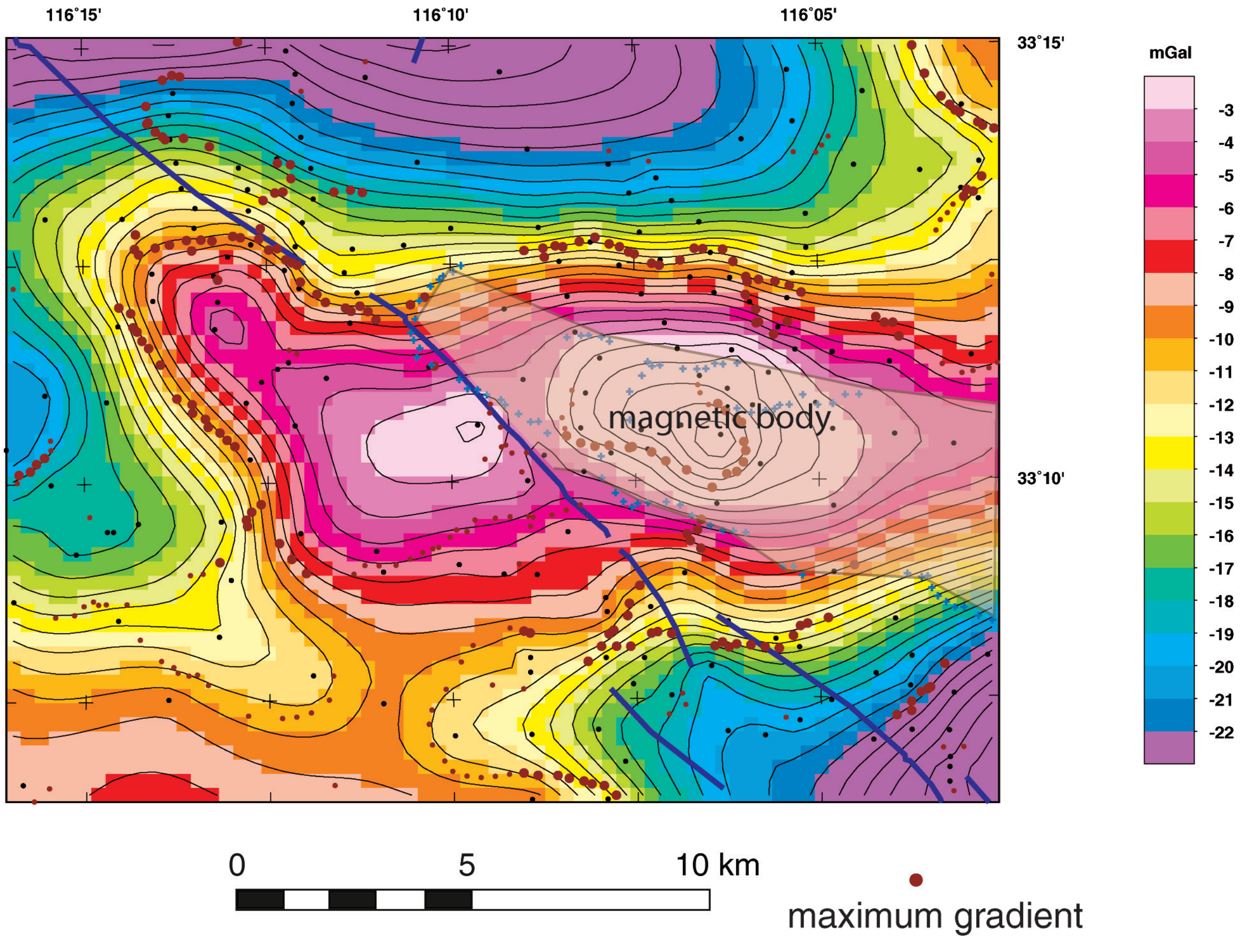

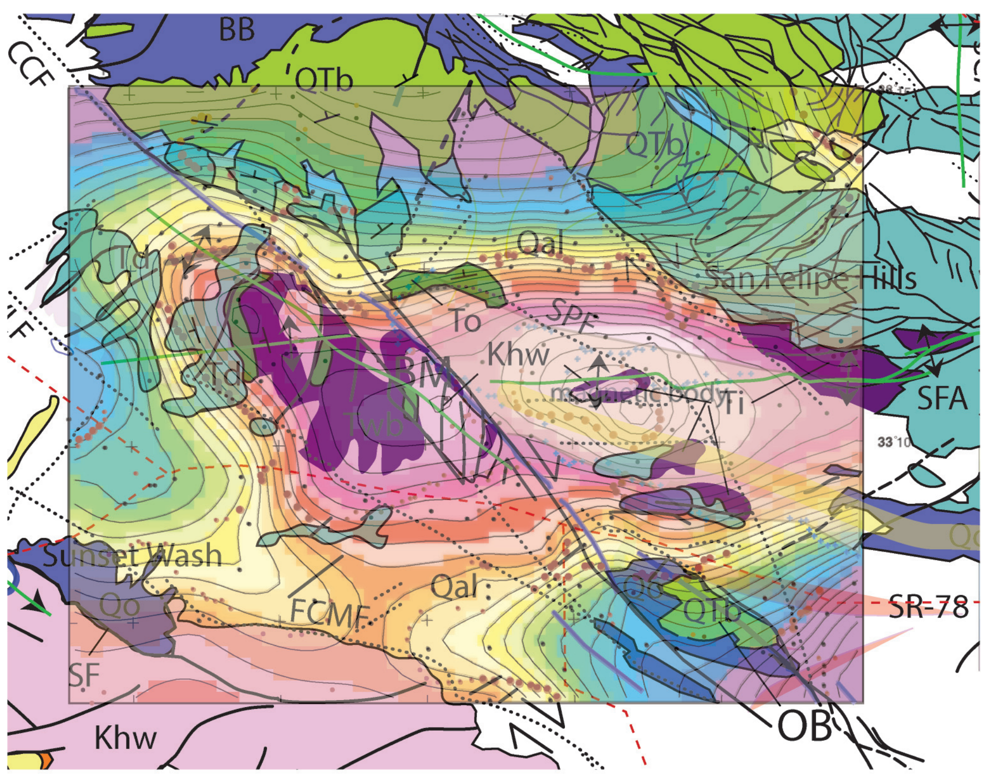

Figure 7. Residual isostatic gravity map of the San Felipe anticline where the Coyote Creek and San Felipe Hills faults cross it. Brown dots show the locations of maximum horizontal gravity gradients. Black dots are gravity measurements. Blue crosses show edges of magnetic body, which produces a magnetic high on the east side of the Coyote Creek fault. The lower figure shows the correspondence between the gravity field and mapped structures in Figure 3.

folds may still be active, but if they are active, they must be forming so slowly that they do not obviously fold the overlying patchy late Pleistocene to Holocene deposits.

We dated five samples from the highest widespread pediment-related deposits around the southern Santa Rosa Mountains using optically stimulated luminescence (OSL) in order to provide some constraint on the age of folding in this area (Table 3). All of these exposures belong to a group of fairly thin deposits that were correlated to the Font's Point sandstone in the Borrego Badlands and estimated to be ca. 0.5 Ma (Ryter, 2002; Lutz et al., 2006). The OSL ages range from ca. 22 to 62 ka and thus indicate a late Pleistocene age of the pediment-capping deposits with no obvious time-space pattern from east to west (Table 3). Each pediment deposit lies in angular unconformity on tilted and folded Pliocene to Pleistocene sedimentary rocks within the Clark fault zone (Dibblee, 1984; Bartholomew, 1970; Pettinga, 1991; Belgarde and Janecke, 2006; Belgarde, 2007; Weismeyer, 1968). The discordance beneath the pediment-related deposits is typically 20°–30° but locally up to 90°. Undated higher and older pediment-related deposits are up to ~75 m above active washes (Belgarde, 2007). Field relationships, sedimentological similarities to strath terraces in the study area, and the wide range of ages from pediment-capping deposits that were collected in roughly similar positions beneath the highest widespread pediment surface, show that the pediment-capping deposits are ancient strath terraces formed in the beds of downcutting streams, and do not represent remnants of once laterally continuous bench pediments. From these data alone we cannot determine whether the folds are still active.

Coyote Creek Fault Zone

Displacement near Coyote Mountain

We carried out new mapping and analysis along two parts of the Coyote Creek fault zone for this study and developed two estimates of right slip. Mapping on either side of the Coyote Ridge segment (CRS, Figs. 2B and 5) utilizes the southern and eastern contact of a distinctive biotite- and hornblende-bearing tonalite (the Coyote Creek, Coyote Ridge, and Clark Valley plutons of Sharp, 1967, Fig. 5) and its enclosing, concordant, marker succession of metasedimentary rock and mylonite. The metasedimentary rocks include a marble marker bed several meters thick located a few to tens of meters SE and E of the southern and eastern contact of the pluton, adjacent biotite-rich migmatite up to 2–3 km thick, and a capping mylonite several kilometers thick where plutonic rocks are present (Fig. 5).

Prior estimates of 4.8 km (Sharp, 1967; Bartholomew, 1970) and 6 km (Dorsey, 2002) of right slip across the main trace of the Coyote Creek fault along the Coyote Ridge segment are too high in part because they used the western base of the Eastern Peninsular Ranges mylonite zone as a strain marker (CRS, Fig. 2; Janecke et al., 2005a). Field relationships show that the western edge of the Eastern Peninsular Ranges mylonite zone is not a reliable marker unit for displacements because this feature has

TABLE 3A. OPTICALLY STIMULATED LUMINESCENCE (OSL) AGE OF BASAL DEPOSITS WITHIN A PEDIMENT

Sample no.	USU no.	Location	Deposit type	Number of aliquots*	Dose rate (Gy/ka)	De, Gy (SD)	OSL age (cal ka)
ST-1-BB	USU-222	Salada Arroyo pediment, Qao	Base of pediment	21 (30)	3.00 ± 0.14	92.11 ± 23.70	30.71 ± 2.34
ST-2-BB	USU-223	North Fork Arroyo, W Tower pediment	Base of pediment	20 (20)	3.04 ± 0.14	55.96 ± 5.56	18.40 ± 1.02
ST-3-BB	USU-224	NE side of Tower pediment	Base of pediment	23 (25)	2.91 ± 0.13	143.14 ± 23.22	49.27 ± 2.98
ST-4-BB	USU-225	Palo Verde Wash pediment	Base of pediment	23 (29)	2.64 ± 0.12	132.71 ± 27.21	50.28 ± 3.36
ST-5-BB	USU-226	Tower pediment easternmost sample	Base of pediment	20 (25)	2.69 ± 0.12	167.41 ± 30.70	62.26 ± 4.05

*Number of aliquots used for age calculation and number of aliquots measured in parentheses.

TABLE 3B. DOSE RATE INFORMATION

Sample no.	USU no.	Depth (m)	H_2O (%)*	Latitude/longitude	Cosmic (Gy/ka)	K_2O (%)	Rb_2O (ppm)	Th (ppm)	U (ppm)
ST-1-BB	USU-222	12.0	3.0	N33.275, W116.127	0.04	2.35 ± 0.06	99.5 ± 4.0	9.3 ± 0.8	1.9 ± 0.1
ST-2-BB	USU-223	2.5	3.0	N33.279, W116.107	0.14	2.32 ± 0.06	103.6 ± 4.1	8.8 ± 0.8	1.9 ± 0.1
ST-3-BB	USU-224	3.0	3.0	N33.279, W116.068	0.13	2.13 ± 0.13	90.5 ± 3.6	8.9 ± 0.8	2.0 ± 0.1
ST-4-BB	USU-225	15.0	3.0	N33.288, W116.171	0.03	2.11 ± 0.05	88.1 ± 3.5	7.0 ± 0.6	1.9 ± 0.1
ST-5-BB	USU-226	3.0	3.0	N33.275, W116.051	0.13	2.08 ± 0.05	80.3 ± 3.2	7.0 ± 0.6	1.8 ± 0.1

*In situ water content, dry when measured in lab, assumed 3 ± 3% as representative of burial history. Error on De is 1 standard deviation (SD). Error on age includes random and systematic errors calculated in quadrature. Age analysis using the single-aliquot regenerative-dose (SAR) procedure of Murray and Wintle (2000) on 90–150 µm quartz sand using 2-mm aliquots.

gradational and variable margins that include interleaved strongly sheared and weakly sheared rocks. On the southwest side of the Coyote Creek fault, the distinctive bedrock marker succession strikes N91° W and dips 84° S (α_{95} = 10.7; N = 7), and the attitude of the pluton margin and the enclosing metamorphic rocks are very similar over a trace length of at least 2 km, except where north-striking faults displace the contact (Fig. 5). The metamorphic wall rocks envelope the biotite-hornblende–bearing tonalite pluton. This smooth and regular geometry is expected in the wall rocks of mesozonal to catazonal plutons, like the Coyote Creek pluton, that were emplaced into migmatitic country rock under upper amphibolite facies conditions (Buddington, 1959; Theodore, 1967, 1970; Sharp, 1967).

On the northeast side of the Coyote Creek fault, the marble, migmatite bodies and their foliations strike N50° E and dip 42° SE (α_{95} = 10°; N = 6) in their closest exposures to the fault (within 0.5 km from the buried fault trace). About 0.5 km farther north the migmatite adjacent to the pluton strikes north and then north-northwest and dips between 55° and 65° ENE (Theodore and Sharp, 1975). Still farther north, the NNW strike of the pluton wall and its adjacent metamorphic and mylonitic rocks persists northward through Coyote Mountain with a fairly uniform strike (Theodore and Sharp, 1975). Smaller offset dextral faults between the Coyote Creek and Clark fault displace the marker succession right laterally between 1 and 2.5 km (Forand, 2010). Although these faults are shown in Figure 5, they were not added to the displacement estimate in Table 2 because our analysis is incomplete. Altogether the mapping, field, and structural data indicate that the pluton margin and wall rocks are steep, smooth, and gently curving where the Coyote Creek fault cuts across them, and all lithologic units have a moderate to steep dip with a concave NW surface trace.

No correction for elevation was applied because exposures of the marble marker bed are at the same elevation (~300 m) where they are closest to the fault on the NE and SW side of the Coyote Creek fault zone. By bracketing the range of plausible trends of bedrock fabrics across the covered area, the dextral separation across the Coyote Creek fault is bracketed between 2.2 and 4.8 km (3.5 ± 1.3 km) with two preferred estimates of ~2.8 and 4.3 km. One preferred estimate (~2.8 km) was measured by projecting each thin marble layer to the fault using the average attitude in nearby exposures and by inferring that the concave NW bend was located at the Coyote Creek fault. The ~4.3 km estimate of right slip is based on projecting the marble layer assuming that the bend is located halfway between the two offset exposures and therefore ~1 km SW of the Coyote Creek fault (Fig. 5).

Strike-slip displacement produced most of the right separation of these units because the marker marble, the contact of the pluton, and the foliation in the migmatites are moderately dipping to vertical near the fault zone. Therefore vertical displacements produce little right-lateral separation of these steep units and have almost no effect on our estimate of right-lateral slip. Off-fault damage might increase this estimate of displacement so this estimate refers to slip across the central main traces of the fault zone and does not include any displacement in the adjacent damage zone or from the newly mapped faults within Coyote Mountain between the Clark and Coyote Creek fault (Forand, 2010). Offset linear markers are not available to provide an unequivocal slip estimate, but slip may be in the 1–2 km range.

The Coyote Creek fault probably has some SW-side-down slip near Coyote Mountain because restoring the right separation on the offset marker succession to its pre-fault position does not restore all of the relief across the fault zone at Coyote Mountain (Sharp, 1967; Dorsey, 2002). Examination of precisely relocated earthquake hypocenters (Lin et al., 2007) shows that the Coyote Creek fault, like almost all of the strands of the San Jacinto fault zone, dips steeply NE (Sanders, 1989; Belgarde, 2007; Janecke and Belgarde, 2008). Hundreds of meters of SW-facing relief remain after restoration of fault offset, and crystalline rocks on the NE side of the fault restore opposite basin fill on the southwest. It is unclear how much of this relief is due to SW-down slip across the Coyote Creek fault and how much is the result of vertical components of slip on the East and West Coyote Creek faults nearby. Based on the minimum throw of a pediment surface west of the West Coyote Mountain fault and northeast of the main trace(s) of the Coyote Creek fault, we estimate the vertical component of slip to be as much as 365 m. This is the relief between the pediment surface NE of the Coyote Creek fault and the alluviated surface of Upper Borrego Valley SW of the fault. Approximately 350 m of vertical slip reduces the right slip by 35–420 m, and supports the interpretation that the vertical component of displacement across the Coyote Creek fault is much smaller than the ~3.5 ± 1.3 km horizontal component. The presence of the early to middle Ocotillo Formation units on both sides of the fault, 2–6 km to the SE, along the Borrego Badlands segment of the fault, further supports our estimated magnitude of vertical slip because significant (>200 m, using data in Lutz, 2005) vertical slip would expose older units on the uplifted side of the fault (Sharp, 1967; Sharp, 1972a, 1972b; Sharp and Clark, 1972; this study; Figs. 2B and 3).

Sharp (1967) mapped a distinctive steeply dipping sill on opposite sides of the Coyote Creek fault near Monkey Hills (<10 km NW of our displacement site) that has 2.3 km of right separation (see upper left corner of Fig. 5). This low value represents displacement across both the main Coyote Creek fault and the inferred northward continuation of the Veggie Line–Henderson Canyon faults, and indicates that displacement across the Coyote Creek fault decreases along strike to the NW.

Displacement near Borrego Mountain

Mapping near Borrego Mountain (Figs. 2B and 8; BMS) suggests that the two main fault traces of the Coyote Creek in that area fault have less right separation than they do along the Coyote Ridge segment at Coyote Mountain (Steely, 2006). The Coyote Creek fault in the Borrego Badlands and Borrego Mountain segments is probably ~0.3–0.5 m.y. younger than it is in the Coyote Ridge segment (Lutz et al., 2006; see below). In this area two independent methods constrain the right slip across the Coyote Creek

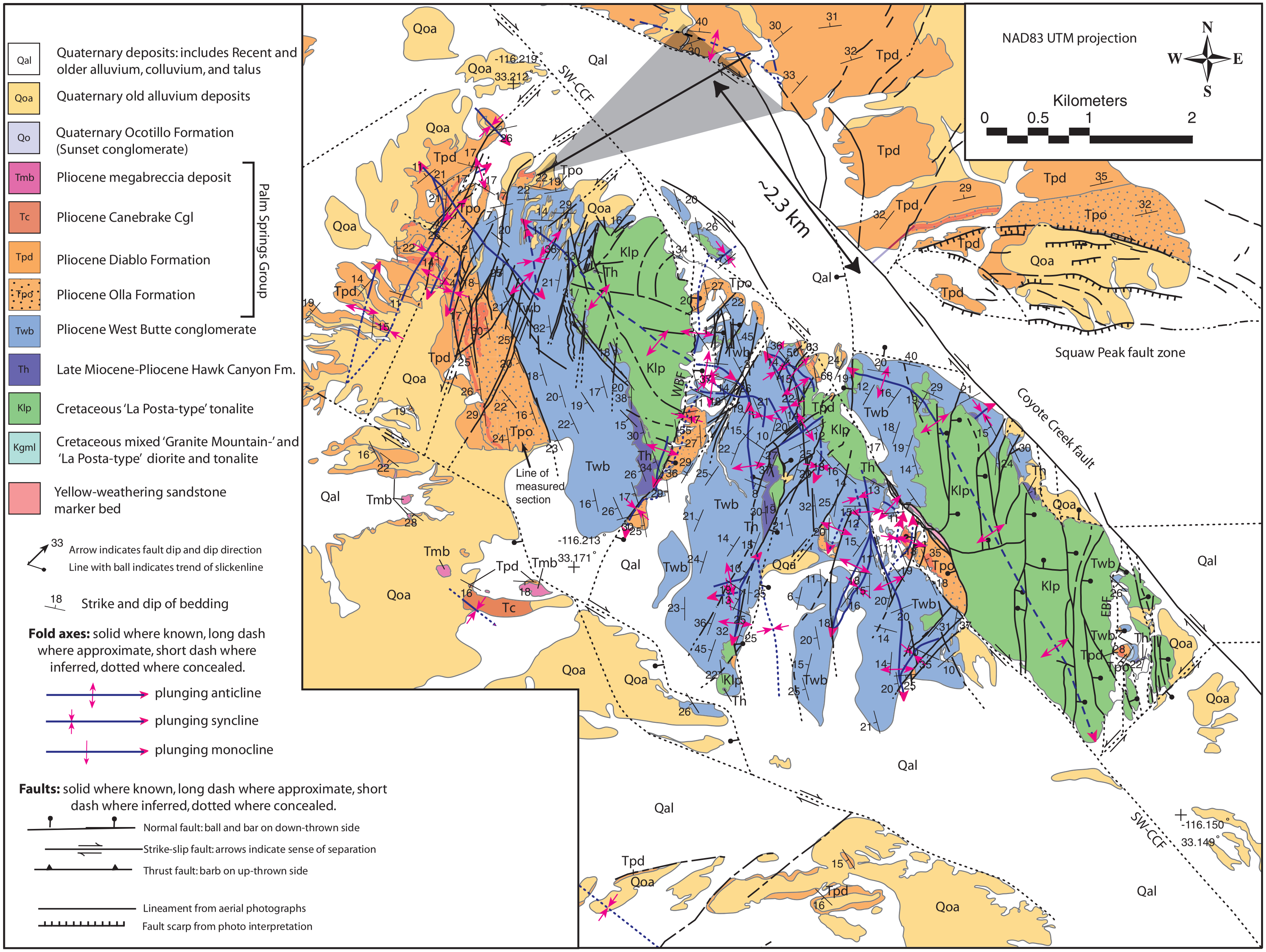

Figure 8. Geologic map of Borrego Mountain area showing the distinctive yellow-weathering sandstone bed on the NE and SW side of the Coyote Creek fault. Modified from Steely (2006).

fault to at most a few kilometers. A distinctive, broadly folded, yellow-weathering sandstone bed in the Pliocene Palm Spring Group lies just below the contact between the Olla and Diablo formations and is displaced ~2.3 ± 0.7 km across both major strands of the Coyote Creek fault (Fig. 8). Key features of the sandstone include its unusually large thickness, well-cemented character, distinctive 1–2 cm poorly lithified concretions, position in the stratigraphy, and weathering color. The range of possible separations varies with the strike of bedding used to project the marker bed across ~3 km of alluvium (Fig. 8). Detailed mapping shows only one marker bed to be present in the Pliocene stratigraphy on the southwest side of the fault and reconnaissance mapping on the NE side revealed one correlative bed. Faulting complicates the geology on the NE side of the fault and removed most of the units stratigraphically below the marker bed.

The topography and geology in the Borrego Mountain area and the NE-side down component of slip documented during the 1968 Borrego Mountain earthquake near the offset marker bed (Clark, 1972) suggest that some of the right separation of the north-dipping marker is due to a NE-down vertical component of slip. Therefore, the right slip must be somewhat less than the ~2.3 ± 0.7 km of right separation of the planar marker bed.

Gravity data provide some additional constraints on the displacement across the Coyote Creek fault because the Borrego Mountain segment of the Coyote Creek fault displaces the early Pleistocene San Felipe anticline (Kirby et al., 2007). Basement in the core of the San Felipe anticline produces a strong gravity high with an overall E-W trend (Fig. 7). Maximum horizontal gravity gradients along the northern and southern limbs of the anticline suggest ~2.3 and 2.8 km of right-lateral separation, if they reflect a steep, moderately to steeply dipping basement contact on the dipping limbs of the San Felipe anticline. Bedding dips in this area rarely exceed 40° (Fig. 8), however, and Janecke interprets the steep gravity gradients as locations of younger steep faults that displace a gently dipping basement-cover contact. Interpretations of the gravity data are further complicated by the presence of at least three generations of faults and folds in this area and the possibility of buried faults, The oldest complicating structure is a NW-trending Pliocene anticline with >400 m of structural relief near Borrego Mountain that formed SW of the future Coyote Creek fault (Steely, 2006). The west end of the younger early Pleistocene San Felipe anticline refolded the older Pliocene Borrego Mountain anticline at Borrego Mountain producing a highly faulted elongate dome. Faults adjacent to the Coyote Creek fault and the northeastward continuation (?) of the late Miocene to Pliocene Vallecito Frontal fault (Fig. 3) also may also have produced gradients in the gravity and magnetic field near Borrego Mountain (Fig. 7).

The early Pleistocene crest of the San Felipe anticline is likely the most robust offset marker of strain across the Coyote Creek fault zone because the hinge is a line that constrains true offset across the fault. The planar north- and south-dipping limbs of the anticline provide separations that are less robust estimates of slip because there is ambiguity regarding vertical displacements whenever planar features are offset. Gravity gradients, however, locate moderately to steeply dipping density contrasts (Grauch and Cordell, 1987), and gravity data are not as effective at defining the locations of a relatively flat and horizontal density contact at the hingeline of the anticline.

Gravity data clearly rule out a large lateral displacement (>3.5–5 km) but are ambiguous about the magnitude of right slip near Borrego Mountain (Fig. 8). The E-W–trending peak of the gravity high, which we interpret as the crest of the Pleistocene San Felipe anticline, shows little right or left separation. An estimate of separation based on gravity in this area awaits additional gravity measurements on the southwest side of the Coyote Creek fault.

Magnetic anomalies are not useful for identifying displacements because the NE side of the Coyote Creek fault has relatively magnetic rocks that are absent on the SW side (Fig. 7). The absence of its offset equivalent suggests that the Borrego Mountain segment of the Coyote Creek fault localized along the NE margin of a less magnetic La Posta–type pluton and its more magnetic country rock. Closely spaced pegmatite-aplite dikes in the tonalite at Borrego Mountain occur in the border phase of the La Posta–type pluton in the San Isidro Mountains, farther west (Holk et al., 2006). The absence of an offset magnetic anomaly on the southwest side of the fault may also be related to a much older (pre–Peninsular Ranges batholith) history of the San Jacinto fault as suggested by geophysical and isotopic data to the northwest (Langenheim et al., 2004).

The overlap between the geologic data (2.3 ± 0.7 km of right slip) and the geophysical analysis (~2.3–2.8 km) shows that the large displacements of the Clark fault zone are not present along the Coyote Creek fault. We use the geologic estimate (2.3 ± 0.7 km) as our preferred estimate to calculate slip rates in Table 2 because the geophysical estimates are too uncertain.

Geologic mapping suggests that the small slip deficit at Borrego Mountain (1–2 km) relative to the Coyote Ridge segment cannot be due to undetected dextral strike-slip faults near the main strand of the Coyote Creek fault near Borrego Mountain (Figs. 3 and 8) (Steely, 2006; Steely et al., 2009). We considered the possibility that additional slip may be localized on two newly identified but poorly exposed dextral faults located ~4 km NE and 5–7 km SW of the main strand of the Coyote Creek fault in the Borrego Mountain area (Fig. 3, the Squaw Peak and Veggie Line faults), but this is unlikely because these two faults have branch points NW and SE of the displaced yellow-weathering marker bed, respectively (Figs. 3 and 8). The offset marker lies in an area where neither adjacent fault can add strain to the Coyote Creek fault zone.

The Squaw Peak fault (SPF, Fig. 3) branches east from the main strand of the Coyote Creek fault ~1.5 km southeast of a major restraining bend in the Coyote Creek fault. It curves to the southeast for ~15 km and reconnects to the main trace of the Coyote Creek fault in the SE Ocotillo Badlands. Much of the fault is covered, but its existence is documented by faulted pediment-related deposits along its NW end, microseismicity downdip of its surface trace (Belgarde, 2007), and uplift of late

Cenozoic sedimentary rocks on its W side. A gravity gradient and the western 8 km of the northern edge of a magnetic body coincide with the NW part of the Squaw Peak fault (Fig. 7).

The main shock of the 1968 Borrego Mountain earthquake nucleated 3 km northeast of the Borrego Mountain segment of the Coyote Creek fault within the Squaw Peak fault zone (Fig. 3; Allen and Nordquist, 1972; Sharp and Clark, 1972). Aftershocks of this earthquake and microseismicity that continues today form a steeply NE-dipping plane beneath the trace of the Squaw Peak fault at 8–12 km depth (Hamilton, 1972; Shearer et al., 2005; Janecke and Belgarde, 2008). This correlation confirms that the Squaw Peak fault exists in this area, is active, and penetrates to the base of the seismogenic crust at 12 km. Overall, the Squaw Peak fault is an oblique-dextral fault with a SW- and W-up component of slip that exhumed hills and faulted and folded basin fill and basement between the main trace of the Coyote Creek fault and the Squaw Peak fault. Several E-W–striking strike-slip faults connect the Coyote Creek fault and the Squaw Peak fault and form a fault array of E-striking strike-slip faults connecting between master NNW-striking dextral faults (Sharp, 1972b; Kirby, 2005; Steely, 2006; Steely et al., 2009).

The second newly identified fault within the Coyote Creek fault system is the Veggie Line fault that lies southwest of the main strands of the Coyote Creek fault and west of Borrego Mountain (Figs. 3 and 8; Steely et al., 2009). The name of the Veggie Line fault is based on NW-trending vegetation lineaments in the Borrego Sink area that appear to coincide with its trace(s). It strikes ~320°.

This NW-striking strike-slip fault is mostly covered by unfaulted alluvium, but it is well expressed geomorphologically and in the gravity and magnetic fields (Steely, 2006). A gravity gradient along the Veggie Line fault is consistent with a SW-down component of slip across it, and the magnetic field shows a slight 2–3 nanoTesla magnetic high along its trace (Steely, 2006).

The Veggie Line fault bounds the SW margin of a dozen active northeast-trending folds and small thrust faults in the Borrego Sink fold belt (Figs. 2 and 3; Dibblee, 1984; Ryter, 2002; Steely et al., 2009; this study). This fold belt is ~2.5–3 km wide along the structural grain and ~5 km long across strike. Deformation affects the Diablo Formation and overlying middle Pleistocene to Holocene surficial deposits, and some of the oblique-thrust faults preserve scarps. Elongate ridges with relief of up to 20–30 m coincide with the active fault-cored folds (Dibblee, 1984; Ryter, 2002). The NE-striking faults in the fold belt define the rungs of a ladder-like fault mesh between the master Coyote Creek fault in the NE and the master Veggie Line fault in the SW (Figs. 3 and 8).

Small earthquakes occur in the Borrego Sinks area (Shearer et al., 2005) and Quaternary fault scarps are present along thrust and strike-slip faults in the Borrego Sink fold belt (Ryter, 2002; this study). From this we infer that the Veggie Line fault currently transfers slip across the Borrego Sink fold belt to the adjacent traces of the Coyote Creek fault zone, as also inferred by Ryter (2002). It may also have been active in early to middle Pleistocene time (see below).

The Veggie Line fault has a trace at least 5 ± 1 km long SW of the Borrego Sink fold belt. Its NW continuation is uncertain NW of the Borrego Sink fold belt, but it probably continues NW along the same strike directly to the Henderson Canyon fault (Fig. 3). Engel and Schultejann (1984) mapped the Henderson Canyon dextral fault in reconnaissance, and we observe a minimum of 1–2 km of mismatch of rock types across its SE end (Janecke and Dorsey, unpublished mapping). Some of the strain of the Veggie Line fault probably transfers westward to the Hell Hole Canyon fault zone, and ultimately SW to the San Felipe fault zone. This transfer occurs across the large Tubb Canyon syncline and the small active out-of-syncline blind thrusts on the south flank of the syncline (Fig. 3; Steely, 2006).

The southeast tip of the Veggie Line fault (a master fault) coincides roughly with (1) the western end of the early to middle Pleistocene San Felipe anticline; (2) the southwest end of the SE-most fold of the Borrego Sink fold belt (connector faults); and (3) the NE end of a buried normal fault of a horsetail fan of faults (connector faults) emanating from the NW end of the Sunset dextral-oblique fault (a master fault) (Figs. 2B and 3) (Lutz et al., 2006; Steely, 2006; Kirby et al., 2007). These multiple linkages could reflect temporal changes in the connections between faults and/or the partitioning of slip southeastward from the Veggie Line fault onto more than one adjacent structure.

Including the Veggie Line and Squaw Peak faults widens the Coyote Creek fault zone from 0 to 2 km to ~8 km perpendicular to the local strike near Borrego Mountain (Figs. 2 and 3). Farther to the SE, beyond the Ocotillo Badlands, the Coyote Creek fault may return to the single-stranded geometry for ~20 km (Fig. 2) and then broadens again to encompass the Superstition Mountains and Superstition Hills faults. Mapping between the Ocotillo Badlands and Superstition Mountains, however, has documented a second fault ~4 km farther NE with an unknown displacement history (T.K. Rockwell and students, unpublished mapping, 2007). There are many significant structural changes along the strike of the Coyote Creek fault system, and many segments that have been mapped as narrow, single-stranded faults are composed of multiple active strands spaced up to 8 km apart (Kirby, 2005; Steely, 2006; Belgarde, 2007; this study).

San Felipe Fault Zone

Structural Geometry

The San Jacinto and Elsinore fault zones are commonly interpreted as the main dextral faults of the Peninsular Ranges, but the intervening San Felipe fault is another long and continuous fault (Dibblee, 1954, 1984; Todd, 1977, 2004; Lowman, 1980; Magistrale and Rockwell, 1996; Steely, 2006; Steely et al., 2009). More than 160 km long, the San Felipe fault has a sigmoidal map trace and projects toward the Elsinore fault in the northwest and the San Jacinto fault zone in the southeast (Fig. 1). In the NW this fault has also been called the Agua Caliente and Murrieta Hot Springs fault zones (Rogers, 1965). Most of the fault strikes more westerly than the San Andreas, San Jacinto, and Elsinore faults

(Fig. 2). Structural segment boundaries along the fault coincide with major bends, steps, and branch points and include a major 9-km-wide double left step and fault bend at Yaqui and Pinyon ridges (Fig. 9). The San Felipe fault steps left to the short Sunset fault and then steps to the ~30 km long Fish Creek Mountains fault (Figs. 2B and 9; Steely et al., 2009).

The Fish Creek Mountains fault bounds the northeast edge of the Vallecito and Fish Creek mountains (Figs. 2 and 3). These two mountain blocks separate the San Felipe–Borrego subbasin in the north (SFBB, Fig. 2A) from the Fish Creek–Vallecito subbasin in the south (FCVB, Fig. 2A) within the much larger Salton basin (Fig. 11). Little of the Fish Creek Mountains fault is exposed, but it must have a significant northeast-side-down slip component northeast of the Fish Creek Mountains in addition to an inferred dextral sense of displacement because it separates a sedimentary basin ~3 km deep estimated from gravity data (Biehler and Rothstein, 1979; Langenheim and Jachens, 1993) beneath Lower Borrego Valley from uplifted fault blocks with up to 1.9 km of topographic relief (Fig. 3). The magnitude of right slip across the Fish Creek Mountains fault is not known.

The San Felipe fault zone south of Pinyon and Yaqui ridges branches, steps, and connects to several adjacent structures. Overall the fault zone steps left ~9 km and consists of numerous short, en echelon strands that splay from a central, more easterly-striking fault zone (Figs. 2 and 3). This complex geometry makes it difficult to identify the central main strands of complex faults where continuous scarps are lacking. Most of the strain in the San Felipe fault zone transfers northeastward across the double contractional stepover to the Sunset fault and the Fish Creek Mountains fault (Fig. 2; Steely, 2006). Slip through this oblique left step resulted in uplift and deformation of syntectonic deposits shed from the fault zone during the first half of its development (Steely, 2006; Steely et al., 2009). Some strain also transfers south via cross faults toward subsidiary faults SE of the Earthquake Valley fault zone in an extensional stepover zone that connects to a still-active segment of the West Salton detachment fault on the northeast flank of Whale Peak (Fig. 2; Magistrale and Rockwell, 1996; Steely, 2006; Steely et al., 2009; Kairouz, 2005; Axen et al., 2006). Cross faults also connect the San Felipe fault zone northward to the Veggie Line–Henderson Canyon fault and San Felipe anticline.

Reconnaissance studies suggest that the San Felipe fault zone has been less active than the San Jacinto and Elsinore fault zones in the late Pleistocene and Holocene (Magistrale and Rockwell, 1996; Steely, 2006; Steely et al., 2009). It produces little microseismicity and has no documented Holocene ruptures (Shearer et al., 2005; U.S. Geological Survey Quaternary Fault and Fold Database, accessed 2008). Newly identified fault scarps are present along the Fish Creek Mountains and Sunset faults (Steely et al., 2009; this study), but the age of last slip is uncertain there. In contrast, two structural segments and several subsidiary faults of the San Felipe fault south of Yaqui Ridge and Pinyon Mountain ruptured in latest Pleistocene time and produced fault scarps ~5 m high (T. Rockwell, 2006, oral commun.; Steely, 2006). About 7 km of fault scarps are distributed across five strands of the San Felipe fault zone, including a fault scarp on an east-dipping fault on a connector fault along the west edge of Mescal Bajada (Steely, 2006; Steely et al., 2009; Axen, unpublished mapping, 2006).

The San Felipe fault zone has dominantly dextral offset with some vertical displacement in contractional and extensional segments. Slickenlines on the main fault trace near the boundary between the Pinyon Ridge and Mescal Bajada segments (Fig. 9) are subhorizontal and show that this vertical strand of the fault is dominantly a dextral fault (Steely et al., 2009). South-down fault scarps several meters high along the Pinyon Ridge segment of the fault and northeast-down scarps on north and northwest-striking fault splays south of the Mescal Bajada segment reflect some vertical displacements (Steely et al., 2009). Some of the right separation of the east-dipping markers is probably related to north-up reverse slip and folding north of the Pinyon Ridge and Mescal Bajada segments. Eastward the vertical component of displacement drops to zero in the Mescal Bajada segment, where cross sections disallow significant (<~0.3 km) vertical displacement across the Mescal Bajada segment farther east (Steely, 2006). Vertical separations are >600 m and NNE-side down across the Sunset fault (Steely et al., 2009).

Displacement

We estimate that the San Felipe fault zone at Pinyon and Yaqui ridges has between 4 and 12.4 km of right slip based on three separate measurements (Fig. 9). Because our three estimates measure slip in the same place—the Mescal, Bajada, and Pinyon Ridge fault segments—they should produce a similar result. The first estimate is based on correlation of the older folded West Salton detachment fault across the San Felipe fault zone. This fault is low angle and deformed by younger strike-slip faults. As a result there is large uncertainty in the estimate of right separation, which ranges from 6.5 to 12.4 km (Figs. 3 and 9; Steely 2006; G. Axen, unpublished data, 2006). South of the fault we project an overturned part of the detachment fault (Axen, unpublished mapping, 2006) across ~2–2.5 km of alluvium to the San Felipe fault trace. On the N side of the San Felipe fault zone the low-angle detachment is eroded at its cutoff point, but diagnostic altered and brecciated rocks in the damage zone closely constrain its original location (Fig. 9). Vertical displacements of a gently dipping surface can produce large right separations, but subhorizontal slickenlines from nearby exposures of the San Felipe fault, and negligible vertical motion across the Mescal Bajada segment of the San Felipe fault, suggest that the right separation is probably close to the right slip (Steely et al., 2009).

A second estimate of >4 km to 6.5 km right slip is based on the separation of the western base of the Eastern Peninsular mylonite zone across the fault (Fig. 9). This estimate has a few kilometers of uncertainty because the gradational base of the eastern Peninsular Ranges mylonite zone spans a considerable thickness of rock (>500 m; Sharp, 1979; this study). The

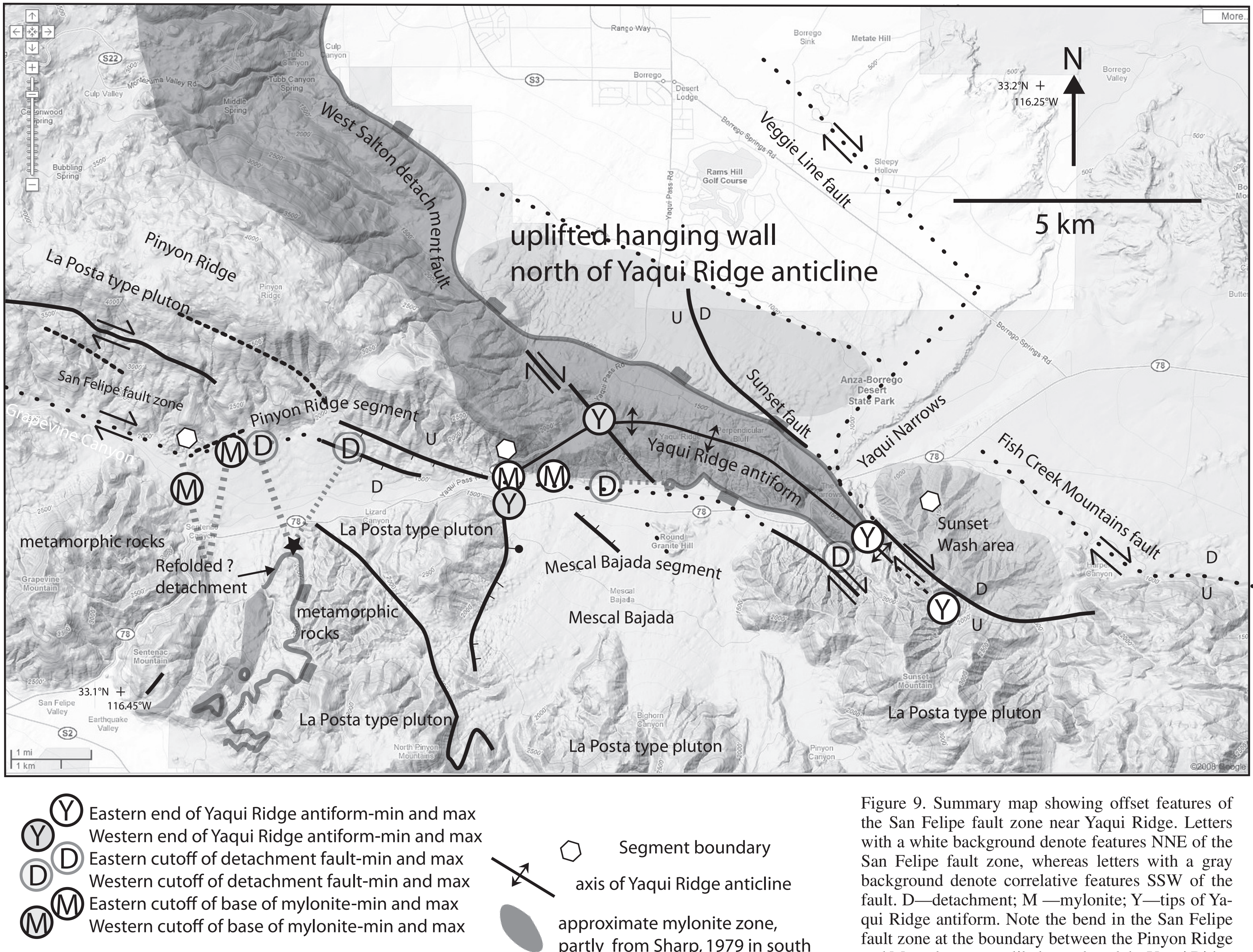

Figure 9. Summary map showing offset features of the San Felipe fault zone near Yaqui Ridge. Letters with a white background denote features NNE of the San Felipe fault zone, whereas letters with a gray background denote correlative features SSW of the fault. D—detachment; M —mylonite; Y—tips of Yaqui Ridge antiform. Note the bend in the San Felipe fault zone at the boundary between the Pinyon Ridge and Mescal segments likely produced the Yaqui Ridge fault-bend fold in the manner shown in Figure 10.

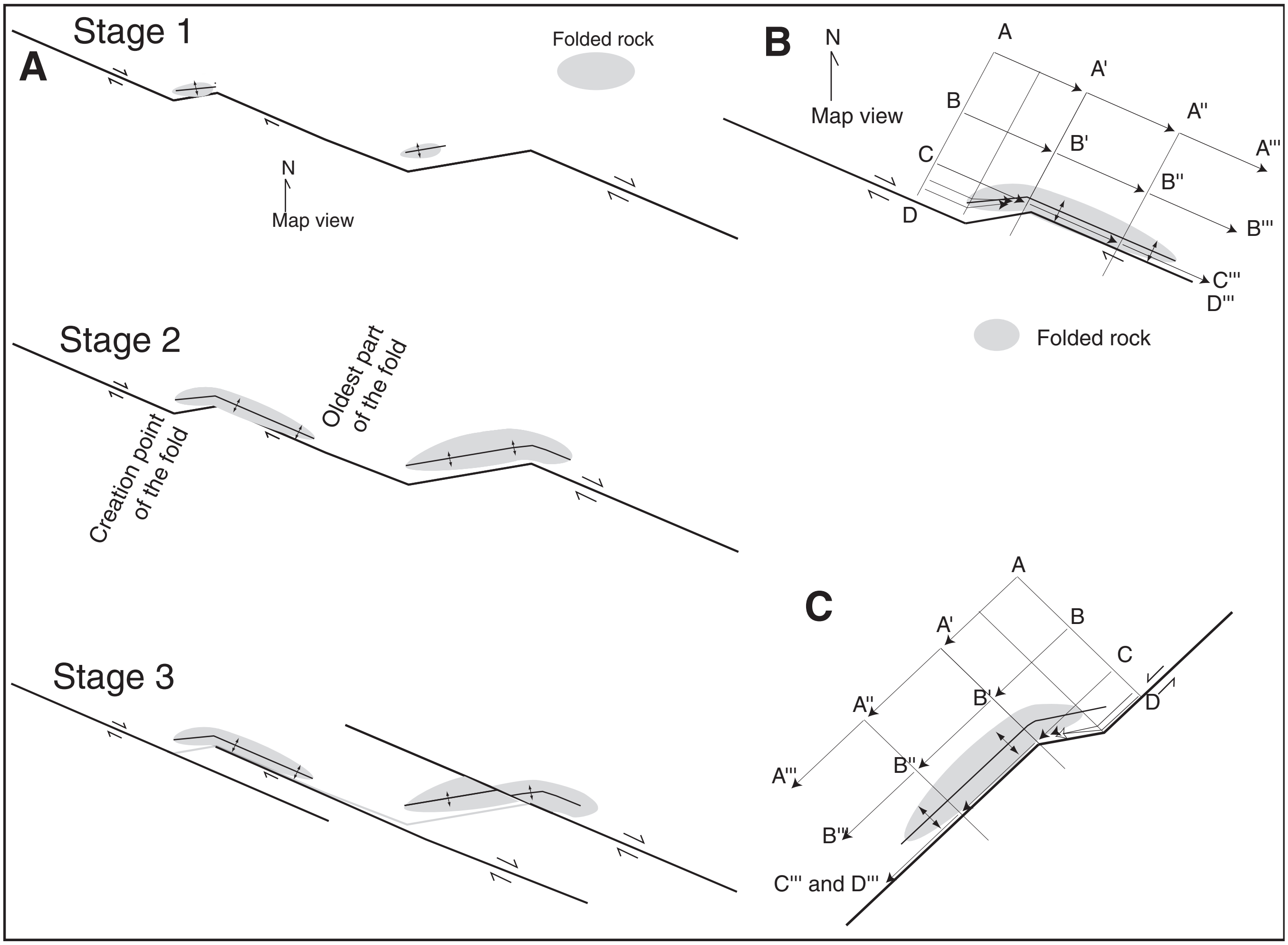

Figure 10. Conceptual model of strike-slip fault-bend folds showing how the length of the fold parallel to its hingeline is equivalent to the displacement past a bend in the adjacent fault. (A) illustrates the progressive evolution of folds adjacent to a smaller bend (left) and larger bend (right). Stage 1 to stage 3 showing how folds form parallel to strike-slip faults and shortening is proportional to the width of the steps in the fault zone (CD). Stage 1: Initiation of folds north of fault bends. Vertical faults are assumed in all models. Creation point of the fold is at the bend, and the youngest part of the fold is always located here. Stage 2: Folds grow as deforming north side of fault moves past the bend. Oldest part of the fold is translated lateral along the fault zone. Stage 3: Faults break to surface in en echelon pattern. Notice that the lengths of the folds parallel to their axis are identical, but the amount of shortening perpendicular to the strike-slip fault varies. Less shortening occurs adjacent to smaller perturbations. (B) and (C) define parameters along a right- and left-lateral fault-bend fold. (B) Right-lateral fault with a weaker NE side than SW side. Fold is shortened by distance CD. AD—shortening required to clear the left step; displacement past bend in fault—AA″; length of fault-bend fold—AA″; particle path—A to A′ to A″ to A‴; CD—magnitude of the left step across both bends; CD—shortening required to clear the left step; displacement past bend in fault—AA″. (C) Left-lateral fault with NW side that is weaker than SE side.

Figure 11. Paleogeographic map of the Ocotillo and Brawley formations during early slip across the San Felipe and San Jacinto fault zones (ca. 1 Ma). Slip has been accumulating on the new dextral faults for a few hundred thousand years and produced a closed local basin in the central Borrego Badlands, between adjacent fault-related uplifts. The outline of this basin coincides with the maximum extent of the mudstone lithofacies of the Ocotillo Formation from Lutz et al. (2006). The mudstone lithofacies records suspension settling of clay and silt in a low-energy, marshy palustrine or lacustrine environment punctuated by input of fine sand from fluvial, or possibly fluvial-deltaic distributary channels during river floods (Lutz, 2005). A bajada formed NE of the newly uplifted Fish Creek and Vallecito Mountains, and was formed from uplifted sediment and basement SW of the fault. Note that the triangular distribution of the finest deposits in the Borrego Badlands area (after Lutz et al., 2006) is predicted by this fault geometry. The Coyote Creek fault zone SE of Coyote Mountain (CM) did not form until after an additional reorganization ca. 0.6–0.5 Ma. Twelve kilometers were restored across Clark fault, and 2 km were restored across the Coyote Creek fault. Notice that these facies relationships, patterns of uplift and subsidence, paleocurrent directions, and locations of basin margins are well explained by an early Pleistocene inception of the faults and are difficult to explain with the alterative late Pliocene inception. For simplicity, there was no restoration of rocks SW of the San Felipe fault zone. Latitude and longitude marks apply to present locations of rocks on NE of Clark fault and SW of the Coyote Creek fault. BB—Borrego Badlands; BM—Borrego Mountain; CM—Coyote Mountain; CF—Clark fault; HVLF—Henderson–Veggie Line fault; OB—Ocotillo Badlands; OWW—Oil Well Wash; SP—Squaw Peak. Paleocurrents and facies from Lutz et al. (2006) (measured at black circles), Kirby et al. (2007), and Steely et al. (2009).

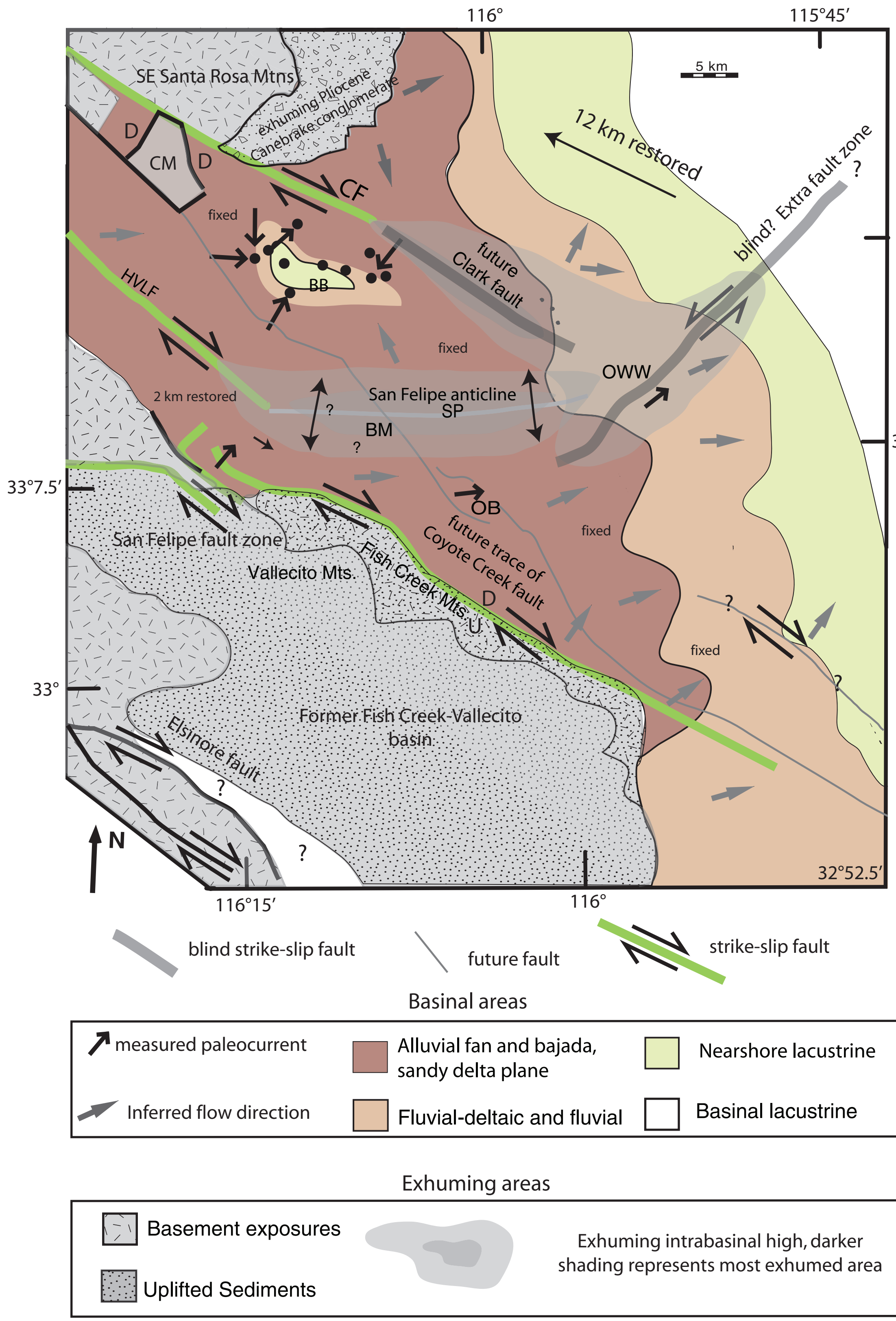

116°
115°45′
5 km
SE Santa Rosa Mtns
exhuming Pliocene Canebrake conglomerate
12 km restored
D
CM
D
CF
fixed
BB
future Clark fault
blind? Extra fault zone ?
33° 15′
HVLF
fixed
OWW
2 km restored
San Felipe anticline
SP
BM
?
33°7.5′
33°7.5′
OB
fixed
San Felipe fault zone
Vallecito Mts.
Fish Creek Mts.
future trace of Coyote Creek fault
D
U
?
fixed
?
33°
Former Fish Creek-Vallecito basin
Elsinore fault
?
?
N
116°15′
116°
32°52.5′
blind strike-slip fault
future fault
strike-slip fault
Basinal areas
measured paleocurrent
Inferred flow direction
Alluvial fan and bajada, sandy delta plane
Fluvial-deltaic and fluvial
Nearshore lacustrine
Basinal lacustrine
Exhuming areas
Basement exposures
Uplifted Sediments
Exhuming intrabasinal high, darker shading represents most exhumed area

mylonite zone is diffuse and variable in character, and has interleaved deformed and undeformed rocks, particularly where metasedimentary rocks are present.

A third estimate of right slip (6.4–9.5 km) interprets the fault-parallel Yaqui Ridge antiform as resulting from shortening north of a bend in the San Felipe fault at the boundary between the E-striking Mescal Bajada and WNW-striking Pinyon Ridge fault segments (Fig. 9). We infer that folding north of the Mescal Bajada segment results from the bend and contraction in the fault zone. If the Yaqui Ridge antiform is a fault-bend antiform, as we interpret, its length is directly related to the amount of right slip across the fault (Fig. 10; also discussed below).

The lengths of other fault-parallel anticlines that form by fault-bend folding in strike-slip fault zones can be directly related to the slip across the fault since creation of the fault bend (Fig. 10; Meisling and Weldon, 1989; Weldon et al., 1993; Kenney 1999; Kenney and Weldon, 1999; Morton, 1999; Kendrick et al., 2002). This process produces flower structures and folds and faults that could be misinterpreted as "strain partitioned" above geometric complexities in the fault zone. It also produces a direct record of the displacement across the fault zone (Fig. 10).

If our structural analysis is correct, the length of the Yaqui Ridge anticline is equivalent to the right slip across the San Felipe fault zone. The length of the anticline ranges from 6.4 to 9.5 km depending on whether the damage zone structurally above the West Salton detachment fault is folded in exposures southeast of the detachment fault (Fig. 9). Although large-scale folding of the damage zone is certainly possible, superposed damage adjacent of the nearby Sunset fault could produce a "folded-looking" damage zone where none exists. This third slip estimate is high and overlaps within errors with the other two slip estimates (Fig. 12). This suggests that our geometrical model and right-slip estimates are robust despite the fairly large uncertainty envelope. About 6.5 km of right slip agree with all three slip estimates (Fig. 12). Right slip may range from 4 to 12.4 km. Mapping farther to the west could refine these estimates and test our hypothesis.

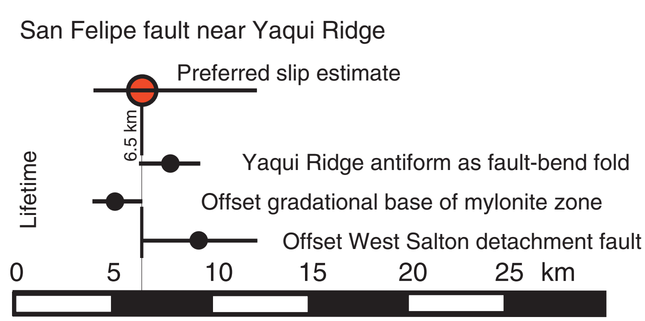

Figure 12. Graphical comparison of three independent estimates of right slip across the Mescal Bajada and Pinyon Ridge segments of the San Felipe fault zone. Refer to Figure 9 for locations of features.

Folds within the Dextral Fault Zones

Folds in the western Salton Trough vary in scale, spacing, dominant trend, relationship to faults, and degree of shortening. Some of the folds are measures of dextral strain and were used earlier to estimate displacement across the Clark and San Felipe faults. Most folds either trend nearly E-W or parallel the NW-striking dextral faults. Folds with other orientations are less common and localized in specific areas parallel to N-striking normal and NE-striking left-lateral faults. Large map-scale folds tend to be singular named structures, whereas more closely spaced folds form trains of subparallel folds and occur in domains that are a few kilometers in dimension (Heitman, 2002; Lilly, 2003; Kirby, 2005; Steely, 2006; Belgarde, 2007).

The San Felipe anticline (SFA, Fig. 3) is the largest and most significant of a half dozen basin-scale folds (Dibblee, 1954, 1984; Heitman, 2002; Lilly, 2003). It trends E-W and was most active from ca. 1.1 to ca. 0.6 Ma (Lutz et al., 2006; Kirby et al., 2007). It lies within the San Jacinto fault zone between the SE tip zone of the Clark fault and the Extra fault in the east and the southeast tip of the Veggie Line fault in the west. The west half of the anticline extends west across the Coyote Creek fault, and has been displaced right laterally by it (Figs. 3 and 7). The San Felipe anticline produced discrete small subbasins and depocenters within the larger San Felipe–Borrego subbasin when it was active and deflected rivers to parallel its axis (Fig. 11, Lutz et al., 2006; Kirby et al., 2007).

Other E-trending map-scale folds include the Grave's Wash anticline, the Carrizo Wash syncline, and a large faulted unnamed anticline east of Whale Peak that has a smaller syncline on part of its crest (Figs. 2 and 3) (Dibblee, 1996; Kairouz, 2005). NW-trending fault-parallel folds include the Split Mountain anticline, the Borrego syncline, the Yaqui Ridge antiform, the Church Ridge antiform, and Salton City anticline (Dibblee, 1954, 1984, 1996; Kirby, 2005; Steely, 2006; Shirvell, 2006; Belgarde, 2007). The basin-scale folds contrast with hundreds of smaller closely spaced folds within the sedimentary basins that both parallel the larger dextral faults and trend oblique to them. The latter geometry is somewhat more common. Flexural slip and detachment folding produced this group of folds (Wells, 1987; Feragen, 1986; Wells and Feragen, 1987; Heitman, 2002; Lilly, 2003; Kirby, 2005; Belgarde, 2007).

How Robust Are the New Slip Estimates?

The consistent 21.9–23.4 km estimates of right separation across the Clark fault documented at five locations by Sharp (1967) provide a useful constraint on the new separation estimates reported here (Table 2). The Clark fault branches northwest of the Salton Trough, and some of its displacement transfers southeastward onto the Coyote Creek fault (Sharp, 1967, 1972a, 1972b, 1979; Sharp and Clark, 1972). The sum of displacement across the Coyote Creek fault and Clark fault at cross-strike positions should therefore sum to ~22–25.6 km, if slip is as consistent as

Sharp's analysis suggest. The 16.8 +3.7/–6.0 km separation across the Clark fault (Forand, 2010) and 3.5 ± 1.3 km across the Coyote Creek fault have almost the ideal spatial location for this test, and they sum to 21.3 +5.0/–7.3 km. Because this value is very similar to the separations calculated by Sharp (1967) a little farther to the northwest along the Clark fault, we have additional confidence in the accuracy of these slip estimates. Addition of the poorly quantified small slip across the Mid Ridge fault would likely raise the total slip to 21.8–23.8 km near Coyote Mountain (Fig. 5).

The displacement data of Sharp (1967) and this study thus demonstrate that the Clark fault and the Clark–Coyote Creek fault pair have fairly consistent amounts of separation along their central 50 km. These results conflict with Blisniuk et al. (2010), who reported that there is a "decrease in total bedrock displacement (Sharp, 1967) from Anza (22–24 km)" that parallels decreasing latest Quaternary slip rates southeastward.

BASIN ANALYSIS AND FAULT ACTIVITY

Structural Setting of the Study Sites

Integrated basin analysis, magnetostratigraphy, and structural studies provide ages of initiation for six segments or faults of the San Felipe and San Jacinto fault zones (Table 4). Our four study areas all lie within the San Jacinto or San Felipe fault zone but differ in their structural position relative to the West Salton detachment fault and in their proximity to the master dextral fault zones. The Ash Wash section (Fig. 13) is located in the footwall of the now-inactive West Salton detachment fault and is deformed by dextral and sinistral strands of the Coyote Creek fault zone. The oldest basin fill in this area provides a minimum age of the Coyote Creek fault because, prior to dextral faulting, the footwall of the detachment fault was being exhumed, uplifted, and eroded, and therefore there should be no syndetachment basin fill. We also consider the implications of a possible lag time between initiation of the Coyote Creek fault and onset of related sedimentation in the new fault zone. Exposures of Pleistocene sedimentary rocks at the three other field sites are situated in the hanging wall of the West Salton detachment fault, and therefore preserve both late Miocene to Pleistocene syndetachment strata and Pleistocene to Holocene postdetachment strata (Figs. 3 and 4; Dibblee, 1954, 1984; Winker and Kidwell, 1996; Dorsey et al., 2006a, 2006b, 2007; Lutz et al., 2006; Kirby et al., 2007; Steely, 2006; Steely et al., 2009). In each of these areas, we examined the stratigraphic, sedimentologic, and structural record for evidence of when the West Salton detachment fault became inactive and the San Jacinto and San Felipe faults started to deform the Salton Trough and Peninsular Ranges.

The three basinal sites are located in the Sunset Wash area, the Borrego Badlands, and the San Felipe Hills (Fig. 3). The deposits at Sunset Wash are exhumed within a double-left stepover along the San Felipe fault zone (Figs. 2 and 3). The Borrego Badlands (BB, Fig. 3) lie between the Santa Rosa segment of the Clark fault in the northeast and the Borrego Badlands segment of the Coyote Creek fault in the southwest. The East Coyote Mountain fault is located west and NW of the Borrego Badlands site (Lutz et al., 2006). The San Felipe Hills are located in a more distal setting relative to the other sites and preserve the southeast tip zone of the Clark strand in the Tarantula Wash and Arroyo Salada structural segments (Kirby, 2005; Belgarde, 2007). The Tarantula Wash segment is NW of the intersection between the northeast-striking sinistral-normal Extra fault and the SE tip of the Clark fault (Figs. 2 and 3).

Stratigraphy of Pleistocene and Holocene Deposits

Tens to hundreds of meters of early to middle Pleistocene sediment are exposed in both the Salton Trough and adjacent to the San Jacinto, San Felipe, and Elsinore faults where they cross the Peninsular Ranges (Fig. 3) (Dibblee, 1954, 1984; Rogers, 1965; Sharp, 1967; Dorsey and Roering, 2006). Some of these deposits preserve a record of initial slip on the dextral faults of this region and overlie up to 1–1.5 km of syndetachment lacustrine mudstone and siltstone of the Borrego Formation in the San Felipe–Borrego subbasin (Fig. 4; Dorsey, 2002; Lutz et al., 2006; Kirby et al., 2007). Pleistocene coarse alluvial conglomerate and sandstone in the western parts of the Salton Trough are assigned to the Ocotillo Formation, whereas age-equivalent sandstone, siltstone, and mudstone in the central to eastern parts of the basin are assigned to the Brawley Formation (Dibblee, 1954, 1984, 1996; Lutz et al., 2006; Kirby et al., 2007). In the Peninsular Ranges, the equivalent sedimentary unit is called the Bautista beds (Frick, 1921; Sharp, 1967).

Prior to our study, the Pleistocene age of the Ocotillo and Brawley formations was known from vertebrate biostratigraphy, chemical correlation of ashes near the top of the Ocotillo Formation with the 0.76 Ma Bishop and ca. 0.74 Ma Thermal Canyon ashes, and reconnaissance magnetostratigraphy (Brown et al., 1991; Remeika and Beske-Diehl, 1996; Jefferson and Remeika, 1995). Our more detailed magnetostratigraphy in the Borrego Badlands and San Felipe Hills refined these ages and showed that the Ocotillo and Brawley formations were deposited rapidly starting at the beginning of the Jaramillo subchron, ca. 1.1 Ma, and that deposition continued until ca. 0.6–0.5 Ma (Lutz et al., 2006; Kirby et al., 2007). Deposition ended during the Brunhes magnetochron, sometime after 0.76 Ma. Magnetostratigraphic studies in three widely separated areas record nearly instantaneous arrival of coarse sand and gravel of the Ocotillo and Brawley formations across the San Felipe–Borrego subbasin at ca. 1.1 Ma. Continuing studies confirm this age assignment in a fourth location (Remeika et al., 2008). Basin-wide subsidence and sediment accumulation SW of the Salton Sea ended ca. 0.5–0.6 Ma and was followed by transpressional deformation, uplift, and exhumation that is clearly related to the active dextral faulting along the San Jacinto and San Felipe fault zones.

Middle Pleistocene to Holocene pediment and terrace gravels and pebbly sand overlie folded and faulted early to middle Pleistocene sedimentary rocks and older rocks along

TABLE 4. EVIDENCE FOR THE AGE OF INITIATION AND SURFACE DEFORMATION WITHIN EACH FAULT ZONE

Fault or fold	Fault or fault segment being considered	Key relationship(s)	Interpretation	Source of data and interpretation
San Felipe fault	Sunset Wash fault	Angular unconformity beneath Pleistocene Ocotillo Formation near the fault zone near Harper Canyon.	A fault bend monocline formed above the upward growing tip of the San Felipe fault zone between ca. 1.3 and 1.1 Ma and produced this unconformity. San Felipe fault zone had initiated at depth by this time.	Steely (2006); Steely et al. (2009)
	Sunset Wash fault	NE fining of the Ocotillo Formation away from the Sunset fault.	The San Felipe fault zone uplifted the SW side of the Sunset fault, and this uplift was the source of the coarse, tonalite-bearing gravel of the Ocotillo Formation. San Felipe fault zone had breached the surface by the time the Ocotillo Formation was being deposited.	Steely (2006); Steely et al. (2009)
	Sunset Wash fault and Fish Creek Mountains fault	NE- to ENE-directed paleocurrent in the Ocotillo Formation near Sunset Wash, San Felipe Hills, and southern Borrego Badlands.	Flow was away from the uplifted blocks along the San Felipe fault zone toward the San Felipe–Borrego basin to the NE of the fault zone. These faults were basin-bounding faults at this time.	Steely (2006); Steely et al. (2009); Kirby et al., 2007; Lutz et al. (2006)
	Sunset Wash fault and Fish Creek Mountains fault	Many recycled sandstone clasts in the Ocotillo Formation in the Borrego Badlands, San Felipe Hills, and Sunset Wash area.	Part of the Pliocene supradetachment basin above the West Salton detachment fault was uplifted and exhumed by the cross-cutting San Felipe fault zone. The uplifted basinal deposits supplied the sandstone clasts.	Steely (2006); Steely et al., 2009; Lutz et al. (2006), Kirby et al. (2007)
San Jacinto fault zone	San Felipe Hills segment of the Clark fault	Disconformity at the base of the Brawley Formation that is localized near the Tarantula Wash segment at the SE tip of the Clark fault.	Incipient slip on the Clark strand at depth produces a broad flat-topped anticline above its blind trace at 1.1 Ma. The Clark fault in the San Felipe Hills segment had not propagated to the surface at this time.	Kirby et al. (2007); this study
	Santa Rosa segment of the Clark fault	Conglomerate shed from upthrown NE side of the Clark fault is preserved in the NE Borrego Badlands in the lower Ocotillo Formation.	The Santa Rosa segment of the Clark fault had propagated to the surface and produced a local highland on the NE side of the fault. Correlation to magnetostratigraphically dated section shows an age of ca. 1.0 Ma for first conglomerate derived from the NE.	Lutz et al. (2006)
	Santa Rosa segment of the Clark fault	NE thickening of the Ocotillo Formation in the Borrego Badlands toward the Clark fault and away from the crest of the San Felipe anticline.	Both structures were active during deposition of the Ocotillo Formation between 1.1 and 0.6 Ma.	Lutz et al. (2006); this study
	San Felipe anticline	West end of the San Felipe anticline is the Veggie Line fault. The east end coincides with both the Extra fault zone and the SE tip of the Clark fault in the reconstructed geometry of Figure 13.	The E-W–trending San Felipe anticline is a transpressive fold within the early San Jacinto fault zone.	Kirby et al. (2007); this study
	East Coyote Mountain fault. This cross fault probably links the Clark and Coyote Creek fault on east side of Coyote Mountain	Conglomerate was shed SE from footwall of East Coyote Mountain fault starting ca. 1.1–1.0 Ma. This overlies silts, clays, and fine sandstone of the Borrego Formation.	East Coyote Mountain fault is part of the San Jacinto fault zone and currently lies between the Clark and Coyote Creek fault. Activity on East Coyote Mountain fault started ca. 1.1–1.0 Ma and shows that the adjacent parts of the San Jacinto fault zone were active at that time.	Lutz et al. (2006)
	SE part of the Tarantula Wash segment	Closely spaced folds of the San Felipe Hills segment did not produce growth relationships in the folded Brawley or Ocotillo formations.	Closely spaced folds within this segment postdate the youngest Brawley and Ocotillo formations, and the fault segment is therefore less than ca. 0.6 to 0.5 Ma. We infer that deformation started to propagate to the surface at about this time.	Kirby et al. (2007)

(*continued*)

TABLE 4. EVIDENCE FOR THE AGE OF INITIATION AND SURFACE DEFORMATION WITHIN EACH FAULT ZONE (*continued*)

Fault or fold	Fault or fault segment being considered	Key relationship(s)	Interpretation	Source of data and interpretation
Coyote Creek fault	Coyote Ridge segment	Megabreccias are present in the Pleistocene Bautista beds west of Coyote Mountain area (this study).	Active tectonism and steep relief was produced along the Coyote Creek fault zone during deposition of these sedimentary rocks. The Coyote Ridge segment of the Coyote Creek fault had breached the surface by the time the megabreccia was deposited.	Dorsey (2002); this study
	Coyote Ridge segment	There are Pleistocene conglomerate and sandstone deposits localized along the fault zone.	Coarse-grained sedimentary rocks were shed from within the fault zone and deposited within fault-controlled basins. Later adjustments in the fault zone uplifted the basinal deposit. The Coyote Ridge segment of the Coyote Creek fault had breached the surface by the time the sedimentary rocks were first being deposited.	Sharp (1967); Dorsey (2002); Dorsey and Roering (2006); this study
	Coyote Mountain segment	Paleocurrents show flow parallel to the Coyote Creek fault zone when deposition of the Bautista beds initiated and again near the end of deposition.	The eroded damage zone of the fault zone and/or graben structures along the fault controlled the stream systems and guided them into dominantly NW and SE directions.	Dorsey (2002); this study
	Coyote Mountain segment	Fanning dips in the upper half of the section along Ash Wash (Dorsey, 2002).	The Coyote Ridge segment of the Coyote Creek fault had breached the surface by this time, and there were adjustments and tilting within the fault zone.	Dorsey (2002)
	Borrego Badlands and Borrego Mountains segments of the Coyote Creek fault	Thickness patterns in the Ocotillo Formation and angular relationships at its base are consistent with one another on the NE and SW side of these segments and show no disruption of the landscape at the Coyote Creek fault.	The Borrego Badlands and Borrego Mountains segment of the Coyote Creek fault probably initiated after deposition of the Ocotillo Formation. If so, the segment is younger than ca. 0.6 Ma. The west tip of the San Felipe anticline was probably actively growing and tilting the Ocotillo Formation on its north limb. Prior to their initiation, during early Pleistocene time, the Veggie Line fault may have been a major fault within the San Jacinto fault zone, transferring slip from the Coyote Ridge segment of the Coyote Creek fault south to the west end of the San Felipe anticline. This geometry bypasses the Coyote Creek fault near Borrego Mountain until after ca. 0.6 Ma and may have connected the San Jacinto fault zone east to the Extra fault and perhaps even to the SE tip of the San Andreas fault.	Lutz et al. (2006); Steely (2006)
San Felipe anticline	SW Borrego Badlands and Borrego Mountain area east to central San Felipe Hills	Angular unconformity and progressive unconformity on flanks of the San Felipe anticline. The Ocotillo Formation thickens by a factor of two on the northeast flank of the anticline. The Ocotillo Formation thickens from about 250 m to >500 m on the NE side of the San Felipe anticline and the SW side of the Clark fault. The presence of dozens of soils in the southwest near the crest of the San Felipe anticline and few to no soils in the expanded sections farther north-northeast indicate that the thinner sections in the south are condensed relative to those in the north (Lutz et al., 2006).	The San Felipe anticline was an active structure within the early San Jacinto fault zone. We relate formation of the anticline to deformation along the San Jacinto fault zone because it links the SE tip of the Veggie Line fault in the west to the Extra fault and SE tip of the Clark fault zone in the east. All of these faults are part of the San Jacinto fault zone or were part of it in the past. Younger deformation complicates the eastern end of the San Felipe anticline somewhat.	Kirby et al. (2007); Lutz et al. (2007); Steely (2006)
	South side of San Felipe anticline from Ocotillo Badlands east to SE San Felipe Hills	Paleocurrents indicate east flow in Ocotillo Badlands, south of the San Felipe anticline, and NE flow in most other areas.	Flow in Ocotillo Formation was deflected eastward by the east-trending crest of the San Felipe anticline because it was actively uplifting in the early to middle Pleistocene within the San Jacinto fault zone.	Kirby (2005); Kirby et al. (2007)

an angular unconformity in most depocenters SW of the Salton Sea. The pediment-related deposits are lithologically and morphologically identical to strath terraces along the active streams but are located higher in the landscape and cannot be related to any modern stream. These thin pediment-related deposits and their upper surfaces are broadly warped and faulted in some areas but are much less folded and faulted than the underlying strata (Reitz, 1977; Dibblee, 1996; Heitman, 2002; Kirby, 2005). Dips are so low that it is difficult to discriminate between original depositional dips and younger tilting of the pediment-related deposits.

Optically stimulated luminescence (OSL) dating of five pebbly sandstone samples from widely separated parts of the highest (oldest) widespread pediment-related deposits of the San Felipe–Borrego subbasin in the SE Santa Rosa Mountains are ca. 18–62 ka (late Pleistocene) (Table 3). These pediment-related deposits are 5–30 m above the modern drainages (Belgarde, 2007; Janecke et al., 2010). We sampled the stratigraphically lowest part of the pediment-related deposits that was not contaminated by the underlying Pliocene basin-fill deposits. Beryllium surface exposure dating of a small remnant of a faulted pediment surface nearby produced an age of ca. 35 ka (Le et al., 2008) that is consistent with the OSL ages from sample 1. There is no physical continuity between the pediment-related deposits dated by OSL and the surface dated using Be exposure dating, so it is difficult to make a more detailed comparison between the results of the two methods. There are small erosional remnants of higher pediment-related deposits as much as ~100 m above the active drainages.

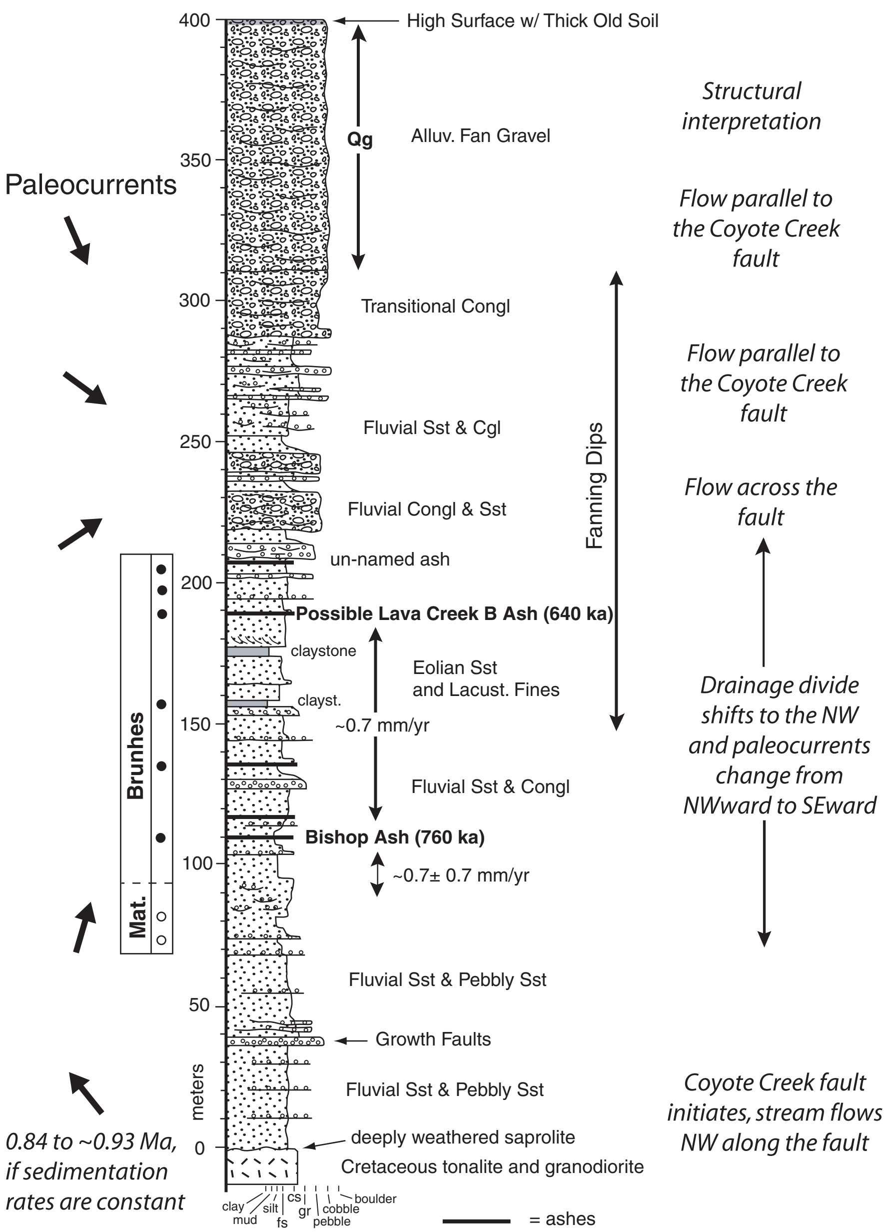

Figure 13. Relationships in Pleistocene sandstone and conglomerate along the Coyote Creek fault zone at Ash Wash. These indicate initiation of strike-slip faulting ca. 0.8–0.9 Ma. New interpretations are italicized. Modified from Dorsey (2002). Sst—sandstone; cgl—conglomerate; fs—fine sand; cs—coarse sand; gr—granule.

Dating Initiation of the San Jacinto and San Felipe Fault Zones in the Western Salton Trough

Thickness patterns, the marked increase in grain size of the sandy to conglomeratic Ocotillo and Brawley formations relative to the underlying mud-rich Borrego Formation, coarsening toward dextral-oblique faults at the margins of the San Felipe–Borrego subbasin, presence of recycled pebbles to cobbles of older basin-fill deposits, and angular unconformities at the base of and within these two formations, all clearly show that widely separated parts of the San Jacinto and San Felipe fault zone initiated in early Pleistocene time and then changed their geometries in middle to late Pleistocene time. Most of the detailed observations and data sets that support this interpretation are published elsewhere (Lutz et al., 2006; Kirby et al., 2007; Steely, 2006; Steely et al., 2009) and are summarized here in tabular form (Table 4). Below we highlight additional interpretations and expand on prior analyses.

These data sets were used to reconstruct the San Felipe–Borrego subbasin to a time early in the history of the San Jacinto and San Felipe fault zones (Fig. 11) and show that deposition was strongly controlled by the new fault systems. Evidence for structural control on deposition includes (1) thickness variations in the Pleistocene deposits that record basin tilting; (2) lateral coarsening toward new basin-bounding dextral-oblique faults at the margins of the San Felipe–Borrego subbasin; (3) recycled clasts in the Ocotillo Formation that were eroded from older basin-fill deposits; and (4) locally developed angular unconformities at the base of—and progressive unconformities within—the Ocotillo and Brawley formations (Table 4 and Fig. 11).

The timing of regional deformation in the new fault zone is recorded by rapid progradation of the conglomeratic and sandy Ocotillo and Brawley formations over the mud-rich Borrego Formation across a large area at 1.1 Ma (Lutz et al., 2006; Kirby et al., 2007). We considered the possibility that Pleistocene climate changes produced the sedimentary signal in the basinal deposits, but rejected that hypothesis because angular unconformities cannot be produced by changing climates nor would recycled clasts or lateral thickening toward faults and away from growing fault-related anticlines result from climate change (Lutz et al., 2006; Kirby et al., 2007; Steely et al., 2009). Progressive unconformities do not result from climate change nor will changing climate deflect rivers to flow parallel to the crests of growing anticlines. The Ocotillo Formation thickens by several factors toward the Santa Rosa segment of the Clark fault of the San Jacinto fault zone (Lutz et al., 2006), thickens toward cross faults within the San Jacinto fault zone, and has its thickest preserved section within the San Felipe fault zone (Steely et al., 2009). None of these structural controls on deposition could result from climate change. Finally, climate change is not documented in the western USA in the early Pleistocene, with the major changes occurring earlier in the Pliocene, between ca. 3.0 and 2.5 Ma (sources in Lutz et al., 2006).

We include the possibility of a lag time between earliest fault activity and arrival of the stratigraphic signal in the basin (gravel progradation) by adding 0.2 m.y. to derive an upper age limit of 1.3 Ma for initiation of the San Jacinto and San Felipe faults. Based on modeling studies that indicate a basinal response time of ~50 k.y. for changes in sediment flux from the uplifting footwall of an active normal fault (e.g., Allen and Densmore, 2000), we infer that 0.2 m.y. substantially overestimates the time required for gravel to prograde into the basin in response to new fault-related uplift and erosion. Including a lag time of 0.2 m.y. is consistent with the presence of a thin conglomerate and sandstone unit 90 m below the base of the Ocotillo Formation in the Borrego Badlands that contains a few clasts of sandstone reworked from Pliocene basinal deposits. If the sedimentation rate in the basal Ocotillo formation applies to the uppermost Borrego Formation, the age of this lens is ca. 1.2 Ma. We err on the conservative side and include a time lag that is twice as long as indicated by this evidence.

Another alternative hypothesis suggests that significant slip on the dextral fault zones occurred prior to 1.1–1.3 Ma within the Borrego Lake basin and produced no sedimentary signal. We reject this "silent fault" hypothesis for two main reasons: (1) because the change in facies, grain size, flow directions, depositional environments, dramatic thickening patterns, and basin boundaries are so abrupt at the base of the Ocotillo and Brawley formations, it is highly unlikely that the San Jacinto fault zone could have been both "depositionally silent" during deposition of the Borrego Formation and then abruptly became "depositionally exuberant" during deposition of the Ocotillo and Brawley formations. A gradational pattern of sedimentary change is predicted by this silent fault hypothesis, yet none is present (Lutz et al., 2006; Kirby et al., 2007; Steely et al., 2009). The 0.2 m.y. lag time discussed above already accounts for the possibility of a silent fault, even though it is not supported by the data.

Finally, our research and abundant prior studies show that strike-slip faults usually produce a sedimentary record in adjacent basins despite their dominantly horizontal translation (e.g., Crowell, 1974, 2003; Sylvester and Smith 1976; Christie-Blick and Biddle, 1985). Janecke made a survey of the modern strike-slip faults in the Salton Trough (excluding the completely buried Brawley seismic zone) and found that every strike-slip fault has a noticeable vertical component along half or more of its trace (Table 5). On average 75% of the fault traces (560 km of the 740 km in the Salton Trough) produce clear basinal responses. The Cerro Prieto fault, for example, has uplifted the basin fill on its northeast side and confines the lower delta of the Colorado River on its SW side along 160 of its 200 km trace length. The San Andreas fault is the basin-bounding fault along its 200 km trace length from Cajon Pass to the Salton Sea and produced major changes in thickness of coeval deposits in the Mecca Hills (Sylvester and Smith, 1976; Sheridan and Weldon, 1994). The San Jacinto fault connects spaced uplifts that lie ~20 km apart and average ~15 km in length. Half of its trace length bounds uplifts that are detectable at the surface, and additional buried uplifts are likely in the

TABLE 5. TRACE LENGTHS OF ACTIVE DEXTRAL FAULTS IN THE SALTON BASIN AND THE PORTIONS THAT LACK DETECTABLE VERTICAL COMPONENT OF SLIP

Fault	Total	No uplift
Clark in basin	50 km	7 km (14%)
San Andreas fault from Cajon Pass to the Salton Sea	200 km	>10 km (>5%)
Cerro Prieto fault	200 km	40 km, only where it is buried by very young sediment of the Colorado River delta (<20%)
Imperial fault	62 km	30 km (48%)
Coyote Creek fault zone, two parts	130 km (Coyote Creek fault and Superstition Mountains strand, following Lin et al. [2007] to the Imperial fault)	77 km (<59%)
	50 km (of the Superstition Hills fault following seismic alignments of Lin et al., 2007) to the Imperial fault	19 km (<38%)
Elsinore fault in basin	50 km	0 km (0%)
Totals	742 km	183 km (25%)

Salton basin. A perfect strike-slip fault with no bends, steps, or misalignment with the regional stress field lacks a sedimentary signal (like the one required for the San Jacinto fault zone to have slipped silently during deposition of the upper Borrego Formation), yet few of the dextral faults of southern California are perfectly straight. Complexities are particularly common along young emergent faults (like the San Jacinto fault would have been if it was active before 1.1 Ma), along faults with widespread block rotation, cross faults, and other interactions. All in all, this analysis casts serious doubt on the silent fault hypothesis.

CHANGES AFTER INITIATION OF THE SAN JACINTO AND SAN FELIPE FAULT ZONES

Early San Jacinto Fault Zone

Formation of the San Felipe Anticline within the Early San Jacinto Fault Zone

The San Felipe anticline is one of the structures of the early San Jacinto fault zone that dates the inception of the fault zone to ca. 1.1–1.3 Ma (Kirby et al., 2007). It was abandoned and cross-cut by the Borrego Badlands and Borrego Mountain segments of the Coyote Creek fault zone after ca. 0.6 Ma (Lutz, 2005; Lutz et al., 2006; Kirby, 2005; Kirby et al. 2007; Steely, 2006; Steely et al., 2009). The San Jacinto fault zone was much wider when the San Felipe anticline was uplifting within the fault zone.

The original geometry and age of the San Felipe anticline are recorded in an angular unconformity and progressive unconformity in the Ocotillo and Brawley formations (Lutz et al., 2006; Kirby et al., 2007). The angular relationships beneath the Ocotillo Formation show that the San Felipe anticline was a broad E-W–trending anticline with gently north- and south-dipping limbs. A gravity high, which corresponds closely to the crest of the Pleistocene San Felipe anticline, is modified by younger structures of the Coyote Creek fault zone (see above).

Clark Fault

Santa Rosa Segment of the Clark Fault

The Borrego Badlands are bounded by active faults of the San Jacinto fault zone, the Clark fault in the NE, and the Coyote Creek fault in the SW. Highlands uplifted by several of these faults abruptly became major suppliers of sediment between 1.0 and 1.1 Ma where previously mudstone and fine sand accumulated in a low-energy lake (Fig. 11) (Lutz et al., 2006). Uplift on the East Coyote Mountain fault began to shed coarse sediment eastward into the former Borrego Lake basin at 1.1 Ma (Lutz et al., 2006). This fault is currently a cross fault between the Clark and Coyote Creek faults, so we interpret its activity as early slip within the San Jacinto fault zone. Older basin-fill deposits exhumed by slip on the Santa Rosa and Arroyo Salada segments of the Clark fault were eroded and recycled into a new depocenter in the eastern Borrego Badlands starting ca. 1.0 Ma (Fig. 11; Lutz et al., 2006). These deposits fine rapidly southwestward into a much smaller local playa lake basin in the Borrego Badlands area that was rimmed by coarser alluvial sediment shed from growing folds and faults of the San Jacinto and San Felipe fault zones starting 1.1–1.3 Ma (Fig. 11). The Ocotillo Formation thickens to the NNE by a factor of 2–3 toward the San Jacinto fault zone and away from the crest of the San Felipe anticline (Lutz et al., 2006). These data provide evidence that the Santa Rosa segment of the Clark fault and the East Coyote Mountain fault propagated to the surface at ca. 1.0 and 1.1 Ma, respectively. The San Felipe anticline was active at the same time to the south (Table 4; Lutz et al., 2006; Kirby et al., 2007).

Initial Blind Slip on the Tarantula Wash Segment of the Clark Fault

The base of the Brawley Formation is a disconformity in the eastern and SE San Felipe Hills and conformable in most other locations (Figs. 2 and 11; Dibblee, 1984; Kirby et al., 2007).

The exposure belt of the Brawley Formation in this area coincides with the southeastern tip of the Clark fault in its Tarantula Wash structural segment. The disconformity is tightly folded near the Clark fault zone, yet there are no thickness changes in the Brawley Formation across the crests and troughs of the many small, closely spaced folds except for structural changes due to flexural-slip, out-of-syncline thrusting, and detachment folding. Broad-scale lateral changes in thickness, like those documented in the Borrego Badlands (Lutz et al., 2006), are possible but difficult to assess because the rocks in the San Felipe Hills are so strongly deformed by faults and folds.

We infer that the disconformity beneath the Ocotillo and Brawley formations resulted from formation of a broad, flat-topped, northwest-trending anticline above a blind Clark fault starting ca. 1.1 Ma (Kirby et al., 2007). Simulation of strike-slip faulting in a heterogeneous clay-rich sedimentary basin (Richard et al., 1989, 1991) illustrates the type of deformation that developed early in the evolution of a strike-slip fault (8 cm stage; Fig. 14A). This geometry is a good match for the relationships documented at ca. 1.1 Ma in the San Felipe Hills above the SE tip of the Clark fault (Fig. 11; Kirby 2005; this study).

More intense near-surface deformation began later, after the end of deposition of the Ocotillo and Brawley formations, and produced closely spaced folds and short discontinuous strike-slip and oblique-slip faults that are organized into separate domains of faults and folds, en echelon sets, disorganized map-scale "breccia" zones, transrotational fault blocks, and fault-fold systems with many cross faults (Figs. 2 and 3, Dibblee, 1986; Reitz, 1977; Dronyk, 1977; Kirby, 2005; Belgarde, 2007; Belgarde and Janecke, 2007). This phase resembles the more deformed 20 cm stage in the analogue model (Fig. 14B; Richard, et al., 1989). These field and map relationships are consistent with ongoing slip on the Tarantula Wash segment of the Clark fault in the subsurface at ca. 1.1 Ma or slightly earlier beneath a broad anticline. Some strands of the Clark fault zone likely propagated upward after ca. 0.5–0.6 Ma (Kirby et al., 2007; this study). As the analogue model and our mapping illustrate, it is likely that some of the slip that accumulated at depth across the Clark fault in the Arroyo Salada and Tarantula Wash segments is distributed onto a myriad of small faults, folds, and décollement surfaces within the mud-rich sedimentary rocks of the Salton basin. This process has produced a strike-slip fault that is "hidden," "effectively blind," and appears "under-slipped" at the surface relative to depth, despite a large amount of deformation being expressed across a broad area at the surface (Fig. 14).

We cannot quantify the *total* slip at the surface in the Arroyo Salada and Tarantula Wash segments since inception of the Clark fault because it is so widely dispersed in the fault's damage zone (≥18 km wide) and because much of it is localized along bedding planes where offset markers are lacking. There is so much pervasive, strong deformation in the field, however, and at least 5.6 km of right slip since ca. 0.5 Ma (see above), that a large fraction of the strain in the crystalline rocks is probably present in the highly deformed mud-rich damage zone around the Clark fault in the Salton basin. The strongly folded and faulted Upper Pliocene and Pleistocene sedimentary rocks in the SE San Felipe Hills are difficult to explain with the alternative end-member interpretation of a rapid southeastward decrease in strain.

Coyote Creek Fault

Coyote Ridge Segment of the Coyote Creek Fault

Initiation of the Coyote Creek fault is recorded in early to middle Pleistocene deposits in the Coyote Badlands (Bautista beds) between the main trace of the Coyote Creek fault and the smaller Box Canyon fault around Ash Wash (Figs. 3 and 5; Dorsey, 2002). These sedimentary rocks nonconformably overlie Cretaceous plutonic rocks and pre-Cretaceous metamorphic wall rocks, in the footwall of the Cenozoic West Salton detachment fault. The Bautista beds consist of sandstone, conglomerate, megabreccia, and at least three ash beds (Fig. 13). The 400-m thickness of this sandy to conglomeratic succession is comparable to the thickness of the Ocotillo and Brawley formations in the San Felipe–Borrego basin. The Brunhes reversal (0.78 Ma) and Bishop ash (0.76 Ma) clearly indicate an early to middle

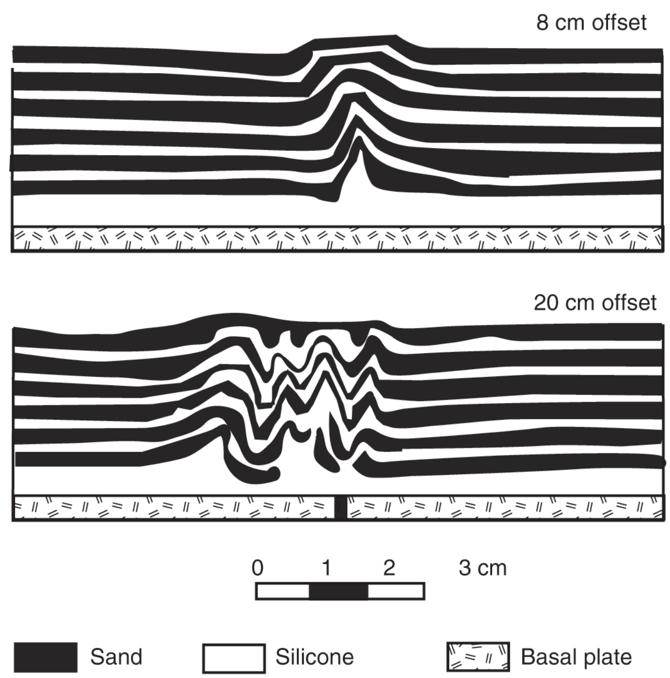

Figure 14. Progressive changes in a deforming anisotropic sedimentary succession above a basement strike-slip fault (from Richard et al., 1989). An early blind geometry evolves into a complex volume of faulted and folded sedimentary rocks with increasing displacement on the basement fault. A broad flat-topped anticline overlies the blind fault (A) With increasing slip, dispersed smaller faults and folds propagate to the surface (B) We infer that the disconformity at the base of the Brawley Formation in the San Felipe Hills (Fig. 11) reflects deformation similar to (A).

Pleistocene age for the sediment around 100 m in the section (Fig. 13) (Dorsey, 2002). Another ash at 188 m in the section is more likely to be the widespread Lava Creek B ash (0.64 Ma), than the Thermal Canyon ash (0.74 Ma) as inferred by Dorsey (2002), because an ash along stratigraphic strike to the southeast was subsequently correlated chemically to the Lava Creek B ash (Fig. 13; A. Sarna-Wojcicki and R. Kesler, 2006, written commun.). Attempts to directly date the ash at 188 m in the measured section at Ash Wash failed due to the absence of zircons or other datable minerals, and altered of volcanic glass prevented a chemical analysis.

If the ash at 188 m in the measured section is the Lava Creek B ash, then the sediment accumulation rate is roughly 0.7 mm/yr above the Bishop ash (Fig. 13), consistent with a weakly constrained sediment accumulation rate estimated for the interval between the Bishop ash and the base of the Brunhes subchron (0.7 ± 0.7 mm/yr). Applying a sediment accumulation rate of 0.7 mm/yr to the entire section at Ash Wash suggests onset of deposition at approximately ca. 0.8–0.9 Ma and cessation at ca. 0.3–0.4 Ma. Fanning dips that first appear in the section at 150 m (Dorsey, 2002) (ca. 0.7 Ma) probably record a structural change within the fault zone after its inception.

Paleoflow within the Coyote Creek fault zone was initially toward the NW, parallel to the fault, and changed progressively to northeastward and southeastward, recording a full reversal of flow direction through time (Dorsey, 2002). We infer that this reversal resulted from northwestward retreat of the drainage divide between the Salton Trough and the west-sloping Peninsular Ranges along the San Jacinto fault zone (Dorsey and Roering, 2006). We interpret the fault-parallel trend of sediment transport at the beginning and end of deposition to reflect flow guided by the NW-SE structural grain of an aggrading half graben within the San Jacinto fault zone (Fig. 13).

The significant thickness of the deposits, the presence of coarse bouldery conglomerates in the section, fanning dips, 180° change in paleoflow, and several megabreccia bodies, are all consistent with tectonism in the Coyote Creek fault zone during deposition of the entire succession of the Bautista beds. This conclusion is a departure from the previous interpretation of Dorsey (2002) of initiation of the Coyote Creek fault after ca. 0.6 Ma. Because the Coyote Canyon area is situated in the previously uplifting and eroding footwall of the West Salton detachment fault, a period of subsidence related to creation of a new strike-slip fault would likely be required to drop the surface below base level and begin accumulating sediment. Based on this we infer a short lag time (~100–200 k.y.) between fault initiation and onset of Bautista beds deposition. We therefore interpret the data from the Coyote Canyon area to record formation of the Coyote Ridge segment of the Coyote Creek fault zone slightly before ca. 0.9 Ma, possibly around the same time as initiation of the Clark and East Coyote Mountain faults at 1.0–1.1 Ma farther to the SE. Structural changes in the Coyote Creek fault zone produced the oldest fanning dips at ca. 0.7 Ma, and later caused exhumation and erosion of sediments after ca. 0.3–0.4 Ma (Dorsey, 2002).

Borrego Badlands and Borrego Mountains Segments and Their Possible Precursors

The central strands of the Coyote Creek fault near the Borrego Badlands and Borrego Mountain (Figs. 2B and 3) probably initiated later, at ca. 0.6 Ma, based on evidence presented by Lutz et al. (2006). If the apparent continuity of Pleistocene strata on either side of these two segments of the fault zone is correct, then slip on the Coyote Creek fault must have bypassed this area and utilized a different set of structures before ca. 0.6 Ma (Lutz et al., 2006). The low (2.3 ± 0.7 km) right separation measured across the Borrego Mountain segment of the Coyote Creek fault (Steely, 2006; this study) relative to 3.5 km measured at Coyote Mountain is consistent with these segments of the fault being ~0.3–0.5 m.y. younger than the Coyote Ridge fault segments.

The Veggie Line fault and its along-strike continuation, the Henderson Canyon fault, are the most likely mapped structures to have bypassed the Borrego Mountain area in early Pleistocene time. These two faults may have localized the slip in the evolving San Jacinto fault zone before the Borrego Badlands and Borrego Mountains segments of the Coyote Creek fault cut across the San Felipe anticline (Fig. 11). If so, the Veggie Line and Henderson Canyon faults connected the NW end of the Coyote Ridge segment of the Coyote Creek fault to the west end of the San Felipe anticline. It may also have provided a connection between the San Jacinto fault zone and the San Felipe fault zone by way of connector faults and the Sunset fault.

This inferred fault-fold connection is difficult to prove but is consistent with evidence for greater slip rates across San Felipe anticline and parts of the San Felipe fault zone in the early to middle Pleistocene than later on. The ~1.3 km of early Pleistocene north-south shortening measured in the western half of the San Felipe anticline (Kirby, 2005) requires only ~1.7 km of right slip across the Veggie Line–Henderson Canyon fault zone to produce it by strain transfer (Figs. 6 and 11). This magnitude of slip is well within the plausible range across this fault. Because much of the area around the Veggie Line fault is buried beneath Holocene cover, it is difficult to further test and verify the existence of these possible linkages in the early to middle Pleistocene.

San Felipe Fault Zone

The basal contact of the Ocotillo Formation in the San Felipe fault zone at Sunset Wash is an angular unconformity (10°–15°) where it overlies north-dipping Pliocene Diablo and Canebrake formations (Steely, 2006; Steely et al., 2009). Either erosion of Borrego and/or Hueso formations occurred prior to deposition of the Ocotillo Formation, or the Borrego and Hueso formation were never deposited in this area. Using a conceptual model of Gawthorpe et al. (1997) and Sharp et al. (2000), we interpret these relationships to record a period of monoclinal folding above the upward propagating tip of the San Felipe fault zone starting between ca. 1.1 and 1.3 Ma (Steely, 2006; Steely et al., 2009). Voluminous arkosic and recycled sediment shed from the uplifted Fish Creek and Vallecito Mountain block first appeared in the adjacent San Felipe–Borrego subbasin at 1.1 Ma (Table 4; Lutz et al., 2006; Kirby et al., 2007; Steely et al., 2009). This probably marks the time when the San Felipe fault zone propagated to the surface and produced a steep, fault-bounded mountain front that exposed crystalline rocks for the first time in this part of the Salton basin (Steely, 2006).

The San Felipe fault zone, like every dextral fault in this area, has changed its geometry since its inception. About 600 m of sediment that accumulated within a stepover of the fault zone, is now being folded, uplifted, and exhumed (Steely et al., 2009). We infer that exhumation began at roughly the same time that it did in dated sites farther north, sometime after ca. 0.6–0.5 Ma, but we are unable to date it directly along the San Felipe fault zone at Sunset Wash.

Insights into Structural Reorganizations from Lithology, Provenance, Paleocurrents, and Depositional Environment of Basinal Deposits

Paleocurrent, provenance, grain size data, and facies panels show that most of the coarse sediment in the Ocotillo and Brawley formations was derived from a newly formed intrabasinal highland along the San Felipe fault zone. This highland consists of the Fish Creek and Vallecito Mountains and the transpressive Yaqui Ridge antiform within a double left-step and contractional bend in the San Felipe fault zone (Kirby et al., 2007; Lutz et al., 2006; Steely, 2006; Steely et al., 2009). Fault blocks uplifted along the San Jacinto fault zone in the SE Santa Rosa Mountains and Coyote Ridge were also an important new source of sediment in the NW part of the San Felipe–Borrego subbasin (Lutz et al., 2006). Pebbles, cobbles, and some boulders of tonalite clasts and feldspathic sand dominate the Ocotillo and Brawley formations, unlike the underlying Borrego Formation, which consists mostly of mudstone, siltstone, and sandstone derived from the Colorado River (Guthrie, 1990; Lutz et al., 2006; Kirby et al., 2007).

The presence of abundant cemented sandstone clasts recycled from older Pliocene formations indicates that part of the Pliocene sedimentary basin that formed above the West Salton detachment fault during transtension was uplifted and exhumed during deposition of the Ocotillo and Brawley formations (Lutz et al., 2006; Kirby et al., 2007; Steely, 2006). Paleoflow was to the NE near the Fish Creek and Vallecito Mountains (Steely, 2006), eastward parallel to the intrabasinal San Felipe anticline, and northeast in a fluctuating deltaic system east of the eastern end of the San Felipe anticline near Oil Well Wash (Fig. 11) (Kirby et al., 2007). In the Borrego Badlands, paleoflow was more complex, but the southern areas consistently record north to NE flow away from the uplifted crystalline rocks along the San Felipe fault zone and across the west tip of the San Felipe anticline (Lutz et al., 2006). Elsewhere in the Borrego Badlands, coarse sediment was shed to the east from uplifted crystalline rocks west of the East Coyote Mountain fault during early deposition of the Ocotillo Formation (ca. 1.1–1 Ma), and to the southwest from the northeast side of the Clark fault starting before ca. 1 Ma (Lutz et al., 2006). These relationships show that the San Felipe fault zone initiated between ca. 1.3 and 1.1 Ma, propagated to the surface ca. 1.1 Ma, experienced a period of fault-related uplift and folding. Starting after 0.5–0.6 Ma, faulting inverted a formerly subsiding area within the fault zone (Table 4; Steely et al., 2009). The oldest sedimentologic evidence for the San Jacinto fault zone is also ca. 1.1 Ma or slightly older, with other segments producing their first sedimentary signal at ca. 1.0, ca. 0.8, and ca. 0.6 Ma (Table 4).

Younger Deformation

Detailed stratigraphic analysis reveals major structural changes in the past 0.5 m.y. in the Borrego Badlands, San Felipe Hills, Coyote Badlands, and San Felipe fault zone. In each of the basinal study sites, widespread subsidence and gentle tilting and folding across widely spaced large folds took place during deposition of early Pleistocene deposits (Ocotillo, Brawley, and Bautista formations). Deposition ended ca. 0.5–0.6 Ma, when closely spaced folds and faults began to strongly deform the Ocotillo, Brawley, and Bautista formations, perhaps as seen in Figure 14B. Slight deformation affects overlying late Pleistocene to Holocene pediment gravel and sand and eolian deposits. Former basinal areas are now being exhumed in the San Felipe Hills, Borrego Badlands, Coyote Badlands, and Sunset Wash areas. All of these sites lie within or adjacent to the San Jacinto and San Felipe fault zones where structural fault geometries result in local uplift and subsidence. Initiation of the San Felipe and San Jacinto faults separated the ~2100 km^2 San Felipe–Borrego subbasin from the much larger Salton supradetachment basin (Kirby et al., 2007; Steely et al., 2009). After ca. 0.5 Ma the San Felipe–Borrego subbasin was further subdivided into even smaller depocenters in the Upper and Lower Borrego Valleys and Clark Lake Valley, each with areas of <200, <400, <85 km^2 (Fig. 3). The rest of the San Felipe–Borrego subbasin has been exhumed and is undergoing pedimentation (Figs. 3 and 11).

These data indicate major structural adjustments of the San Felipe, Coyote Creek, and Clark faults after ca. 0.6–0.5 Ma. These changes modify the entire upper crust and cannot be localized to the thin sedimentary basin fill because the basin fill is at most a few kilometers thick in our study areas yet faults shift their locus and main central strands by up to 13 km at that time. Microseismic alignments are well developed along the San Jacinto fault zone and show that most of the larger active faults penetrate to the base of the seismogenic crust at 10–14 km and have fairly consistent steep dips (Shearer et al., 2005; Lin et al., 2007; Belgarde, 2007; Forand, 2010). Changing fault networks in crystalline bedrock cut by the San Jacinto fault zone are less well documented but also suggested by the presence of many less active fault strands adjacent to the central Holocene ones (Sharp, 1967). All of this provides evidence that the changing fault patterns are deep-seated, fundamental changes in fault systems, not superficial changes limited to weak cover rocks. Significant structural changes redistributed strain onto new right- and left-lateral faults and folds far removed from the older central fault strands. In some instances, the fault zones simplified, but often fault patterns became more complex and broader after ca. 0.5 Ma (Fig. 11).

DISCUSSION

Summary of Results from the Western Salton Trough

Early Pleistocene reorganization of faults in the Western Salton Trough area produced a radical change from low-energy deposition in a large perennial lake, which formed the fine-grained Borrego Formation to alternating alluvial fan, fluvial, deltaic, nearshore lacustrine and eolian environments recorded in the Ocotillo, Bautista, and Brawley formations (Fig. 11; Table 4). The West Salton detachment fault was structurally dissected and became inactive ca. 1.3–1.1 Ma when segments of the San Jacinto and San Felipe fault zones cut across it. This dissection produced basement-cored folds like the San Felipe anticline and Yaqui Ridge anticline within the new dextral fault zones. Differential uplift of the Peninsular Ranges in the footwall of the detachment ceased, and continued subsidence and deposition in its hanging wall became localized adjacent to faults and folds of the newly formed San Felipe and San Jacinto fault zones. In the hanging wall of the West Salton detachment fault, the original, much larger Salton supradetachment basin broke up into the smaller San Felipe–Borrego subbasin in the north and Fish Creek–Vallecito subbasin in the south (Fig. 3). Intervening highlands grew along the San Felipe and San Jacinto fault zones. Deposition ceased in the Fish Creek–Vallecito basin shortly after 0.9 Ma (Dorsey et al., 2011), but deposition of the Ocotillo and Brawley formations continued at a high rate in the San Felipe–Borrego subbasin until ca. 0.5–0.6 Ma. In the subsiding former footwall of the detachment fault in the Peninsular Ranges, sandstone and conglomerate of the Bautista beds accumulated on a pre-Pleistocene erosion surface near the developing San Jacinto, San Felipe, and Elsinore fault zones. Areas farther from the dextral faults continued to be the sites of erosion and/or pedimentation in the Peninsular Ranges in the Pleistocene. The San Felipe fault zone may have propagated to the surface slightly before the San Jacinto fault zone, but a difference in age cannot be discerned with the available data.

Folding has been a component of deformation within the San Jacinto and San Felipe fault zones since their inception, and produced the basin-scale San Felipe, Split Mountain, and Yaqui Ridge anticlines and Borrego syncline starting in the early Pleistocene. The scale and style of folding evolved and changed significantly after the end of deposition of the Ocotillo and Brawley formations in the middle Pleistocene (compare Figs. 14A and 14B). Hundreds of closely spaced folds started to form at that time, basin-wide deposition ceased southwest of the Salton Sea, and exhumation and pedimentation began to dominate the San Felipe–Borrego subbasin.

The changes at ca. 0.5–0.6 Ma may reflect a natural progression of evolving fault zones that are embedded in a mud-rich sedimentary basin. The analogue model of Richard et al. (1989) (Fig. 14) illustrates this hypothesis. Alternatively, it is possible that a more contractional mode of dextral faulting was initiated at ca. 0.5–0.6 Ma. The fact that most of the San Jacinto and San Andreas fault zone SE of their branch point currently dips steeply to the northeast and has a small reverse northeast-side-up component of slip (Sanders and Magistrale, 1997; Lin et al., 2007; Belgarde, and Janecke, 2007; Fuis et al., 2007) is consistent with the latter interpretation but does not require it. Both interpretations are plausible, and more detailed structural studies are needed in the Peninsular Ranges and Salton Trough to resolve this question. Careful analysis of focal mechanisms to determine whether there is a consistent contractional component of the ongoing deformation would support the second hypothesis. Examination of adjacent dextral faults in the Superstition Hills and Durmid Hill areas may reveal evolutionary patterns that are more consistent with one of these hypotheses.

The sedimentary signal of input from the San Felipe fault zone has been much greater than that of the San Jacinto fault zone in our area of study. This may be due to enhanced contractional deformation and uplift along the central WNW-striking fault segments of the San Felipe fault zone near Yaqui and Pinyon ridges and the Fish Creek Mountains. There was also a significant vertical component of southwest side up across the Fish Creek Mountains fault. Because the San Felipe fault zone produced more vertical uplift than the less oblique San Jacinto fault zone, the San Felipe fault zone had a greater impact on the subsidence, deposition, and facies patterns in the San Felipe–Borrego subbasin than the San Jacinto fault zone. The vertical slip component of the San Felipe fault zone exhumed broad expanses of crystalline rocks near our study sites, whereas much of the San Jacinto fault zone is still encased in basinal deposits where we studied it. Nevertheless, numerous indicators of activity on both faults appear abruptly in the basinal record in the early Pleistocene.

Total Slip and Age of the San Jacinto Fault Zone

Our finding that the northwestern margins of the Coahuilla pluton (SW of the fault) and Clark Valley pluton (NE of the fault) are offset ~23.1 km along the Clark fault (Fig. 2) contradicts a recent assertion that this part of the fault has only 14.5–17 km of total bedrock displacement (Blisniuk et al., 2010). This discrepancy is important because it bears on the age and evolution of the San Jacinto fault zone. The estimate of Blisniuk et al. (2010) substantially underestimates total bedrock offset in this area because it matches mafic mineral assemblages within the zoned pluton instead of matching the more distinctive margins of the pluton (compare fig. 2 of Blisniuk et al., 2010, to plate 1 of Sharp, 1967). In contrast, the bold red lines on either side of the Clark fault in Figure 2A (this paper) represent bedrock separation of at least 23.1 km that is obtained using well-mapped, correlative intrusive contacts of Sharp (1967, plate 1). Combining their late Quaternary slip rate and estimate of total bedrock offset, and assuming that slip rate has been constant since fault initiation, Blisniuk et al. (2010) suggested that the San Jacinto fault zone may have initiated at ca. 1.8 ± 0.5 Ma, significantly earlier than the 1.1–1.3 Ma age documented above. Their analysis is unconvincing because it is based on a weak compositional correlation and on assuming that a fault zone with documented two fold changes in slip rate (Blisniuk et al., 2009) instead had a constant slip rate since its inception. Perhaps more importantly, late Quaternary slip rates are based on offsets averaged over only a small fraction (<3–5%) of the total lifetime of the fault zone. It is unlikely that late Quaternary slip rates are a reliable measure of the lifetime behavior of a fault zone of latest Pliocene to earliest Pleistocene age.

Comparison to the Northwestern San Jacinto Fault Zone

Our results are consistent with those of Morton and Matti (1993), Matti and Morton (1993), and Albright (1999). Based on analysis of Pliocene–Pleistocene deposits in the San Timoteo Badlands along the northwestern part of the San Jacinto fault zone (Fig. 1), these studies estimated an age of ca. 1.2–1.4 Ma for initiation of the San Jacinto fault SE of its branch point with the San Andreas fault. They inferred that the San Jacinto fault formed as a result of increasing structural complexity, crustal convergence, and resistance to strike-slip motion through San Gorgonio Pass, a major restraining bend and left step between the Coachella Valley and Mojave sections of the San Andreas fault.

Initiation of the NW San Jacinto fault zone at ca. 1.2–1.4 Ma is similar to and slightly older than the initiation age of ca. 1.1–1.3 Ma that we document for the oldest segments of the San Jacinto fault zone in the western Salton Trough. Uncertainty in initiation ages and possible short lag times between tectonic changes and the first appearance of a signal in the stratigraphic record suggests that fault initiation was either synchronous in the NW and SE or propagated very rapidly to the SE along the fault zone. In either case, our work confirms the young age of the San Jacinto fault and the high average lifetime slip rates that those ages imply (e.g., Morton and Matti, 1993; Matti and Morton, 1993; Albright, 1999; Kendrick, et al., 2002). It is noteworthy that the end of deposition in the San Timoteo area between 0.5 and 0.8 Ma overlaps with the 0.5–0.6 Ma end of deposition and onset of widespread exhumation and folding in the western Salton Trough. This could record a regional kinematic change at that time.

Lifetime and Interval Fault Slip Rates

We use the age of initiation of slip across segments of the Clark, Coyote Creek, and San Felipe fault zones, combined with the new estimates of dextral slip, to calculate lifetime and incremental slip rates for individual faults and the fault zone as a whole (Fig. 15; Tables 2 and 4). Several of the slip estimates are based on offsets of east-dipping planar or folded marker units. For east- to SE-dipping markers, significant SW-down motion across a NW-striking strike-slip fault will increase the right separation. We discuss the impact of possible vertical components of slip above and show that impacts are small to modest.

Clark Fault

Lifetime Slip Rate. When the lifetime slip across the Santa Rosa segment of the Clark fault of 16.8 +3.7/–6.0 km (Forand, 2010) is divided by the preferred age of 1.05 Ma (and plausible age between 1.0 and 1.3 Ma, (Table 2), it yields a slip rate between 8.3 and 20.5 mm/yr. The preferred and most likely value is 16.0 +4.5/–7.7 mm/yr across the Clark fault since the early Pleistocene. The unequal positive and negative errors reported here (see Table 2) result from dividing a displacement estimate with an uncertainty by an age with its own uncertainty and from the geologic constraints that rule out symmetric projections of the marker succession toward the fault (Figs. 3 and 5). Slip-rate estimates that report equal error bars assume that either age or displacement is perfectly known.

The lifetime slip rate across the Clark fault of 16.0 +4.5/–7.7 mm/yr is a slip rate for almost all of the displacement across the Buck Ridge, Santa Rosa, and Clark fault zones because the offset marker succession used to measure displacement is located east of the branch points between the Clark and Santa Rosa strands of the San Jacinto fault zone in the SE Santa Rosa Mountains. Minor offsets within the damage zone may be missing from this estimate.

Interval Slip Rate. We calculate a post–0.55 Ma slip rate of >10.2 +7/–3 mm/yr across the Tarantula Wash segment of the Clark fault by assuming that >5.6 ± 0.4 km of right slip across the Clark fault produced closely spaced folds near the fault tips, and that folding began 0.55 ± 0.2 m.y. and continues today (Table 2 and Fig. 6) (Kirby, 2005). As noted above, the >5.6 ± 0.4 km

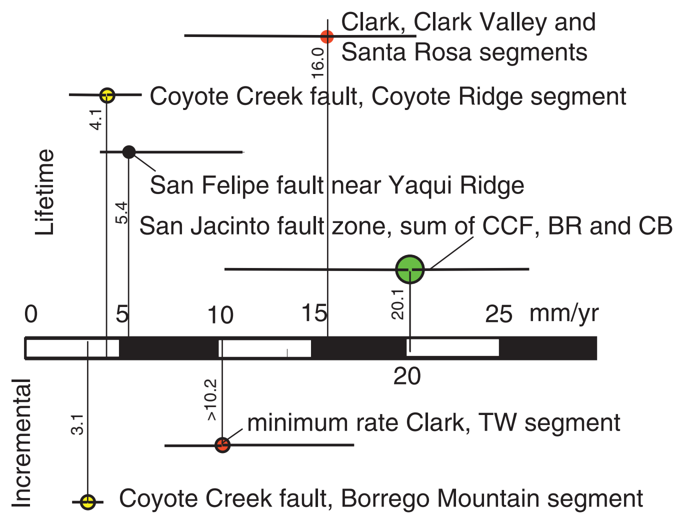

Figure 15. Graphical comparison of lifetime (top) and incremental (below) slip rates across segments of faults of the San Jacinto and San Felipe fault zones. See Table 2 for additional data. CCF—Coyote Creek fault; BR—Buck Ridge; CF—Clark fault; TW—Tarantula Wash.

estimate of right slip is a minimum because it does not include deformation in the NE part of the Clark fault zone, the strain from one of the Tarantula Wash segment's largest dextral faults (San Felipe Hills fault), block rotation, or blind deformation (Figs. 3 and 6). Slip across the San Felipe Hills fault cannot be quantified because some of the folding at the tip of the San Felipe Hills fault overlaps spatially with folding produced earlier in the Pleistocene San Felipe anticline (Fig. 3).

It is possible that tight folding at the tips of fault strands in the Tarantula Wash segment spanned less than ~0.5–0.6 m.y., perhaps only 0.5–0.3 m.y., because late Pleistocene pediment-related deposits are much less folded than the Brawley and Ocotillo formations within the Clark fault zone and because folding may not have initiated immediately after the end of Brawley deposition. It is also plausible that tight folding began right above the Clark fault zone before the end of deposition of the Brawley Formation, and later spread outward from the central fault strands in a manner depicted in the analog models of (Figs. 3, 11, and 14; Richard et al., 1989). Because no deposits of the Brawley Formation are preserved directly above the central strands of the Clark fault zone in the Tarantula Wash segment, we applied a large uncertainty of 0.2 m.y. to the duration of the tight folding (0.55 ± 0.2 Ma).

The resultant slip rate of >10.2 +7/−3 mm/yr across the Tarantula Wash segment of the Clark fault since ca. 0.55 Ma underestimates the slip rate because it is likely that some strain is taken up by distributed faulting and block rotation that cannot currently be quantified. In addition, some of the displacement across the Clark fault may still be focused in crystalline rocks at depth. We do not know the proportion of the strain that has propagated to the surface into folds and faults and the proportion localized at depth in the SE part of the Tarantula Wash segment of the Clark fault.

Coyote Creek Fault

Lifetime Slip Rate. Total slip across the Coyote Creek fault in the Coyote Ridge segment is well constrained at 3.5 ± 1.3 km, based on correlation of a distinctive biotite-hornblende–bearing tonalite and its wall rocks (as explained above). Four kilometers of displacement of some of the same contacts were reported by Sharp (1967), and this value was reduced slightly to 3.5 ± 1.3 km by our more detailed mapping and correlation across the fault. Dividing the plausible range of displacements (2.2 km to 4.8 km) by the age of the fault (0.8–1.1 Ma) yields a lifetime slip rate of 4.1 +1.9/−1.7 mm/yr (Table 2). This is a significant reduction from the prior estimate (10 mm/yr, Dorsey, 2002) (Figs. 15 and 16).

Interval Slip Rates. Along the Borrego Mountain and Borrego Badlands segments, we calculate a minimum interval slip rate across the Coyote Creek fault zone of >3.8 ± 1.2 mm/yr since creation of this part of the fault zone at ca. 0.6 Ma (Table 1). This interval slip rate of >3.8 ± 1.2 mm/yr overlaps with the lifetime rate of 4.1 +1.9/−1.7 mm/yr calculated along the Coyote Creek fault in the Coyote Ridge segment (Table 2 and Fig. 15).

San Felipe Fault Zone

The San Felipe fault zone near Pinyon Ridge has between 4 and 12.4 km of right slip, with 6.5 km being our preferred estimate (Fig. 12). This is more displacement than across most of the central and southern Elsinore fault (~2–3 km), all of the Coyote Creek fault, and all of the Earthquake Valley fault (which displaces a pluton margin ~2.5–3 km) (Rogers, 1965; Todd, 1977, 2004; this study; Magistrale and Rockwell, 1996). The San Felipe fault zone may carry much of the extra 8–9 km of displacement across the NW end of the Elsinore fault (McCulloh et al., 2000; Langenheim et al., 2006) that does not persist to the central and SE Elsinore fault zone, as suggested by Magistrale and Rockwell (1996). In their model, slip across the NW Elsinore fault is transferred onto the SE San Jacinto fault zone by the San Felipe fault zone. More data are required to test this hypothesis.

Right slip has accumulated across the contractional Pinyon Mountain and Mescal Bajada segments of the San Felipe fault zone since ca. 1.1–1.3 Ma (Steely, 2006), indicating a lifetime right slip rate of ~5.4 +5.9/−1.4 mm/yr. Such a high lifetime slip rate is unexpected for a fault with no documented Holocene fault scarps and no microseismicity (Steely, 2006; Lin et al., 2007; Table 2). The San Felipe fault is not currently included in compilations of active faults in southern California (e.g., Southern California Earthquake Center and U.S. Geological Survey fault databases (http://www.data.scec.org/faults/sofault.html; http://earthquake.usgs.gov/regional/qfaults/ca/sta.html) nor in the Working Group's report (http://www.wgcep.org/), yet it is unequivocally an active Quaternary fault zone that has produced surface ruptures in the past (Steely, 2006; Steely et al., 2009; this study).

The small number of Quaternary fault scarps on the Fish Creek Mountains and Sunset faults relative to other parts of the San Felipe fault zone around Mescal Bajada and Pinyon Ridge (and southward near Whale Peak) (Kairouz, 2005; Steely, 2006; Steely et al., 2009; this study) are consistent with more latest Quaternary activity on extensional parts of the San Felipe fault zone than on the contractional stepover near Yaqui Ridge. Alternation of activity levels and switching between extensional connector faults and contractional steps of the San Felipe fault zone could produce this pattern, in a manner grossly similar to that proposed by Bennett et al. (2004) for the San Andreas and San Jacinto fault zones, and by Dolan et al. (2007) for the San Andreas, Eastern California shear zone, and Garlock fault systems. Whatever the process, it must produce slip rates in the latest Quaternary that are much lower than the lifetime average across the San Felipe fault zone.

Total Lifetime Slip Rate across the San Jacinto Fault Zone

Addition of the lifetime slip rate across the Clark fault and Buck Ridge–Santa Rosa faults in the Santa Rosa segment (16.0 +4.5/−7.7 mm/yr) and the nearby Coyote Ridge segment of the Coyote Creek fault (~4.1 +1.9/−1.7 mm/yr) yields a time-averaged slip rate of 20.1 +6.4/−9.4 mm/yr across most of the San

Jacinto fault zone at the western edge of the Salton basin (Table 2). Future field studies may increase these estimates slightly, if unquantified dextral slip across the Henderson Canyon fault is significant, and if it can be confirmed that there is roughly 1–2 km of right slip across one to three faults between the Clark and Coyote Creek fault in the Coyote Mountain area (Forand, 2010).

Our calculated lifetime geologic rate of 20.1 +6.4/–9.4 mm/yr approaches or exceeds slip rates determined for the southern San Andreas fault since the late Pleistocene (e.g., compare to van der Woerd et al., 2006; Lundgren et al., 2009; Behr et al., 2010) and overlaps with the faster group of prior estimates for the San Jacinto fault zone (Table 1). Our finding of a high long-term slip rate across the San Jacinto fault zone may suggest that the frequency of large earthquakes could be greater than that predicted when one only considers the Holocene rates from paleoseismic and neotectonic studies—provided that the fault zone had a grossly time-invariant slip rate (but see below).

The Coyote Creek fault has a low lifetime slip rate of ~4.1 +1.9/–1.7 mm/yr at Coyote Ridge (Table 2). This rate is low in absolute value and low when compared with that of the Clark fault nearby (16.0 +4.5/–7.7 mm/yr) (Table 2). This rate is also low (but within uncertainty) when compared with a recent inversion of InSAR and GPS data, which show a slip rate of 12 ± 9 mm/yr across the Coyote Creek fault (Lundgren et al., 2009). It is lower

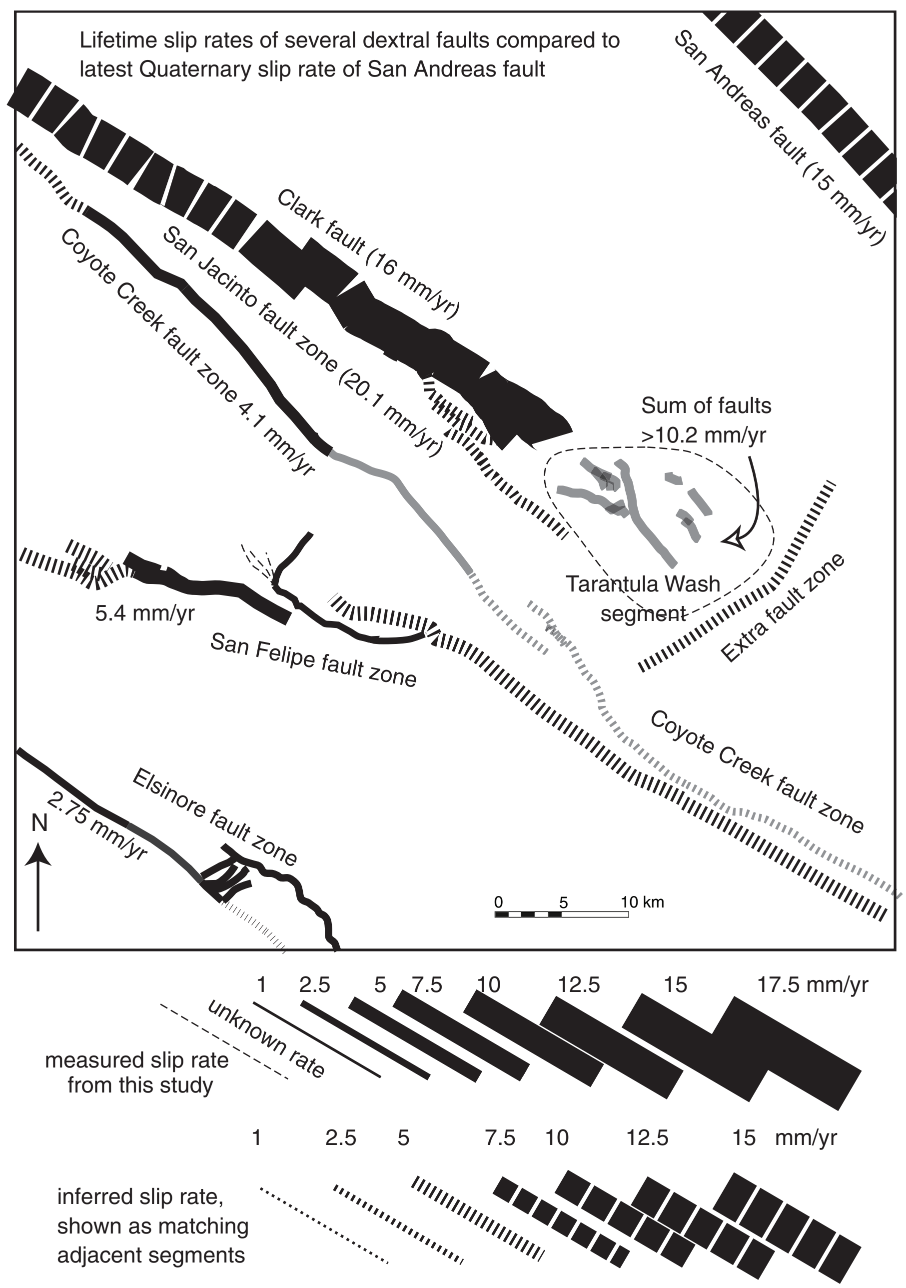

Figure 16. Map showing slip rates from this study as line width. Lifetime slip rates in black are shown for the relevant structural segments. Adjacent segments, where the slip rate is not known, are plotted with the same slip rate and a dashed line. Incremental slip rates are gray. San Andreas fault is shown with a slip rate of 25 mm/yr in accordance with Fialko (2006), but its slip rate is controversial in this area (Table 1). Fault traces are greatly simplified from Figure 3.

than a preliminary paleoseismic rate of 6 mm/yr from the Borrego Mountain segment of the fault (Verdugo et al., 2006).

Comparison of Slip Rates

In the Salton Trough the Coyote Creek fault has a more continuous and well-defined trace than the Clark fault, despite much greater displacement across the Clark fault (~16.8 +3.7/–6.0 km versus ~1–5 km) (Table 1). The Clark fault zone widens to >18 km in the Salton basin, and its fault traces radiate >90° in the Arroyo Salada and Tarantula Wash segments (Belgarde, 2007; Janecke and Belgarde, 2007, 2008), whereas the maximum width of the Coyote Creek fault zone is ~8 km where the Veggie Line and Squaw Peak faults in the Borrego Badlands and Borrego Mountain segments of the Coyote Creek fault zone accommodate some displacement. The fault zone is ~5.5–7 km wide in the Superstition Mountain and Superstition Hills faults, but nowhere does its width approach that of the Clark fault zone in the Arroyo Salada and Tarantula Wash segments (Figs. 1–3).

The Coyote Creek fault zone has nucleated more M>6 earthquakes in historic time and has experienced creep events during regional earthquakes, whereas the Clark fault has not (Sharp, 1972a, 1972b, 1982; Sharp and Clark, 1972; Clark, 1972; Sanders, 1989; Hudnut and Clark, 1989; Hudnut et al., 1989; Rymer et al., 2002; Rymer, 2000). Oddly, the slightly younger, slower, and more seismically active Coyote Creek fault has the more "mature-looking" and continuous fault trace than the slightly older and much faster Clark fault within the Salton basin. Concepts of fault simplification with increased age (Wesnousky, 1990; Stirling et al., 1996) do not predict these relationships. We caution against applying these conceptual models to all fault zones, particularly in areas like the Salton Trough and Peninsular Ranges where abundant cross faults continually roughen the adjacent master faults as they interact. Inheritance may also contribute to the complex geometry of the fault zone (Langenheim et al., 2004).

The lifetime slip rate across the San Felipe fault zone of ~5.4 +5.9/–1.4 mm/yr is unexpectedly high. It is roughly twice that of the southern Elsinore fault (2.5–3 mm/yr = 2.5 km/0.9 Ma; Rockwell et al., 1990), twice the rate of the Coyote Creek fault near Borrego Mountain (>2.5. to 3.3 mm/yr), and greater than the rate on the Coyote Creek fault along the Coyote Ridge segment (4.1 +1.9/–1.7 mm/yr, Table 2). Our analysis of the San Felipe fault clearly shows that lesser known faults have accommodated significant strain during the past 1–1.5 Ma. Such faults can have high lifetime slip rates, are active, and appear to have variable slip rates during their lifetimes. Thus they have the potential to produce large future earthquakes, possibly similar to the 1992 Landers earthquakes in magnitude and character (Sieh et al., 1993; Spotila and Sieh, 1995; Zachariasen and Sieh, 1995).

No GPS-based or InSAR-based analysis has considered the San Felipe fault zone explicitly, but it is plausible that some of the strain accumulation recorded in the area by Lundgren et al. (2009) is localized on the San Felipe fault zone. We speculate that the decadal slip rate (12 ± 9 mm/yr) interpreted across the Coyote Creek fault by Lundgren et al. (2009) is due to the addition of strain adjacent to *both* the Coyote Creek and San Felipe fault zones. These two faults lie within 1–20 km of one another in the area of Lundgren et al.'s (2009) analysis, and resolving strain onto separate San Felipe and/or the Coyote Creek faults may require higher resolution of data than is currently available. The sum of the lifetime slip rates across the Coyote Creek and San Felipe fault zones of 9.5 +7.8/–3.7 mm/yr (Table 2) overlaps Lundgren et al.'s (2009) loading rate of 12 ± 9 mm/yr.

It is challenging to compare our geologic slip rates with prior results because of the large range of GPS-based, paleoseismic, neotectonic, and geologic slip estimates for the San Jacinto fault zone over different periods of observation and using different methods (Table 1). Paleoseismic and neotectonic studies have documented Holocene slip rates as low as 1 mm/yr and as high as 23 mm/yr near Anza and along the Coyote Creek fault (Table 1). The possibility that up to 75% of dextral strain is localized in deforming rocks in the damage zone next to principal slip surfaces—as it is in the Arroyo Salada and Tarantula Wash segments of the Clark fault (e.g., Sieh, 1984; Salyards et al., 1992; Weldon et al., 2002; Rockwell et al., 2002; Shelef et al., 2006; this study), and the very distributed pattern of active faulting along both the San Felipe and San Jacinto fault zones (Figs. 2, 3, and 6)—could introduce a bias toward lower slip rates in paleoseismic and neotectonic studies that sample only the central parts of a deforming fault zone (Table 1). Because there is a tendency for most (but not all, e.g., Verdugo et al., 2006) paleoseismic and neotectonic slip rates to be lower than rates determined using other methods (e.g., Tables 1–3), this bias might be real.

GPS-based slip rates measure the elastic strain that might also accumulate as permanent strain in damage zones. Therefore GPS-based slip rates may have a bias toward higher slip rates than paleoseismic studies, provided that significant permanent slip is localized in damage zones adjacent to the main slip surfaces. Inversions of GPS data depend critically on the model parameters, so some differences are expected between our lifetime geologic slip rates and GPS-based estimates. It is noteworthy that a recent integrated GPS and InSAR inversion yielded a modern slip rate of 19–21 mm/yr across the San Jacinto fault zone (Fialko, 2006), which is indistinguishable from the lifetime rate determined here. This comparison suggests the possibility of relatively uniform slip rates through time. Other comparisons are more suggestive of changing slip rates through time.

Prior geologic analyses have produced slip-rate estimates that are among the highest of the different methods (>20 mm/yr). These have very large uncertainties and are controversial (Table 1) (Morton and Matti, 1993; Matti and Morton, 1993; Kendrick et al., 2002). Inversions of InSAR and GPS data sets have produced inconsistent slip-rate values, ranging from low values of 9 ± 2 mm/yr (e.g., Bennett et al., 1996) to high values of 24 ± 18 mm/yr (e.g., Fialko, 2006; Lundgren et al., 2009) despite analysis of similar data sets in some instances (Table 1). Our results overlap within error with the majority of prior results from geologic and GPS analyses and with few of the paleoseismic and neotectonic interpretations (Table 1) (Morton and Matti, 1993; Kendrick et al., 2002; Anderson et al., 2003; Fialko, 2006; Rockwell et al., 2006). From these data sets one could posit many different time-varying, spatially varying, or even steady-state slip-rate models without a compelling reason to favor one over another. Clearly more analyses and detailed studies at different time scales and spatial scales are needed before such comparisons become robust, especially in light of the extreme structural complexity that we documented along these fault zones.

Variation of Slip Rates in Time and Space?

Long-term geologic slip rate is an especially critical parameter because any discrepancy between it and shorter-term slip rates suggests changes in slip rate through time. Furthermore, it is important to document whether the high slip rates calculated over the lifetime of faults in southern California have been steady since their initiation, experienced more random temporal variations, or perhaps had systematic, co-varying changes in slip rate such as those hypothesized by Bennett et al. (2004) and Dolan et al. (2007). Steady slip rates greatly simplify hazard analyses and estimation of seismic risk because slip rates calculated over different time intervals should be the same. We therefore examined our data set, prior estimates, each fault's structural evolution, along with empirical and theoretical data from other faults (Table 2), before concluding that the data are most consistent with changing slip rates over time.

Some of the rates in Table 2 are suggestive of changing slip rates over time. The San Felipe fault zone produced a high lifetime slip rate of ~5.4 +5.9/–1.4 mm/yr, yet the fault appears to be much less active since the late Pleistocene (Steely, 2006; Steely et al., 2009; this study). Further analysis of recently discovered fault scarps along the San Felipe fault zone is needed to assess its activity level in the latest Quaternary and to test our impression of a current low slip rate (Steely, 2006). We are confident, however, that the fault zone is not slipping anywhere near the overall lifetime average rate (i.e., there has been much less than 540 m of right slip in the past 100,000 years). This must be due to a recent decrease in slip rate. Possible causes are speculative but include a broadening of the fault zone as the contractional stepover at Yaqui Ridge locked up. There are numerous active faults that bypass this zone north and south of Yaqui Ridge (Fig. 3; Steely et al., 2009; this study) and persistent microseismicity angling northeast across Pinyon Ridge (Lin et al., 2007) could be part of this growing fault system. Transfer of strain onto the left-lateral Hell Hole Canyon fault and then to active west-northwest–striking faults north of Yaqui Ridge may be part of the expansion of the fault zone laterally. The newer fault strands branch north from the main central traces of the San Felipe fault zone along the northwest end of Grapevine Canyon and southward near the confluence of Grapevine Canyon and San Felipe Wash (Figs. 2 and 3). Both fault systems merge back with the central strands of the San Felipe fault zone east of Yaqui Ridge along the Fish Creek Mountains fault. Alternatively, the San Felipe fault zone has been complex and broad since it formed, and the slowing latest Quaternary slip rates on its central strands reflect simple changes in slip rate with time.

The low slip rates reported by Le et al. (2008) and Blisniuk et al. (2010) across individual fault strands in the Clark and Coyote Creek fault zones, when combined with our data, also require changing slip rates with time, as long as their study sites captured enough of the widely distributed strain of the San Jacinto fault zone (Figs. 2 and 3; Belgarde, 2007; Janecke and Belgarde, 2008; Forand, 2010; Janecke et al., 2010) to be representative of its latest Quaternary slip rates. Regardless of these important details, the San Felipe and Clark fault zones both appear to show reductions in slip rate through time. Temporal changes in slip rate are also recorded in the latest Quaternary data sets along identical strands of the fault zone (Blisniuk et al., 2009).

The available data along the Coyote Creek fault zone (Table 2) are more consistent with steady slip rates because the lifetime and ca. 0.5-Ma slip rates overlap within errors. The uncertainties are large, however, and there are preliminary Holocene slip rates along the Coyote Creek fault that are higher (6 mm/yr during the past 1200 years; Verdugo et al., 2006) than either the incremental (>3.8 ± 1.2 mm/yr since 0.6 Ma) or lifetime (4.1 +1.9/–1.7 mm/yr since 0.9–0.8 Ma) slip rate determined here. Verdugo et al.'s (2006) 6 mm/yr estimate and our >3.8 mm/yr lifetime slip rates are from the same rupture segment of the Coyote Creek fault and might therefore record a meaningful acceleration of slip in the Holocene.

The complex and evolving structural history of the Clark, Coyote Creek, and San Felipe fault zones is much more likely to produce time-varying deformation rates on individual faults than constant slip rates. We believe it is unlikely that slip rates were steady along these fault zones through time because all three faults experienced major, deeply penetrating structural adjustments since their initiation. These changes include the addition of new fault segments (Borrego Mountain, Borrego Badlands, and segments of the Coyote Creek fault), blind fault segments that propagated to the surface during this time, fault geometries that produced different types of folds at different stages of development, and even reversals of the dip-slip component of deformation (Table 4).

Major structural changes affected every dextral fault in our study in the Pleistocene (Fig. 11). The San Felipe fault zone illustrates the changes in fault geometry particularly well. Sediment accumulated NE of the Sunset fault during the first half of its history, then after ca. 0.6 Ma this stepover experienced uplift and exhumation and additional shortening (Steely et al., 2009). More recently, the slip rate on the main central segments has decreased, and there is a suggestion that additional faults north and south of Yaqui Ridge are expanding the fault zone up to ~8 km in width. The Tarantula Wash segment of the Clark fault also evolved from a blind fault with a broad flat-topped anticline above its trace at ca. 1.1 Ma (perhaps like Fig. 14A), to a surface-breaking fault in the NW half of the segment. After ca. 0.5–0.6 Ma, dozens of closely spaced detachment folds and discontinuous strike-slip, normal and thrust faults formed in the SE half (as in Fig. 14B; Belgarde, 2007; Kirby et al., 2007).

The Coyote Creek fault initiated and produced a central fault-parallel graben along the Coyote Ridge segment that accumulated ~150 m of sediment with little tilting. Subsequent adjustments initiated a major tilting episode that was followed at ca. 0.3–0.4 Ma by uplift and exhumation of the sedimentary rocks within the fault zone (Fig. 6; Dorsey, 2002). The Borrego Badlands and Borrego Mountain segments of the Coyote Creek fault did not exist before ca. 0.6 Ma (Lutz et al., 2006), and strain may have been accommodated instead by the Veggie Line–Henderson Canyon fault, the San Felipe anticline, and the Extra fault (Fig. 14 and Table 4). Later the Borrego Badlands and Borrego Mountain segments formed and cut across the early and middle Pleistocene San Felipe anticline. These were major adjustments, and it is highly unlikely that slip rates could have been uniform across individual faults and fault segments within such evolving and changing fault zones. Faults are fractal (Okubo and Aki, 1987), and we predict that unsteady changes in slip rate also characterize these fault zones at the 100-k.y., 10-k.y., and 1-k.y. time scale as they respond to smaller geometric and structural adjustments than the ones documented here.

Changes in slip rate and clustering of events have been documented along the San Andreas fault (Weldon et al., 2004; Dolan et al., 2007), the Clark fault, and the Coyote Creek fault at multiple sites (Middleton, 2006; Rockwell et al., 2006; Blisniuk et al., 2009). The northern San Andreas fault system near San Francisco Bay has also experienced major changes in activity within its fault array (Graymer et al., 2002). There "activity on any single fault zone in the system has been sporadic, and alternating periods of activity and inactivity have been recorded on at least some of the fault zones" (Graymer et al., 2002, p. 1471). Parts of the Garlock fault appear to vary temporally in their activity level (Meade and Hager, 2005). Fault and fold patterns in the Mecca Hills and Durmid Hill show that the southern San Andreas fault also has old fault strands that likely resulted in rate changes as the fault system changed from one fault system to another and possibly back again (Sheridan and Weldon, 1994; Janecke, unpublished mapping).

Theoretical and empirical analyses also predict time-varying slip rates along fault zones. Slip rates can be expected to vary in time as a result of earthquake clustering, progressive changes in recurrence times, geometric complexities and reorientation of faults over geologic time scales, viscoelastic effects, and/or blind slip (Bennett et al., 2004; Becker et al., 2005; Dolan et al., 2007). Climate can drive tectonic processes and climate systems cycle at many different time scales (Montgomery et al., 2001). Suppressed or increased slip rates due to lithospheric rebound and loading and unloading by distant continental ice sheets or by Lake Cahuilla may produce transients in the deformation field much as flexure due to highstands of Lake Bonneville nearly stalled the Wasatch Fault during the last glacial and pluvial (Hampel and Hetzel, 2006; Luttrell et al., 2007). All these processes influence slip rates. Thus fault slip rates that are measured on different fault segments over different time periods, during different climate regimes, and within a network of evolving and interacting faults, are unlikely to be constant through time. Accordingly, it is potentially misleading to predict the age of a fault by dividing its total displacement by a slip rate determined from a short period of time, as has been done for many years in the San Jacinto and Elsinore fault zones (e.g., Blisniuk et al., 2010).

Implications for the Southern San Andreas Fault System

The southern San Andreas fault was the main large strike-slip fault in southern California prior to early Pleistocene initiation of the San Jacinto, San Felipe, and other dextral faults farther to the southwest. This major reorganization expanded the southern San Andreas fault system to its current width of 75–80 km (San Andreas to Elsinore fault) from a width of roughly 20–30 km (San Andreas and West Salton detachment faults). Assessing the timing of this reorganization, and the amount of Pacific–North American strain that is no longer localized on the main strand of the San Andreas fault system has profound implications for seismic hazards, fault kinematics, and evolving plate boundary. We predict that studies along the San Andreas fault in Coachella Valley and near San Bernardino will show that slip rates there decreased by roughly half in the early Pleistocene when the San Jacinto and San Felipe fault initiated. Together the San Jacinto and San Felipe fault zones have accommodated slightly more plate motion (~25.5 mm/yr) than the southern San Andreas fault since their inception at ca. 1.1–1.3 Ma. If the westward transfer of plate motion continues in southern California, the southern San Andreas fault in the Salton Trough may change from being the main plate boundary fault to defining the eastern margin of the growing Sierra Nevada microplate, as suggested by Meade and Hager (2005). The transformation of the southern San Andreas fault, south of the Transverse Ranges, from the principal plate boundary fault to the southern section of the Eastern California shear zone is a major change that will transform the dynamics of the fault network. Alternatively, if switching of activity between the San Andreas and Eastern California shear zone fault systems occurs regularly (Dolan et al., 2007), very different dynamics are predicted. Further research into the past behavior of the southern San Andreas fault, south of the Transverse Ranges, may illuminate this question. The early Pleistocene reorganization of faults that we document along the San Jacinto and San Felipe fault zones is now known to have affected the entire Salton Trough–Gulf of California corridor from Cajon Pass south to the Alarcon ridge (~1500 km long) and is the subject of current research (Janecke and DeMets, 2010).

CONCLUSIONS

This study documents early Pleistocene (ca. 1.3–1.0 Ma) initiation of the San Jacinto and San Felipe fault zones in the western Salton Trough, where they cross-cut the West Salton detachment fault and its supradetachment basin. The earliest pulses of gravel input from different segments of the Clark and Coyote Creek fault zone range in age from ca. 0.9 to ca. 1.1 Ma, recording onset of fault activity at that time. We consider a possible short lag time of 0.2 m.y. that could increase the age of the fault zones to ca. 1.3 Ma. The Borrego Mountain and Borrego Badlands structural segments of the Coyote Creek fault probably developed after ca. 0.6 Ma and accumulated ~2.3 km of right slip. Initiation of the San Felipe fault zone at 1.3–1.1 Ma resulted in uplift of the large Fish Creek–Vallecito Mountains fault block and progradation of alluvial gravel and sand (Ocotillo and Brawley formations) ~25 km northeast across the former perennial Borrego Lake.

Total lifetime slip rates across segments of the San Jacinto and San Felipe fault zones sum to >25.5 +12.6/–9.3 (Table 2). This sum exceeds all reported slip rates from the southern San Andreas fault. Our analysis thus shows that starting in early Pleistocene time more than half of the Pacific–North American plate motion shifted southwestward from the northeast margin of the Salton Trough into the Peninsular Ranges and central-western Salton Trough. Discrepancies between lifetime, minimum, 0.5-m.y., paleoseismic, neotectonic, and geodetic slip rates reveal a general lack of consensus regarding the distribution of slip rates across the southern San Andreas fault system in space and time, and show that our understanding of this system is incomplete at most time scales.

The modern geometries and kinematics of the San Felipe and San Jacinto fault zone did not develop until after the end of Ocotillo and Brawley deposition at ca. 0.6–0.5 Ma, and these faults have continued to change and evolve to the present. Despite the young age of the San Jacinto fault zone (1.1–1.3 Ma), it has already undergone one major structural adjustment, formed and abandoned a major basement-cored anticline, created and then largely bypassed a subsidiary fault, and changed its dominant style of folding in the Salton Trough. Although the five slip rates reported here for segments of the San Felipe and San Jacinto fault zones can be interpreted in different ways, the compelling evidence for episodic and changing deformational styles is more consistent with time-varying slip rates since the early Pleistocene than with steady-state models. The lifetime slip rates across the San Jacinto fault zone exceed most previous short-term estimates from paleoseismologic analyses but are consistent with higher rates based on GPS, triangulation, and long-term geologic rates to the northwest. Some of the difference could be due to off-fault damage that is not sampled by some paleoseismic studies. Changing fault geometries probably changed slip rates many times within this complex mash of faults.

ACKNOWLEDGMENTS

We thank the National Science Foundation (NSF), the Petroleum Research fund of the American Chemical Society, the Southern California Earthquake Center, and the National Earthquake Hazard Reduction Program of the U.S. Geological Survey for providing funding. Grants from Geological Society of America, American Association of Petroleum Geologists, J.S. Williams fund, and NSF Advance program assisted various authors. Special thanks to Eric Mustonen for making the last few field seasons the most luxurious ever. We appreciate input, data, and help of many individuals including: Gary Axen, Jerry Bartholomew, Ronald Blom, Brett Cox, Robert Crippen, Jim Evans, Gary Girty, George Jefferson, Susan Kidwell, Eric Layman, Jon Matti, David Okaya, Jarg Pettinga, Tom Rockwell, Peter Shearer, and Charlie Winker. Tom Rockwell and his Neotectonics class at San Diego State University mapped an important strand of the Coyote Creek fault SE of the Ocotillo Badlands, and we thank them for sharing its location with us for inclusion in Figure 3.

REFERENCES CITED

Albright, L.B., 1999, Magnetostratigraphy and biochronology of the San Timoteo Badlands, southern California, with implications for local Pliocene–Pleistocene tectonic and depositional patterns: Geological Society of America Bulletin, v. 111, p. 1265–1293, doi: 10.1130/0016-7606(1999)111<1265:MABOTS>2.3.CO;2.

Allen, C.R., and Nordquist, J.M., 1972, Foreshock, main shock and larger aftershocks of the Borrego Mountain earthquake in The Borrego Mountain Earthquake of April 9, 1968: U.S. Geological Survey Professional Paper 787, U.S. Government Printing Office, p. 16–23.

Allen, C.R., Silver, L.T., and Stehli, F.G., 1960, Agua Blanca fault—A major transverse structure of northern Baja California, Mexico: Geological Society of America Bulletin, v. 71, no. 4, p. 467–482, doi: 10.1130/0016-7606(1960)71[467:ABFMTS]2.0.CO;2.

Allen, P.A., and Densmore, A.L., 2000, Sediment flux from an uplifting fault block: Basin Research, v. 12, p. 367–380, doi: 10.1046/j.1365-2117.2000.00135.x.

Anderson, G., Agnew, D.C., and Johnson, H.O., 2003, Salton Trough regional deformation estimated from combined trilateration and survey-mode GPS data: Bulletin of the Seismological Society of America, v. 93, p. 2402–2414, doi: 10.1785/0120030014.

Axen, G.J., and Fletcher, J.M., 1998, Late Miocene–Pleistocene extensional faulting, northern Gulf of California, Mexico and Salton Trough, California: International Geology Review, v. 40, p. 217–244, doi: 10.1080/00206819809465207.

Axen, G.J., Janecke, S., Steely, A., Shirvell, C., Fluette, A., Kairouz, M., Housen, B., Stockli, D., Dorsey, R., and Grove, M., 2006, The West Salton detachment fault, Salton Trough, California: A primary low-angle normal fault in an evolving dextral wrench zone: Eos (Transactions, American Geophysical Union), v. 87, no. 52, Fall Meeting Supplement, abstract T41D-1602, http://www.agu.org/meetings/fm06/waisfm06.html.

Bartholomew, M.J., 1970, San Jacinto fault zone in the northern Imperial Valley, California: Geological Society of America Bulletin, v. 81, no. 10, p. 3161–3166, doi: 10.1130/0016-7606(1970)81[3161:SJFZIT]2.0.CO;2.

Becker, T.W., Hardebeck, J.L., and Anderson, G., 2005, Constraints on fault slip rates of the southern California plate boundary from GPS velocity and stress inversions: Geophysical Journal International, v. 160, p. 634–650, doi: 10.1111/j.1365-246X.2004.02528.x.

Behr, W.M., Rood, D.H., Fletcher, K.E., Guzman, N.E., Finkel, R., Hanks, T.C., Hudnut, K.W., Kendrick, K.J., Platt, J.P., Sharp, W.D., Weldon, R.J., and Yule, J.D., 2010, Uncertainties in slip rate estimates for the Mission Creek strand of the southern San Andreas fault at Biskra Palms oasis: Southern California: Geological Society of America Bulletin, v. 122, p. 1360–1377, doi: 10.1130/B30020.1.

Belgarde, B.E., 2007, Structural characterization of the three southeast segments of the Clark fault, Salton Trough, California [M.S thesis]: Utah State University, 4 plates, map scale 1:24,000, 216 p.

Belgarde, B.E., and Janecke, S.U., 2006, Structural characterization and microseismicity near the SE end of the Clark fault of the San Jacinto fault zone in the SW Salton Trough: Palm Springs, California, Annual Meeting of the Southern California Earthquake Center, v. 16, p. 75, http://www.scec.org/meetings/2006am/.

Belgarde, B.E., and Janecke, S.U., 2007, A "hidden" fault? Structural geology of three segments of the Clark fault, San Jacinto fault zone, California: Geological Society of America Abstracts with Programs, v. 39, no. 6, p. 375, http://gsa.confex.com/gsa/2007AM/finalprogram/abstract_129101.htm.

Bennett, R., Rodi, W., and Reilinger, R., 1996, Global Positioning System constraints on fault slip rates in southern California and northern Baja, Mexico: Journal of Geophysical Research, v. 101, B10, p. 21,943–21,960, doi: 10.1029/96JB02488.

Bennett, R.A., Friedrich, A.M., and Furlong, K.P., 2004, Codependent histories of the San Andreas and San Jacinto fault zones from inversion of fault displacement rates: Geology, v. 32, p. 961–964, doi: 10.1130/G20806.1.

Biehler, S., and Rothstein, D., compilers, 1979, Salton Sea sheet of Bouguer gravity map of California: Sacramento, California Division of Mines and Geology, scale 1:250,000.

Blisniuk, K., Oskin, M.E., Fletcher, K., Sharp, W.D., and Rockwell, T.K., 2009, ^{10}Be and U-series dating of late Quaternary landforms along the southern San Jacinto fault: Implications for temporal slip rate variability: American Geophysical Union, Fall Meeting 2009, abstract T21D-1861.

Blisniuk, K., Rockwell, T., Owen, L.A., Oskin, M., Lippincott, C., Caffee, M.W., and Dortch, J., 2010, Late Quaternary slip rate gradient defined using high-resolution topography and ^{10}Be dating of offset landforms on the southern San Jacinto Fault zone, California: Journal of Geophysical Research, v. 115, B08401, 11 p., doi: 10.1029/2009JB006346.

Brown, N.N., Fuller, M.D., and Sibson, R.H., 1991, Paleomagnetism of the Ocotillo Badlands, Southern California, and implications for slip transfer through an antidilational fault jog: Earth and Planetary Science Letters, v. 102, p. 277–288, doi: 10.1016/0012-821X(91)90023-B.

Buddington, A.F., 1959, Granite emplacement with special reference to North America: Geological Society of America Bulletin, v. 70, no. 6, p. 671–747, doi: 10.1130/0016-7606(1959)70[671:GEWSRT]2.0.CO;2.

Christie-Blick, N., and Biddle, K.T., 1985, Deformation and basin formation along strike-slip faults, *in* Biddle, K.T., and Christie-Blick, N., eds., Strike-Slip Deformation, Basin Formation, and Sedimentation: Society of Economic Paleontologists and Mineralogists Special Publication 37, p. 1–35.

Clark, M.M., 1972, Surface rupture on the Coyote Creek fault, in the Borrego Mountain Earthquake of April 9, 1968: U.S. Geological Survey Professional Paper 787, p. 55–86.

Crowell, J.C., 1974, Origin of late Cenozoic basins in southern California, *in* Dott, R.H., and Shaver, R.H., eds., Modern and Ancient Geosynclinals Sedimentation: Society of Economic Paleontologists and Mineralogists Special Publication 19, p. 292–303.

Crowell, J.C., ed., 2003, Evolution of Ridge Basin, Southern California: An Interplay of Sedimentation and Tectonics: Geological Society of America Special Paper 367, 247 p.

Dibblee, T.W., Jr., 1954, Geology of the Imperial Valley region, California: Geology of southern California: California Division of Mines Bulletin, v. 170, p. 21–28.

Dibblee, T.W., 1984, Stratigraphy and tectonics of the San Felipe Hills, Borrego Badlands, Superstition Hills, and vicinity, *in* Rigsby, C.A., ed., The Imperial Basin—Tectonics, Sedimentation, and Thermal Aspects: Los Angeles, California, Pacific Section SEPM (Society for Sedimentary Geology), p. 31–44.

Dibblee, T.W., Jr., 1996, Stratigraphy and tectonics of the Fish Creek–Vallecito Mountains, Vallecito Badlands, Coyote Mountains, and Yuha Desert, southwestern Imperial basin, California, *in* Abbott, P.L., and Seymore, D.C., eds., Sturzstroms and Detachment Faults, Anza-Borrego Desert State Park, California: Santa Ana, California, South Coast Geological Society, Annual Field Trip Guidebook 24, p. 59–79.

Dolan, J.F., Bowman, D.D., and Sammis, C.G., 2007, Long-range and long-term fault interactions in southern California: Geology, v. 35, p. 855–858, doi: 10.1130/G23789A.1.

Dorsey, R.J., 2002, Stratigraphic record of Pleistocene initiation and slip on the Coyote Creek fault, lower Coyote Creek, southern California, *in* Barth, A., ed., Contributions to Crustal Evolution of the Southwestern United States: Geological Society of America Special Paper 365, p. 251–269.

Dorsey, R.J., 2006, Stratigraphy, tectonics, and basin evolution in the Anza-Borrego Desert region, *in* Jefferson, G.T., and Lindsay, L.E., eds., Fossil Treasures of Anza-Borrego Desert: San Diego, California, Sunbelt Publications, p. 89–104.

Dorsey, R.J., and Axen, G.J., 2009, End of detachment faulting and initiation of strike-slip faults at 1.0 Ma, western Fish Creek–Vallecito basin, southern California: Geological Society of America Abstracts with Programs, v. 41, no. 7, p. 138.

Dorsey, R.J., and Roering, J.J., 2006, Quaternary landscape evolution in the San Jacinto fault zone, Peninsular Ranges of southern California: Transient response to strike-slip fault initiation: Geomorphology, v. 73, no. 1–2, p. 16–32, doi: 10.1016/j.geomorph.2005.06.013.

Dorsey, R.J., Fluette, A.L., Housen, B.A., McDougall, K.A., Janecke, S.U., Axen, G.J., and Shirvell, C., 2006a, Chronology of late Miocene to early Pliocene sedimentation at Split Mountain Gorge, western Salton Trough: Implications for development of the Pacific–North America plate: Ensenada Mexico, Abstracts for National Science Foundation MARGINS Program, Workshop on Rupturing of Continental Lithosphere, January 9–13, http://rcl-cortez.nsf-margins.org/Workshop_Abstracts.pdf, p. 23–24.

Dorsey, R.J., Housen, B.A., Janecke, S.U., McDougall, K., Fanning, M., Fluette, A., Axen, G.J., Shirvell, C.R., 2006b, Chronostratigraphy of the Fish Creek–Vallecito Basin, SW Salton Trough: A high-fidelity record of slip on the West Salton detachment fault and subsidence in its upper plate: Eos (Transactions, American Geophysical Union), v. 87, no. 52, abstract T41D-1600.

Dorsey, R.J., Fluette, A., McDougall, K.A., Housen, B.A., Janecke, S.U., Axen, G.A., and Shirvell, C.R., 2007, Chronology of Miocene–Pliocene deposits at Split Mountain Gorge, southern California: A record of regional tectonics and Colorado River evolution: Geology, v. 35, p. 57–60, doi: 10.1130/G23139A.1.

Dorsey, R.J., Housen, B.A., Janecke, S.U., Fanning, M., and Spears, A.L.F., 2011, Stratigraphic record of basin development within the San Andreas fault system: Late Cenozoic Fish Creek–Vallecito basin, southern California: Geological Society of America Bulletin, doi: 10.1130/B30168.1 (in press).

Doser, D.I., 1990, Source characteristics of earthquakes along the southern San Jacinto and Imperial fault zones (1937 to 1954): Bulletin of the Seismological Society of America, v. 80, p. 1099–1117.

Dronyk, M.P., 1977. Stratigraphy, structure and a seismic refraction survey of a portion of the San Felipe Hills Imperial Valley, California. [M.S. thesis]: Riverside, California, University of California, 141 p.

Engel, A.E.J., and Schultejann, P.A., 1984, Late Mesozoic and Cenozoic Tectonic History of South Central California: Tectonics, v.3, no.6, p. 659–675.

Erskine, B.E., 1985, Mylonitic deformation and associated low-angle faulting in the Santa Rosa mylonite zone, southern California [Ph.D. thesis]: Berkeley, University of California, 247 p.

Fay, N.P., and Humphreys, E.D., 2005, Fault slip rates, effects of sediments and the strength of the lower crust in the Salton Trough region, Southern California: Journal of Geophysical Research, v. 110, B09401, doi: 10.1029/2004JB003548.

Feragen, E.S., 1986, Geology of the southeastern San Felipe Hills, Imperial Valley, California [M.S. thesis]: San Diego State University.

Fialko, Y., 2006, Interseismic strain accumulation and the earthquake potential on the southern San Andreas fault system: Nature, v. 441, p. 968–971, doi: 10.1038/nature04797.

Fletcher, J.M., Grove, M., Kimbrough, D., Lovera, O., and Gehrels, G.E., 2007, Ridge-trench interactions and the Neogene tectonic evolution of the Magdalena shelf and southern Gulf of California: Insights from detrital zircon U-Pb ages from the Magdalena fan and adjacent areas: Geological Society of America Bulletin, v. 119, p. 1313–1336, doi: 10.1130/B26067.1.

Forand, D.H., 2010, Examination of deformation in crystalline rock from strike-slip faults in two locations, southern California [M.S. thesis]: Logan, Utah State University, 286 p.

Frick, C., 1921, Extinct vertebrate faunas of the Badlands of Bautista Creek and San Timoteo Canyon, southern California: California University, Department of Geology Bulletin, v. 12, p. 277–424.

Fuis, G., Scheirer, D.S., Langenheim, V.E., and Kohler, M.D., 2007, The San Andreas fault in southern California is almost nowhere vertical—Implications for tectonics: Geological Society of America Abstracts with Programs, v. 39, no. 6, p. 279.

Gawthorpe, R.L., Sharp, I., Underhill, J., and Gupta, S., 1997, Linked sequence stratigraphic and structural evolution of propagating normal faults: Geology, v. 25, p. 795–798, doi: 10.1130/0091-7613(1997)025<0795:LSSASE>2.3.CO;2.

Grauch, V.J.S., and Cordell, L., 1987, Limitations of determining density or magnetic boundaries from the horizontal gradient of gravity or pseudogravity data: Geophysics, v. 52, p. 118–121, doi: 10.1190/1.1442236.

Graymer, R.W., Sarna-Wojcicki, A.M., Walker, J.P., McLaughlin, R.J., and Fleck, R.J., 2002, Controls on timing and amount of right-lateral offset on the East Bay fault system, San Francisco Bay region, California: Geological Society of America Bulletin, v. 114, p. 1471–1479, doi: 10.1130/0016-7606(2002)114<1471:COTAAO>2.0.CO;2.

Guthrie, L.L., 1990, An internally standardized study of Cenozoic sand and sandstone compositions, Salton basin, southern California: Implications for rift basin evolution with emphasis on the Palm Spring and Imperial formations [M.S. thesis]: San Diego State University.

Hamilton, R.B., 1972, Aftershocks of the Borrego Mountain earthquake from April 12 to June 12, 1968, *in* The Borrego Mountain Earthquake of April 9, 1968: U.S. Geological Survey Professional Paper 787, p. 31–54.

Hampel, A., and Hetzel, R., 2006, Response of normal faults to glacial-interglacial fluctuations of ice and water masses on Earth's surface: Journal of Geophysical Research, v. 111, B11408, doi: 10.1029/2005JB004124.

Heitman, E.A., 2002. Characteristics of the structural fabric developed at the termination of a major wrench fault [M.S. thesis]: San Diego State University, 77 p.

Hill, R.I., 1984, Petrology and petrogenesis of batholithic rocks, San Jacinto Mountains, southern California [Ph.D. dissertation]: Pasadena, California Institute of Technology, 660 p.

Holk, G.J., Taylor, H.P., Jr., and Gromet, L.P., 2006, Stable isotope evidence for large-scale infiltration of metamorphic fluids generated during shallow subduction into the eastern Peninsular Ranges mylonite zone (EPRMZ), southern California: International Geology Review, v. 48, p. 209–222.

Hudnut, K.W., and Clark, M.M., 1989, New slip along parts of the 1968 Coyote Creek fault rupture, California: Bulletin of the Seismological Society of America, v. 79, p. 451–465.

Hudnut, K., Seeber, L., Rockwell, T., Goodmacher, J., Klinger, R., Lindvall, S., and McElwain, R., 1989, Surface ruptures on cross-faults in the 24 November 1987 Superstition Hills, California, earthquake sequence: Bulletin of the Seismological Society of America, v. 79, p. 282–296.

Ingersoll, R.V., and Rumelhart, P.E., 1999, Three-stage evolution of the Los Angeles basin, southern California: Geology, v. 27, p. 593–596, doi: 10.1130/0091-7613(1999)027<0593:TSEOTL>2.3.CO;2.

Janecke, S.U., and Belgarde, B.E., 2007, The width of dextral fault zones and shallow décollements of the San Jacinto fault zone, southern California: Palm Springs, California, Annual Meeting of the Southern California Earthquake Center, v. 17, http://www.scec.org/meetings/2007am/index.html.

Janecke, S.U., and Belgarde, B.E., 2008, Detecting hidden, high-slip rate faults: San Jacinto fault zone: Final Report for National Earthquake Hazards Reduction Program grant 06HQGR0031, 96 p., http://earthquake.usgs.gov/research/external/research.php?yearID=2006&pi=janecke&regionID=&award=&keyword=&submit=Find+Projects.

Janecke, S.U., and DeMets, C., 2010, Early Pleistocene reorganization of plate motion in the Salton Trough–Gulf of California: Geological Society of America Abstracts with Programs, v. 42, no. 4, p. 44.

Janecke, S.U., Kirby, S.M., Langenheim, V.E., Housen, B.A., Dorsey, R.J., Crippen, R.E., and Blom, R.G., 2004, Kinematics and evolutions of the San Jacinto fault zone in the Salton Trough: Progress Report from the San Felipe Hills area: Geological Society of America Abstracts with Programs, v. 37, no. 5, p. 317.

Janecke, S.U., Kirby, S., Steely, A., Lutz, A., Dorsey, R.J., Housen, B.A., and Langenheim, V., 2005a, Early Pleistocene emergence of new dextral faults SW of the southern San Andreas fault, Salton Trough: Palm Springs, Abstracts for the Annual Meeting of the Southern California Earthquake Center (SCEC), September 2005, p. 41, www.scec.org/meetings/2005am/2005abstracts.doc.

Janecke, S.U., Kirby, S.M., Langenheim, V., Steely, A.N., Dorsey, R.J., Housen, B.A., and Lutz, A., 2005b, High geologic slip rates on the San Jacinto fault zone in the SW Salton Trough, and possible near-surface slip deficit in sedimentary basins: Geological Society of America Abstracts with Programs, v. 37, no. 7, p. 275.

Janecke, S.U., Dorsey, R.J., and Belgarde, B., 2010, Age and structure of the San Jacinto and San Felipe fault zones and their lifetime slip rates, *in* Clifton, H.E., and Ingersoll, R.V., eds., 2010, Geologic excursions in California and Nevada: Tectonics, stratigraphy, and hydrogeology: Pacific Section, SEPM (Society for Sedimentary Geology) Book 108, p. 233–271.

Jefferson, G.T., and Remeika, P., 1995, The mid-Pleistocene stratigraphic co-occurrence of Mammuthus columbi and Mammuthus imperator in the Ocotillo Formation, Borrego Badlands, Anza-Borrego Desert State Park, California, *in* Remeika, P., and Sturz, A., eds., Paleontology and Geology of the Western Salton Trough Detachment, Anza-Borrego Desert State Park, California: San Diego Association of Geologists, Field Trip Guidebook 1, p. 104–108.

Jennings, C.W., compiler, 1977, Geologic map of California: California Division of Mines and Geology Geologic Data Map 2, scale 1:750,000.

Jennings, C.W., 1994, Fault activity map of California and adjacent areas, with locations and ages of recent volcanic eruptions: California Division of Mines and Geology Geologic Data Map No. 6, map scale 1:750,000.

Johnson, N.M., Officer, C.B., Opdyke, N.D., Woodard, G.D., Zeitler, P.K., and Lindsay, E.H., 1983, Rates of late Cenozoic tectonism in the Vallecito–Fish Creek basin, western Imperial Valley, California: Geology, v. 11, p. 664–667, doi: 10.1130/0091-7613(1983)11<664:ROLCTI>2.0.CO;2.

Kairouz, M.E., 2005, Geology of the Whale Peak Region of the Vallecito Mountains: Emphasis on the kinematics and timing of the West Salton detachment fault, southern California [M.S. thesis]: Los Angeles, University of California, 156 p.

Kendrick, K.J., Morton, D.M., Wells, S.G., and Simpson, R.W., 2002, Spatial and temporal deformation along the northern San Jacinto fault, southern California: Implications for slip rates: Bulletin of the Seismological Society of America, v. 92, p. 2782–2802, doi: 10.1785/0120000615.

Kennedy, M.P., 2000, Preliminary geologic map of the Pechanga 7.5′ quadrangle, San Diego and Riverside Counties, California: California Department of Conservation, http://www.consrv.ca.gov/cgs/rghm/rgm/preliminary_geologic_maps.htm.

Kennedy, M.P., 2003, Preliminary geologic map of the Vail Lake 7.5′ quadrangle, San Diego and Riverside Counties, California, http://www.consrv.ca.gov/cgs/rghm/rgm/preliminary_geologic_maps.htm.

Kennedy, M.P., and Morton, D.M., 2003, Preliminary geologic map of the Murrieta 7.5′ quadrangle, Riverside County, California: U.S. Geological Survey Open-File Report 03-189, 17 p., scale 1:24,000, http://geopbs.wr.usgs.gov/open-file/of03-189/.

Kenney, M.D., 1999, Emplacement, offset history, and recent uplift of basement within the San Andreas fault system, northeast San Gabriel Mountains, California [Ph.D. dissertation]: University of Oregon, 357 p.

Kenney, M.D., and Weldon, R.J., 1999, Timing and magnitude of mid to late Quaternary uplift of the western San Bernardino and northeastern San Gabriel Mountains, southern California, *in* Reynolds, R.E., and Reynolds, J., Tracks along the Mojave: A Field Guide from Cajon Pass to the Calico Mountains and Coyote Lake: San Bernardino County Museum Association Quarterly, v. 46, no. 3, p. 33–46.

King, N.E., and Savage, J.C., 1983, Strain-rate profile across the Elsinore, San Jacinto, and the San Andreas faults near Palm Springs, California, 1973–81: Geophysical Research Letters, v. 10, no. 1, p. 55–57, doi: 10.1029/GL010i001p00055.

Kirby, S.M., 2005, The Quaternary tectonic and structural evolution of the San Felipe Hills, California [M.S. thesis]: Logan, Utah State University, 182 p.

Kirby, S.M., Janecke, S.U., Dorsey, R.J., Housen, B.A., McDougall, K., Langenheim, V., and Steely, A., 2007, Pleistocene Brawley and Ocotillo formations: Evidence for initial strike-slip deformation along the San Felipe and San Jacinto fault zones, California: The Journal of Geology, v. 115, p. 43–62, doi: 10.1086/509248.

Langenheim, V.E., and Jachens, R.C., 1993, Isostatic residual gravity map of the Borrego Valley 1:100,000-scale quadrangle, California: U.S. Geological Survey Open-File Report 93-246, scale 1:100,000.

Langenheim, V.E., Jachens, R.C., Morton, D.M., Kistler, R.W., and Matti, J.C., 2004, Geophysical and isotopic mapping of preexisting structures that influenced the location and development of the San Jacinto fault zone, southern California: Geological Society of America Bulletin, v. 116, no. 9, p. 1143–1157, doi: 10.1130/B25277.1.

Langenheim, V.E., Tien-Chang Lee, Biehler, S., Jachens, R.C., and Morton, D.M., 2006, Isostatic gravity map with geology of the Santa Ana 30′ × 60′ quadrangle, southern California: U.S. Geological Survey Scientific Investigations Map 2951, http://pubs.usgs.gov/sim/2006/2951/.

Le, K., Oskin, M., Rockwell, T., and Owen, L., 2008, Temporal and spatial late Quaternary slip rate variability on the southern San Jacinto fault, California, Eos (Transactions, American Geophysical Union), v. 87, no. 52, Fall Meeting Supplement, abstract T44B-08.

Lilly, D.R., 2003, Structural geology of a transitory left step in San Felipe Hills fault [M.S. thesis]: San Diego State University.

Lin, G., Shearer, P.M., and Hauksson, E., 2007, Applying a three-dimensional velocity model, waveform cross correlation, and cluster analysis to locate southern California seismicity from 1981 to 2005: Journal of Geophysical Research, v. 112, B12309, doi: 10.1029/2007JB004986.

Lowman, P.D., 1980, Vertical displacement on the Elsinore fault of southern California: Evidence from orbital photography: The Journal of Geology, v. 88, p. 415–432, doi: 10.1086/628525.

Lundgren, P., Hetland, E.A., Liu, Z., and Fielding, E.J., 2009, Southern San Andreas–San Jacinto fault system slip rates estimated from earthquake cycle models constrained by GPS and interferometric synthetic aperture radar observations: Journal of Geophysical Research, v. 114, 18 p., B02403, doi: 10.1029/2008JB005996.

Luttrell, K., Sandwell, D., Smith-Konter, B., Bills, B., and Bock, Y., 2007, Modulation of the earthquake cycle at the southern San Andreas fault by lake loading: Journal of Geophysical Research, v. 112, B08411, 15 p., doi: 10.1029/2006JB004752.

Lutz, A.T., 2005, Tectonic controls on Pleistocene basin evolution in the central San Jacinto fault zone, southern California [M.S. thesis]: Eugene, University of Oregon, 136 p.

Lutz, A.T., Dorsey, R.J., Housen, B.A., and Janecke, S.U., 2006, Stratigraphic record of Pleistocene faulting and basin evolution in the Borrego Badlands, San Jacinto fault zone, southern California: Geological Society of America Bulletin, v. 118, p. 1377–1397, doi: 10.1130/B25946.1.

Magistrale, H., 2002, The relation of the southern San Jacinto fault zone to the Imperial and Cerro Prieto faults, *in* Barth, A., ed., Contributions to Crustal Evolution of the Southwestern United States: Boulder, Colorado, Geological Society of America Special Paper 365, p. 271–278.

Magistrale, H., and Rockwell, T., 1996, The central and southern Elsinore fault zone, southern California: Bulletin of the Seismological Society of America, v. 86, p. 1793–1803.

Matti, J.C., and Morton, D.M., 1993, Paleogeographic evolution of the San Andreas fault in southern California: A reconstruction based on a new cross-fault correlation, *in* Powell, R.E., Weldon, R J., and Matti, J.C., eds., The San Andreas Fault System: Displacement, Palinspastic Reconstruction, and Geologic Evolution: Geological Society of America Memoir 178, p. 107–159.

McCaffrey, R., 2005, Block kinematics of the Pacific–North America plate boundary in the southwestern United States from inversion of GPS, seismological, and geologic data: Journal of Geophysical Research, v. 110, p. B07401, doi: 10.1029/2004JB003307.

McCulloh, T.H., Beyer, L.A., and Enrico, R.J., 2000, Paleogene strata of the eastern Los Angeles basin, California: Paleogeography and constraints on Neogene structural evolution: Geological Society of America Bulletin, v. 112, p. 1155–1178, doi: 10.1130/0016-7606(2000)112<1155:PSOTEL>2.0.CO;2.

Meade, B.J., and Hager, B.H., 2005, Block models of crustal motion in southern California constrained by GPS measurements: Journal of Geophysical Research, v. 110, p. B03403, doi: 10.1029/2004JB003209.

Meisling, R., and Weldon, K., 1989, Late Cenozoic tectonics of the northwestern San Bernardino Mountains, southern California: Geological Society of America Bulletin, v. 101, p. 106–128, doi: 10.1130/0016-7606(1989)101<0106:LCTOTN>2.3.CO;2.

Middleton, T.J., 2006, Tectonic geomorphology of the southern Clark fault from Anza southeast to the San Filipe Hills: Implications of slip distribution for recent past earthquakes [M.S. thesis]: San Diego State University, 95 p.

Montgomery, D.R., Balco, G., and Willett, S.D., 2001, Climate, tectonics, and the morphology of the Andes: Geology, v. 29, p. 579–582, doi: 10.1130/0091-7613(2001)029<0579:CTATMO>2.0.CO;2.

Morton, D.M., 1999, Preliminary digital geologic map of the Santa Ana 30′ × 60′ quadrangle, southern California, version 1.0.: U.S. Geological Survey Open-File Report 99-172.

Morton, D.M., and Kennedy, M.P., 2003, Geologic map of the Bachelor Mountain 7.5′ quadrangle, Riverside County, California: U.S. Geological Survey Open-File Report 03-103.

Morton, D.M., and Matti, J.C., 1993, Extension and contraction within an evolving divergent strike-slip fault complex: The San Andreas and San Jacinto fault zones at their convergence in southern California, *in* Powell, R.E., Weldon, R.J., and Matti, J.C., eds., The San Andreas Fault System: Displacement, Palinspastic Reconstruction, and Geologic Evolution: Geological Society of America Memoir 178, p. 217–230.

Murray, A.S., and Wintle, A.G., 2000, Luminescence dating of quartz using an improved single aliquot regenerative-dose protocol: Radiation Measurements, v. 32, p. 57–73.

Nicholson, C., Sorlien, C.C., Atwater, T., Crowell, J.C., and Luyendyk, B.P., 1994, Microplate capture, rotation of the western Transverse Ranges, and initiation of the San Andreas transform as a low-angle fault system: Geology, v. 22, p. 491–495, doi: 10.1130/0091-7613(1994)022<0491:MCROTW>2.3.CO;2.

Okubo, P.G., and Aki, K., 1987, Fractal geometry in the San Andreas fault system: Journal of Geophysical Research, v. 92, p. 345–355, doi: 10.1029/JB092iB01p00345.

Pacheco, M., Martín-Barajas, A., Elders, W., Espinosa-Cardeña, J.-M., Helenes, J., and Segura, A., 2006, Stratigraphy and structure of the Altar basin of NW Sonora: Implications for the history of the Colorado River delta and the Salton Trough: Revista Mexicana de Ciencias Geológicas, v. 23, p. 1–22.

Pettinga, J.R., 1991, Structural styles and basin margin evolution adjacent to the San Jacinto fault zone, southern California: Geological Society of America Abstracts with Programs, v. 23, no. 5, p. 257.

Powell, R.E., 1993, Balanced palinspastic reconstruction of Pre-Late Cenozoic paleogeology, southern California, *in* Powell, R.E., Weldon, R.J., II, and Matti, J.C., eds., The San Andreas Fault System: Displacement, Palinspastic Reconstruction, and Geologic Evolution: Geological Society of America Memoir 178, p. 1–106.

Reitz, D.T., 1977, Geology of the western and central San Felipe Hills, northwestern Imperial County, California [M.S. thesis]: Los Angeles, University of Southern California, 155 p.

Remeika, P., and Beske-Diehl, S., 1996, Magnetostratigraphy of the western Borrego Badlands, Anza-Borrego Desert State Park, California: Implications for stratigraphic age control, *in* Abbott, P.L., and Seymour, D.C., eds., Sturzstroms and Detachment Faults, Anza-Borrego Desert State Park, California: South Coast Geological Society Annual Field Trip Guide Book, no. 24, p. 209–220.

Remeika, P., Liddicoat, J. C., and Beske-Diehl, S., 2008, Magnetostratigraphy of the western Borrego Badlands, Anza-Borrego Desert, California: Implications for tectonics and litho- and biostratigraphic control: Eos (Transactions, American Geophysical Union), v. 89, no. 53, Fall Meeting Supplement, abstract GP51A-0739.

Richard, P., Ballard, J.F., Colletta, B., and Cobbold, P.R., 1989, Fault genesis and propagation above a basement strike-slip fault: Analogue modeling and tomography: Comptes Rendus de l'Académie des Sciences, Série II, Mécanique, Physique, Chimie, Sciences de l'Univers, Sciences de la Terre, v. 309, p. 2111–2118.

Richard, P., Mocquet, B., and Cobbold, P.R., 1991, Experiments on simultaneous faulting and folding above a basement wrench fault: Tectonophysics, v. 188, p. 133–141, doi: 10.1016/0040-1951(91)90319-N.

Rockwell, T., Loughman, C., and Merifield, P., 1990, Late Quaternary rate of slip along the San Jacinto fault zone near Anza, Southern California: Journal of Geophysical Research, v. 95, p. 8593–8605, doi: 10.1029/JB095iB06p08593.

Rockwell, T.K., Lindvall, S., Dawson, T., Langridge, R., and Lettis, W., 2002, Lateral offsets on surveyed cultural features resulting from the 1999 Izmit and Duzce earthquakes, Turkey: Bulletin of the Seismological Society of America, v. 92, p. 79–94, doi: 10.1785/0120000809.

Rockwell, T.K., Seitz, G., Dawson, T., and Young, J., 2006, The long record of San Jacinto fault paleoearthquakes at Hog Lake: Implications for regional patterns of strain release in the southern San Andreas fault system: Seismological Research Letters, v. 77, no. 2, p. 270.

Rogers, T.H., 1965, Santa Ana sheet: California Division of Mines and Geology Geologic Map of California, scale, 1:250,000.

Rymer, M.J., Boatwright, J., Seekins, L.C., Yule, J.D., and Jing Liu, 2002, Triggered surface slips in the Salton Trough associated with the 1999 Hector Mine, California, earthquake: Bulletin of the Seismological Society of America, v. 92, no. 4, p. 1300–1317, doi: 10.1785/0120000935.

Rymer, R.M., 2000, Triggered surface slips in the Coachella Valley area associated with the 1992 Joshua Tree and Landers, California, earthquakes: Bulletin of the Seismological Society of America, v. 90, p. 832–848, doi: 10.1785/0119980130.

Ryter, D.W., 2002, Late Pleistocene kinematics of the central San Jacinto fault zone, southern California [Ph.D. dissertation]: University of Oregon, 137 p.

Salyards, S., Sieh, K., and Kirschvink, J., 1992, Paleomagnetic measurement of nonbrittle deformation across the San Andreas fault at Pallett Creek: Journal of Geophysical Research, v. 97, p. 12,457–12,470, doi: 10.1029/92JB00194.

Sanders, C., and Magistrale, H., 1997, Segmentation of the northern San Jacinto fault zone, southern California: Journal of Geophysical Research, v. 102, p. 27,453–27,467, doi: 10.1029/97JB02377.

Sanders, C.H., Magistrale, H., and Kanamori, H., 1986, Rupture patterns and preshocks of large earthquakes in the southern San Jacinto fault zone: Bulletin of the Seismological Society of America, v. 76, p. 1187–1206.

Sanders, C.O., 1989, Fault segmentation and earthquake occurrence in the strike-slip San Jacinto fault zone, California, *in* Schwartz, D.P., and

Sibson, R.H., eds., Proceedings of Conference XLV: A Workshop on Fault Segmentation and Controls of Rupture Initiation and Termination: U.S. Geological Survey Open-File Report 89-0315, p. 324–349.

Sanders, C.O., and Kanamori, H., 1984, A seismotectonic analysis of the Anza Seismic Gap, San Jacinto fault zone, southern California: Journal of Geophysical Research, v. 89, p. 5873–5890, doi: 10.1029/JB089iB07p05873.

Savage, J.C., and Prescott, W.H., 1976, Strain accumulation on the San Jacinto fault near Riverside, California: Bulletin of the Seismological Society of America, v. 66, p. 1749–1754.

Savage, J.C., Prescott, W.H., Lisowski, M., and King, N., 1979, Deformation across the Salton Trough, California 1973–1977: Journal of Geophysical Research, v. 84, p. 3069–3079, doi: 10.1029/JB084iB06p03069.

Schultejann, P.A., 1984, The Yaqui Ridge antiform and detachment fault: Mid-Cenozoic extensional terrane west of the San Andreas fault: Tectonics, v. 3, p. 677–691, doi: 10.1029/TC003i006p00677.

Sharp, I., Gawthorpe, R.L., Underhill, J., and Gupta, S., 2000, Fault propagation folding in extensional settings: Examples of structural style and synrift sedimentary response from the Suez Rift, Sinai, Egypt: Geological Society of America Bulletin, v. 112, p. 1877–1899, doi: 10.1130/0016-7606(2000)112<1877:FPFIES>2.0.CO;2.

Sharp, R.V., 1967, San Jacinto fault zone in the Peninsular Ranges of southern California: Geological Society of America Bulletin, v. 78, p. 705–729, doi: 10.1130/0016-7606(1967)78[705:SJFZIT]2.0.CO;2.

Sharp, R.V., 1972a, Tectonic setting of the Salton Trough, in the Borrego Mountain earthquake of April 9, 1968: U.S. Geological Survey Professional Paper 787, p. 3–15.

Sharp, R.V., 1972b, Map showing recently active breaks along the San Jacinto fault zone between the San Bernardino area and Borrego Valley, California: U.S. Geological Survey Miscellaneous Geologic Investigations Map I-675, scale 1:24,000, 3 sheets.

Sharp, R.V., 1975, En echelon fault patterns of the San Jacinto Fault zone, *in* Crowell, J.C., ed., San Andreas Fault in Southern California: A Guide to San Andreas Fault from Mexico to Carrizo Plain: California Division of Mines and Geology Special Report, no. 118, p. 147–152.

Sharp, R.V., 1979, Some characteristics of in the Peninsular Ranges mylonite zone, *in* Speed, R., and Sharp, R., co-organizers, and Evernden, J.F., conveners, Proceedings of Conference VIII—Analysis of Actual Fault Zones in Bedrock: U.S. Geological Survey Open-File Report 79-1239, Chapter 13, p. 258–267.

Sharp, R.V., 1981, Variable rates of late Quaternary strike slip on the San Jacinto fault zone, southern California: Journal of Geophysical Research, v. 86, p. 1754–1762, doi: 10.1029/JB086iB03p01754.

Sharp, R.V., 1982, Tectonic setting of the Imperial Valley Region, in the Imperial Valley, California, earthquake of October 15, 1979: U.S. Geological Survey Professional Paper 1254, p. 5–14.

Sharp, R.V., and Clark, M.M., 1972, Geologic evidence of previous faulting near the 1968 rupture on the Coyote Creek fault: U.S. Geological Survey Professional Paper, v. 787, p. 131–140.

Shearer, P., Haukkson, E., and Lin, G., 2005, Southern California hypocenter relocation with waveform cross-correlation: Part 2, Results using source-specific station terms and cluster analysis: Bulletin of the Seismological Society of America, v. 95, p. 904–915, doi: 10.1785/0120040168.

Shelef, E., Oskin, M., and Fialko, Y., 2006, Distributed anelastic strain and its relationship to compliant zones surrounding active faults of the eastern California Shear Zone: Eos (Transactions, American Geophysical Union), v. 85, no. 47, Fall Meeting Supplement, abstract T21C-0439.

Sheridan, J.M., and Weldon, R.J., II, 1994, Accommodation of compression in the Mecca Hills, California, *in* McGill, S.F., and Ross, T.M., Geological Investigations of an Active Margin: Geological Society of America Cordilleran Section Guidebook, p. 330–336.

Shirvell, C., 2006, Pliocene exhumation along the West Salton detachment system and tectonic evolution of the Fish Creek–Vallecito supradetachment basin, Salton Trough, southern California [M.S. thesis]: Los Angeles, University of California, 133 p.

Sieh, K., 1984, Lateral offsets and revised dates of large earthquakes at Pallett Creek, California: Journal of Geophysical Research, v. 89, p. 7641–7670, doi: 10.1029/JB089iB09p07641.

Sieh, K., Jones, L., Hauksson, E., Hudnut, K., Eberhart-Phillips, D., Heaton, T., Hough, S., Hutton, K., Kanamori, H., Lilje, A., Lindvall, S., McGill, S.F., Mori, J., Rubin, C., Spotila, J., Stock, J., Thio, H.K., Treiman, J., Wernicke, B., and Zachariasen, J., 1993, Near-field investigations of the Landers earthquake sequence, April to July 1992: Science, v. 260, p. 171–176, doi: 10.1126/science.260.5105.171.

Spotila, J.A., and Sieh, K., 1995, Geologic investigations of a “slip gap” in the surficial ruptures of the 1992 Landers earthquake, southern California: Journal of Geophysical Research, v. 100, B1, p. 543–559, doi: 10.1029/94JB02471.

Steely, A.N., 2006, The evolution from late Miocene West Salton detachment faulting to cross-cutting oblique strike-slip faults in the southwest Salton Trough, California [M.S thesis]: Utah State University, 253 p., 3 plates, scale 1:24,000.

Steely, A.N., Janecke, S.U., Dorsey, R.J., and Axen, G.J., 2009, Early Pleistocene initiation of the San Felipe fault zone, SW Salton Trough, during reorganization of the San Andreas fault system: Geological Society of America Bulletin, v. 121, p. 663–687, doi: 10.1130/B26239.1.

Stirling, M.W., Wesnousky, S.G., and Shimazaki, K., 1996, Fault trace complexity, cumulative slip, and the shape of the magnitude-frequency distribution for strike-slip faults: A global survey: Geophysical Journal International, v. 124, p. 833, doi: 10.1111/j.1365-246X.1996.tb05641.x.

Stock, J.M., and Hodges, K.V., 1989, Pre-Pliocene extension around the Gulf of California and the transfer of Baja California to the Pacific Plate: Tectonics, v. 8, p. 99–115, doi: 10.1029/TC008i001p00099.

Sylvester, A.G., and Smith, R.R., 1976, Tectonic transpression and basement-controlled deformation in the San Andreas fault zone, Salton trough, California: American Association of Petroleum Geologists Bulletin, v. 60, p. 74–96.

Thatcher, W., Hileman, J.A., and Hanks, T.C., 1975, Seismic slip distribution along the San Jacinto fault zone, southern California and its implications: Geological Society of America Bulletin, v. 86, p. 1140–1146, doi: 10.1130/0016-7606(1975)86<1140:SSDATS>2.0.CO;2.

Theodore, T.G., 1967, Structure and petrology of the gneisses and mylonites at Coyote Mountain, Borrego Springs, California [Ph.D. dissertation]: California University, Los Angeles, 268 p.

Theodore, T.G., 1970, Petrogenesis of mylonites of high metamorphic grade in the peninsular ranges of southern California: Geological Society of America Bulletin, v. 81, p. 435–450, doi: 10.1130/0016-7606(1970)81[435:POMOHM]2.0.CO;2.

Theodore, T.G., and Sharp, R.V., 1975, Geologic map of the Clark Lake quadrangle, San Diego County, California: U.S. Geological Survey MF-644, scale 1:24,000.

Todd, V.R., 1977, Geologic map of the Agua Caliente Springs quadrangle, San Diego County, California: U.S. Geological Survey Open-File Report 77-742, 20 p., scale 1:24,000.

Todd, V.R., 2004, Preliminary geologic map of the El Cajon 30° × 60° quadrangle, southern California: U.S. Geological Survey Open-File Report 2004-1361, scale 1:100,000.

Treiman, J.A., and Lundberg, M.M., compilers, 1999, Fault number 125f, San Jacinto fault, Superstition Hills section, in Quaternary fault and fold database of the United States: U.S. Geological Survey website, http://earthquakes.usgs.gov/regional/qfaults, accessed 03/24/2009 03:26 PM.

van der Woerd, J., Klinger, Y., Sieh, K., Tapponnier, P., Ryerson, F.J., and Mériaux, A.S., 2006, Long-term slip rate of the southern San Andreas fault from ^{10}Be-^{26}Al surface exposure dating of an offset alluvial fan: Journal of Geophysical Research, v. 111, abstract B04407, 17 p., doi: 10.1029/2004JB003559.

Verdugo, D., Ragona, D., and Rockwell, T., 2006, New paleoseismic results from the southern San Jacinto fault zone: 2006 Southern California Earthquake Center Annual Meeting abstract volume, p. 175.

Weismeyer, A.L., 1968, Geology of the northern portions of the Seventeen Palms and Fonts Point quadrangles, Imperial and San Diego Counties, California [M.A. thesis]: Los Angeles, University of Southern California.

Weldon, R.J., Meisling, K.E., and Alexander, J., 1993, A speculative history of the San Andreas fault in the central Transverse Ranges, *in* Powell, R.E., Weldon, R.J., and Matti, J. eds., The San Andreas Fault System: Displacement, Palinspastic Reconstruction, and Geologic Evolution: Geological Society of America Memoir 178, p. 161–178.

Weldon, R.J., II, Fumal, T.E., Powers, T.J., Pezzopane, S.K., Scharer, K.M., and Hamilton, J.C., 2002, Structure and earthquake offsets on the San Andreas fault at the Wrightwood, California paleoseismic site: Bulletin of the Seismological Society of America, v. 92, p. 2704–2725, doi: 10.1785/0120000612.

Weldon, R.J., II, Scharer, K.M., Fumal, T.E., and Biasi, G.P., 2004, Wrightwood and the earthquake cycle: What a long recurrence record tells us about how faults work: GSA Today, v. 14, p. 4–10, doi: 10.1130/1052-5173(2004)014<4:WATECW>2.0.CO;2.

Wells, D.L., 1987, Geology of the eastern San Felipe Hills, Imperial Valley, California: implications for wrench faulting in the southern San Jacinto fault zone [M.S. thesis]: San Diego State University.

Wells, D.L., and Feragen, E.S., 1987, Percent strain and slip rate estimates for a proposed buried extension of the Clark fault, southern San Jacinto fault zone, Imperial Valley, California: Geological Society of America Abstracts with Programs, v. 19, p. 6.

Wesnousky, S., 1990, Seismicity as a function of cumulative geologic offsets: Some observations from southern California: Bulletin of the Seismological Society of America, v. 80, p. 1374–1381.

Winker, C.D., 1987, Neogene stratigraphy of the Fish Creek–Vallecito section, southern California: Implications for early history of the northern Gulf of California and Colorado delta [Ph.D. dissertation]: Tucson, University of Arizona, 494 p.

Winker, C.D., and Kidwell, S.M., 1996, Stratigraphy of a marine rift basin: Neogene of the western Salton Trough, California, *in* Abbott, P.L., and Cooper, J.D., eds., Field Conference Guidebook and Volume for the Annual Convention: San Diego, California, American Association of Petroleum Geologists, Pacific Section, p. 295–336.

Woodard, G.D., 1963, The Cenozoic succession of the West Colorado Desert, San Diego and Imperial Counties, southern California [Ph.D. thesis]: Berkeley, University of California, 494 p.

Woodard, G.D., 1974, Redefinition of Cenozoic stratigraphic column in Split Mountain Gorge, Imperial Valley, California: American Association of Petroleum Geologists Bulletin, v. 58, p. 521–539.

Zachariasen, J., and Sieh, K., 1995, The transfer of slip between two en echelon strike-slip faults: A case study from the 1992 Landers earthquake, southern California: Journal of Geophysical Research, v. 100, no. B8, p. 15,281–15,301, doi: 10.1029/95JB00918.

Manuscript Accepted by the Society 29 June 2010

Printed in the USA